Ministère de l'Enseignement Supérieur et de la Recherche Scientifique

Université Hassiba Benbouali de Chlef

Faculté des Sciences Exactes et Informatique

Département de physique

THÈSE

Présentée pour l'obtention du diplôme de

DOCTORAT

Filière : Physique

Spécialité : Physique théorique

Par

GUEBLI NADIA

Thème :

Quantum droplets in Bose-Bose mixtures

Soutenue le 03/07/2023, devant le jury composé de :

Habib RACHED	Professeur	UHB Chlef	Président
Abdelaali BOUDJEMAA	Professeur	UHB Chlef	Rapporteur
Kamel BENCHEIKH	Professeur	Université de Setif	Examinateur
Sid Ahmed DIAF	Professeur	Université de Khemis Meliana	Examinateur
Mohamed BELABBAS	MCA	UHB Chlef	Examinateur

Abstract

Most recent sensational breakthrough in the field of ultracold atomic quantum gases is the creation of self-bound droplet state. This exotic phase of matter which can be formed in dipolar condensates and binary Bose mixtures, results from the competition between an attractive mean-field energy and the repulsive Lee-Huang-Yang correction. This thesis looks to answer the question of effects of higher-order quantum and thermal fluctuations on the stabilization of self-bound droplets in Bose-Bose mixtures. Within the Hartree-Fock-Bogoliubov theory we calculate the ground-state energy, the droplet equilibrium density, the depletion and anomalous density of the droplet as well as the critical temperature as a function of the relevant parameters. Our findings for the ground-state energy are compared with recent available analytical predictions and diffusion Monte Carlo simulations and excellent agreement is found. We compute the density profiles and breathing modes of the droplet of this novel state of matter by numerically solving the underlying generalized finite-temperature Gross-Pitaevskii equation. This latter is derived selfconsistently from our theory using the local density approximation. We study also in this thesis the bulk and surface properties of ultradilute self-bound quantum droplets in a heteronuclear Bose-Bose mixture. Within the realm of the Hartree-Fock-Bogoliubov theory, we calculate beyond the Lee-Huang-Yang corrections to the ground-state energy, the droplet equilibrium density, the surface tension, and the critical number of particles. Our predictions coincide perfectly with recent diffusion Monte Carlo simulation and density functional theory method.

Acknowledgements

"Praise be to Allah, the Most Gracious and the Most Merciful, who has blessed us with existence and is the source of all success." I am grateful to countless individuals who played a part in the completion of my thesis, and though it's challenging to acknowledge all of them in brief, there are a few whom I would like to specifically thank.

First and foremost, I would like to express my sincerest gratitude to my supervisor, Prof. Abdelaali Boudjemaa, for his unwavering support, guidance, and encouragement throughout the course of my research. His vast knowledge and expertise in the field have been instrumental in shaping my understanding of the subject matter and in guiding me through the challenges of the research process. I am deeply grateful for his patience, encouragement, and understanding throughout the entire journey. His support has been crucial in helping me to complete this thesis, and I am deeply appreciative of all that has done for me. This work would not have been possible without invaluable support, and I am honored to have had the opportunity to work with such a talented and dedicated supervisor.

I would like to extend my sincere gratitude to the members of my thesis jury, Prof. Habib Rached, Prof. Kamel Bencheikh, Prof. Sid Ahmed Diaf and Dr. Mohamed Belabbas for their valuable time, effort, and insightful feedback during the examination of my thesis. I am grateful for the opportunity to present my research and receive constructive criticism from such knowledgeable and experienced professionals in the field. Their suggestions and recommendations have been instrumental in improving the quality of my work and have helped to deepen my understanding of the subject

matter.

Contents

List of Figures

Chapter 1

General Introduction

In 1924 Satyendra Nath Bose, along with Albert Einstein (in 1925) predicted a new state of matter- at very low temperature a macroscopic number of bosons coalesce into the ground state [1, 2]. This phase, later coined the Bose-Einstein condensate (BEC). In 1995, arround 70 years after the original works by Bose and Einstein, BEC was first observed experimentally in dilute atomic gases at JILA, MIT and Rice University [3, 4, 5]. A route to achieve such ultracold structures comprises a combination of laser cooling and subsequent evaporative [6, 7, 8]. The experimental realization of BEC has lead to a resurgence of interest in the theory of weakly interacting Bose gases (see for reviews and books [9, 10, 11, 12, 13]). More generally, these systems offer an unprecedented opportunity for investigating many-body quantum phenomena.

The great interest in the ultracold gases field and the high controllable interactions allowed in 2005 the experimental achievement of a ^{52}Cr BEC with inter-atomic magnetic dipole dipole interaction (DDI) [14]. Ultracold dipolar gases, in which magnetic or electric DDIs play a crucial role, differ substantially from their nondipolar counter-

parts due to the long-range character and the anisotropy (being partially repulsive or attractive). By virtue of this interaction, dipolar gases are expected to open fascinating prospects for the observation of novel quantum phases and many-body phenomena (see for reviews [15, 14, 16, 17]).

The ability to control interactions using Feshbach resonances offer a plethora of research directions. Feshbach resonances are dramatic enhancements of the scattering cross section between two atoms for certain values of an external magnetic field [12]. Utilizing these resonances, it has then become possible to produce binary BECs either in different hyperfine levels [18, 19, 20, 56, 22], in different isotopes of the same species [23, 24], in different atomic species [25, 26, 27, 28, 29, 30], or even with different statistics [31]. In recent years, degenerate dilute Bose-Bose gases have prompted considerable interest in the community of cold atoms physics due to their rich phase diagram. One of the most amazing features of such multi-component structures is their miscibility-immiscibility transition which depends on the ratio of the intra- and interspecies interactions [32, 33, 34], on the condensate numbers [35], and on thermal fluctuations [36, 37, 38]. A mixture of two-component Bose-Einstein condensate (BEC) plays a crucial role in various systems, such as solitons (see e.g. [39]), vortices (see e.g. [40]), and disordered enviroment [41, 42, 43]. The focus on understanding dilute, ultracold quantum Bose-Bose mixtures increased dramatically after the theoretical proposal by Petrov [44] in 2015 on the formation of self-bound droplets.

Recently, the investigation of self-bound droplet states has become a burgeoning area of interest. The existence of such a liquid droplet cannot be explained by a Van der Waals-like mechanism but instead originates from a many-body effect. This novel state of matter is stabilized by quantum fluctuations and requires a minimum number

of particles. Such an exquisite stabilization mechanism originates from the delicate competition between the attractive mean-field energy and repulsive beyond mean-field effects furnished by the Lee-Huang-Yang (LHY) corrections [45], arresting the mean-field collapse, forming ultradilute quantum droplet. This latter has opened a new avenue to explore a broad range of exciting physical phenomena such as supersolid states and polarons. Quantum droplets are also potentially promising for future technologies, including gravitational wave detectors and quantum sensors.

As suggested by Petrov in his seminal work [44], qauntum droplets can emerge in mixtures of binary BECs with repulsive intraspecies and attractive interspecies interactions. The inclusion of the repulsive LHY quantum fluctuations leads to stabilize the mechanical collapse predicted by the mean-field theory giving rise to the formation of a self-bound liquid-like droplet. The same stabilization scenario has been recognized responsible for the formation of self-bound droplets in single and binary dipolar BECs, where the competition between the mean-field energy associated with short and long-range interactions and the LHY corrections arrests the dipolar instability at high density [46, 47, 48, 49, 50, 51]. Both droplets are characterized by ultralow densities, six to eight orders of magnitude more dilute than a Helium ^{4}He liquid droplet [52] and orders of magnitude thinner than air. Despite these ultradilute structures share many peculiar properties, they present several differences. The most important among them is that in the case of dipolar case, anisotropic character of the magnetic DDI gives rise to the nucleation of filament-like self-bound droplets with highly anisotropic properties [47, 53, 54]. Conversely, the self-bound systems created from Bose-Bose mixtures are spherical in free space. Droplets should also exist in other systems with pure isotropic contact interactions. For instance, in a seminal

3

paper by Bulgac [55], the mechanism that creates the droplet state is based on a balance between two- and three-body interactions.

Experimentally, such liquid droplets have been first observed in dipolar BECs of ^{164}Dy atoms, in Stuttgard in the group led by Tilman Pfau [46, 47], and with ^{166}Er atoms, in Innsbruck in Francesca Ferlainos group [48]. Shortly after, the first experiments have been realized also with homonuclear mixtures of ^{39}K, in the group led by Leticia Taruell in Barcelona in confined spatial geometries [56, 57] and the group in Florence in three-dimensional (3D) free space [58]. The observation of heteronuclear quantum droplets in an attractive bosonic mixture of ^{41}K-^{87}Rb and ^{23}Na-^{87}Rb have been reported quite recently in [59, 60].

Theoretically, quantum droplets in both dipolar and binary BECs have been attracted considerable interests in studying their incredible properties, such as self-bound feature [46, 47, 56], collective modes [61, 62], soliton to droplet transition [57], vortices [63, 64], droplet-droplet collision [65], supersolid states [66, 67, 68, 69], low-dimensional properties [70, 71, 72, 73], finite-temperature effects [73, 74, 75, 76, 77, 78, 79] and so forth (see recent reviews [80, 47, 81] and references therein). Furthermore, recent numerical results based on Quantum and Diffusion Monte Carlo simulations (QMC) and (DMC) [70, 82, 83, 84, 85, 86, 87, 88, 89] have checked the important role played by the quantum fluctuations for the description of the self-bound droplets of both dipolar and nondipolar BECs realized in recent experiments.

Almost all previous works are based on the zero-temperature generalized Gross-Pitaevskii (GGP) equation which is derived from the Petrov's prescription [44]. Frankly speaking, this model, although generally accepted, is somewhat artificial since the LHY term has not been properly included. Indeed, in the relevant regime of droplet

4

formation, the Petrov's theory predicts a purely imaginary phonon velocity for one of the two gapless Bogoliubov low-lying excitations and hence a complex energy functional [76, 77]. To overcome this technical problem, Petrov supposed a weak dependence of the LHY energy on the interspecies interaction strength and explicitly setting to zero the value of the imaginary phonon velocity [44]. Omitting a small imaginary contribution to the LHY energy might be justified only close to the droplet formation point. Intersting models such as the pairing approach and the perturbation theory [76, 77], concentrate on accounting for additional terms to the energy functional, have been introduced recently in order to cure this imaginary excitation energies. Moreover, recent DMC calculations of [85] revealed that the accuracy of method of [44] becomes worse as one increases the attractive interspecies interaction. Owing to such an inconsistency the GGP equation fails to predict the ground-state energy, the critical atom number and the effects of higher-order (beyond LHY) quantum corrections compared to recent experiments and QMC and DMC results [70, 85, 86, 88].

This thesis

In this thesis we aim to investigate effects of higher-order quantum and thermal fluctuations on the occurrence and on the stabilization of quantum droplets in both homonuclear and heteronuclear Bose-Bose mixtures. To this end, we develop a versatile theoretical model in order to remove the handicaps of the standard Petrov's theory [44]. Our analysis is based on the Hartree-Fock-Bogoliubov (HFB) theory that can go beyond the LHY description and self-consistently evaluate the quantum and thermal fluctuations exhibited by weakly-interacting binary BECs [73, 74, 78, 79].

The HFB theory includes automatically higher-order corrections originating from the normal and anomalous correlations to the equation of state (EoS) generalizing all existing models in the literature. The intriguing coupling between the order parameter, and the normal and anomalous fluctuations makes the HFB a promising approach for exploring quantum self-bound droplets in a dipolar single BEC [74] and Bose-Bose mixtures [49, 73, 78, 79] at both zero and finite temperatures.

We first focus on the role of higher-order quantum and thermal fluctuations in a symmetric (homonuclear) mixtures using our self-consistent HFB theory. We show that at zero temperature, our theory not only provides interesting results but also captures genuine higher-order quantum effects predicted from recent diffusion Monte Carlo (DMC) simulations for the ground-sate energy and the equilbrium density [85]. The regime of relatively strong interactions, where the quantum corrections become more pronounced is also discussed. Furthermore, we deal with the ground-state properties of the droplet such as the density profiles and the collective modes. Our treatment is based on the GGP equation which we derive self-consistently from the HFB formalism taking into account higher-order quantum corrections under the local density approximation. We aim here to understand how the density distribution and the collective oscillations behave when varying the interaction.

On the other hand, we discuss the effects of higher-order fluctuations on the bulk and surface properties of quantum droplets in a heteronuclear Bose-Bose mixture of ^{41}K-^{87}Rb. The longer lifetime of this new liquid mixture due to a lower three-body recombination rate of the system allows the observation of more complex scenarios arising from the interactions between self-bound droplets. Within the realm of the HFB theory, we calculate beyond the LHY corrections to the ground-state energy,

6

the equilibrium density, the surface tension, and the critical number of particles of the droplet. Our predictions are compared with recent QMC simulation and Density Functional Theory (DFT) method [89] and excellent agreement is found.

The dearth of finite temperature work motivates also the focus of this thesis, that is, the finite-temperature analysis of ultradilute binary liquid mixtures. An outstanding question here is, how the thermal fluctuations affect the formation and the stabilization of the self-bound droplet? Based on the free energy of the bulk mixture, calculated within our HFB approach, corrections to the equilibrium density and the critical temperature are presented. For the homonuclear droplet, we find that the droplet evaporates when the temperature becomes slightly larger than the ground-state energy of the droplet, in good agreement with recent results inferred from the macroscopic approach [76] and the pairing theory [77]. Finite-temperature effects on the shape and the frequencies of the breathing oscillations of the self-bound droplet are also addressed by numerically solving the finite-temperature GGP equation derived from our HFB theory. We investigate in addition the effects of temperature on the formation and on the robustness of heteronuclear self-bound mixtures. It is pointed out that the self-bound droplet remains robust even for relatively large thermal fluctuations in contrast to the homonuclear case.

Outline of the thesis

In chapter 2, we present the physics of ultracold Bose-Bose mixtures and their fundamental properties. We introduce in particular the coupled HFB equations which are designed to be applied to a Bose-Bose mixture at any temperature. A full three-

dimensional study on miscible-immiscible conditions is performed. We derive the HFB-de Gennes equations that enabling us to calculate the collective excitations in the presence of the noncondensate and anomalous densities. The ultraviolet divergence of the anomalous averages and of the ground-state energy is properly regularized obtaining useful analytical expressions. We apply the developed HFB method to a homonuclear Bose mixture. Quantum and thermal fluctuation corrections in the excitations and the thermodynamics of such a system are deeply analyzed.

Chapter 3 concerns the theory of quantum droplets made in bosonic mixtures which predicts in particular the conditions for their formation, their equilibrium properties and their collective excitations. We present the theoretical model introduced by Petrov [44] which is based on the zero-temperature GGP equation. We then briefly review the key steps for the experimental realization of such droplets in 3D free space. The general properties of the self-bound droplet and its future impressive technological applications are also discussed.

The major achievements of this thesis are presented in chapters 4, 5 and 6.

Chapter 4 is dedicated to the study of the effects of higher-order quantum fluctuations on the ground-state properties of the self-bound droplet. We extract useful analytical results for the ground-state energy and the equilibrium density that extend naturally the seminal equations of Petrov [44]. Explicit expressions connecting normal and anomalous correlations to the droplet equilibrium density are also obtained for the first time to the best of our knowledge. We show that at zero temperature, our theory not only provides fascinating results but also captures genuine higher-order quantum effects predicted from recent DMC simulations. We further analyze the equilibrium properties of the self-bound droplet, by numerically solving the adjusted

GGP equation which takes into account higher-order effects.

In chapter 5, the properties of uniform self-bound quantum liquid droplets in heteronuclear Bose-Bose mixtures of ^{41}K-^{87}Rb [59] are studied in the presence of higher-order quantum corrections. We calculate in particular, the ground-state energy, the equilibrium bulk densities, and the compressibility of the system by means of numerical simulations. The surface properties of a ^{41}K-^{87}Rb self-bound quantum droplet are also discussed. The density profile of the droplet and the surface tension are analyzed by means of a variational scheme and numerical simulations. The critical number of particles is also adequately computed.

Chapter 6 presents a comprehensive theoretical study of finite-temperature effects on both homonuclear and heteronuclear self-bound Bose droplets. Within the HFB theory we determine the free energy, the critical temperature and the thermal equilibrium density of the droplet. The shape and the collective excitations of self-bound droplet are also obtained for different values of temperature based on finite-temperature GGP equation. Our analysis is then extended to the heteronuclear self-bound droplet.

Finally, we present conclusions and an outlook.

Chapter 2

Physics of ultracold Bose-Bose mixtures

2.1 Introduction

Recently, binary mixtures of BEC have afforded an intriguing glimpse into the macroscopic quantum world since they exhibit an incredible richness in terms of holding different kinds of phases not achievable in a single component BEC. This places these ensembles at a remarkable interface between atomic physics, nonlinear, condensed physics, and non-equilibrium statistical physics.

Theoretical investigations of degenerate binary Bose mixtures have mainly addressed the determination of the ground-state and the density profiles of trapped systems [32, 34, 33], the stability, and the phase separation [90, 33, 91, 92, 93, 94, 95]. The dynamics of the center-of-mass oscillation (dipole modes) of two-component BECs was studied analytically and numerically by Sinatra et *al.* [96], whereas, the excitations

of quadrupole and scissors modes have been explored by Kasamatsu et *al.* [97]. Furthermore, the properties of homogeneous double condensate systems were analyzed in [98, 99, 100, 101, 102] using the Bogoliubov theory. At finite temperature, uniform binary Bose gases have been worked out using the Bogoliubov approach [103], the Hartree-Fock theory [104] and a large-N approximation [105]. The phase separation, the dynamics, and the thermalization mechanisms of trapped binary mixtures at finite temperatures have been also examined utilizing the local-density approximation [106], the Popov theory [107, 108], and the Zaremba-Nikuni-Griffin model [109, 35, 110]. There has been also an extensive amount of work addressing Bose mixtures in disordered media (see eg. [111, 112, 113, 114, 41, 42, 43]).

Although the above theories received great success in describing the behavior of dual BECs, much remains to be investigated regarding effects of quantum and thermal fluctuations on the phase separation and collective excitations of such mixtures. They ignored also the importance of the anomalous density in such Bose mixtures. This quantity which quantifies the correlations of pairs of noncondensed atoms with pairs of condensed atoms has a crucial contribution especially at intermediate temperatures [115, 116].

The main focus of this chapter is to introduce the basis of the HFB theory for dilute Bose-Bose mixtures [37] that we will rely on throughout this thesis. The approach that we develop here offers a self-consistent theoretical framework to study the properties of dilute Bose-Bose mixtures including the two condensates, thermal clouds and pair anomalous correlations, as well as the coupling between the theses components at both zero and finite temperatures. In addition, the HFB equations allow us to include many-body effects on scattering processes through the anomalous

pair average. This latter plays a key role in the phenomenon of phase separation in binary Bose condensates. We shall see also, in the next chapters, that the theory provides an excellent starting point to study the behavior of ultradilute quantum droplets. The HFB theory has been successfully tested against experiments in a wide variety of issues for single BECs namely: effects of anomalous correlations, low-dimensional Bose gases, collective modes, vortices, solitons and Bose polarons, and so on [115, 116, 117, 118, 119, 120, 121, 122, 123, 124, 125].

In this chapter we present the finite-temperature criterion for the phase separation where the effects of anomalous correlations lead to modify the condition for the miscible-immiscible scenario of the system. On the other hand, starting from our HFB equations, we develop a random-phase theory for the elementary excitations in a homogeneous mixture. Additionally, we derive meaningful analytical expressions for the condensed depletion, the anomalous density, the equation of state for Bose mixtures.

2.2   Hartree-Fock-Bogoliubov theory

Let us consider a weakly interacting two-component BEC with atomic mass m_j (see figure 2.1). The many-body Hamiltonian describing this mixture reads:

$$
\begin{aligned}
\hat{H} = \sum_{j=1}^{2} \Bigg[& \int d\mathbf{r}\, \hat{\psi}_j^\dagger(\mathbf{r}) h_j^{sp} \hat{\psi}_j(\mathbf{r}) \\
& + \frac{1}{2} \int d\mathbf{r} \int d\mathbf{r}'\, \hat{\psi}_j^\dagger(\mathbf{r}) \hat{\psi}_j^\dagger(\mathbf{r}') V_j(\mathbf{r}-\mathbf{r}') \hat{\psi}_j(\mathbf{r}') \hat{\psi}_j(\mathbf{r}) \Bigg] \\
& + \int d\mathbf{r} \int d\mathbf{r}'\, \hat{\psi}_1^\dagger(\mathbf{r}) \hat{\psi}_2^\dagger(\mathbf{r}') V_{12}(\mathbf{r}-\mathbf{r}') \hat{\psi}_2(\mathbf{r}') \hat{\psi}_1(\mathbf{r}),
\end{aligned}
\tag{2.1}
$$

where $\hat{\psi}_j^\dagger$ and $\hat{\psi}_j$ denote, respectively the usual creation and annihilation field operators, satisfying the usual canonical commutation rules

$$[\hat{\psi}_j(\mathbf{r}), \hat{\psi}_j^\dagger(\mathbf{r}')] = \delta(\mathbf{r} - \mathbf{r}'). \tag{2.2}$$

The single particle Hamiltonian is defined as $h_j^{sp} = -(\hbar^2/2m_j)\nabla^2 + U_j(\mathbf{r})$, where $U_j(\mathbf{r})$ is the external traps. At very low temperature, the usual procedure is to make a contact interaction approximation to the intra- and interspecies two-body interaction potentials.

The intraspecies two-body interaction potential is

$$V_j(\mathbf{r} - \mathbf{r}') = g_j\delta(\mathbf{r} - \mathbf{r}'), \tag{2.3}$$

where $g_j = 4\pi\hbar^2 a_j/m_j$ with a_j being the intraspecies s-wave scattering lengths. The interspecies two-body interactions potential reads

$$V_{12}(\mathbf{r} - \mathbf{r}') = g_{12}\delta(\mathbf{r} - \mathbf{r}'), \tag{2.4}$$

where $g_{12} = g_{21} = 2\pi\hbar^2(m_1^{-1} + m_2^{-1})a_{12}$ which is characterized by the interspecies $a_{12} = a_{21}$ s-wave scattering lengths.

Substituting the definitions (2.3) and (2.4) into the Hamiltonian (2.1), one obtains:

$$\hat{H} = \sum_{j=1}^{2} \int d\mathbf{r}\, \hat{\psi}_j^\dagger(\mathbf{r}) \left[h_j^{sp} + \frac{g_j}{2}\hat{\psi}_j^\dagger(\mathbf{r})\hat{\psi}_j(\mathbf{r}) \right] \hat{\psi}_j(\mathbf{r}) + g_{12} \int d\mathbf{r}\, \hat{\psi}_2^\dagger(\mathbf{r})\hat{\psi}_2(\mathbf{r})\hat{\psi}_1^\dagger(\mathbf{r})\hat{\psi}_1(\mathbf{r}),$$

$$\tag{2.5}$$

In order to describe Bose-Bose mixtures at finite temperature, we divide the Bose-field operator into two parts: the condensate contribution Φ, which corresponds to the macroscopic occupation of a single quantum state and noncondensed part $\hat{\tilde{\psi}}$, which

corresponds to thermally-excited atoms (at $T = 0$ this contribution is only due to quantum fluctuation):

$$\hat{\psi}_j(\mathbf{r}, t) = \Phi_j(\mathbf{r}, t) + \hat{\bar{\psi}}_j(\mathbf{r}, t). \tag{2.6}$$

Within this, the Hamiltonian (2.1) takes the form of a sum

$$\hat{H} = \hat{H}^{(0)} + \hat{H}^{(1)} + \hat{H}^{(2)} + \hat{H}^{(3)} + \hat{H}^{(4)}, \tag{2.7}$$

where

$$\hat{H}_0 = \sum_{j=1}^{2} \int d\mathbf{r} \left(\Phi_j^* h_j^{sp} \Phi_j + \frac{g_j}{2} n_{cj} \right) + g_{12} \int d\mathbf{r} n_{c1} n_{c2}, \tag{2.8a}$$

$$\hat{H}_1 = 0, \tag{2.8b}$$

$$\hat{H}_2 = \sum_{j=1}^{2} \int d\mathbf{r} \left[\bar{\Psi}_j^\dagger h_j^{sp} \bar{\Psi}_j + g_j \left(2 n_{cj} \bar{\Psi}_j^\dagger \bar{\Psi}_j + \frac{1}{2} \Phi_j^{*2} \bar{\Psi}_j \bar{\Psi}_j + \frac{1}{2} \Phi_j^2 \bar{\Psi}_j^\dagger \bar{\Psi}_j^\dagger \right) \right]$$
$$+ g_{12} \int d\mathbf{r} \left(\bar{\Psi}_2^\dagger \bar{\Psi}_2 n_{c1} + \bar{\Psi}_1^\dagger \bar{\Psi}_1 n_{c2} \right), \tag{2.8c}$$

$$\hat{H}_3 = \sum_{j=1}^{2} g_j \int d\mathbf{r} \left(\Phi_j \bar{\Psi}_j^\dagger \bar{\Psi}_j^\dagger \bar{\Psi}_j + \Phi_j^* \bar{\Psi}_j^\dagger \bar{\Psi}_j \bar{\Psi}_j \right)$$
$$+ g_{12} \int d\mathbf{r} \left(\Phi_1 \bar{\Psi}_2^\dagger \bar{\Psi}_2 \bar{\Psi}_1^\dagger \Phi_1^* \bar{\Psi}_2^\dagger \bar{\Psi}_2 \bar{\Psi}_1 + \Phi_2 \bar{\Psi}_2^\dagger \bar{\Psi}_1^\dagger \bar{\Psi}_1 + \Phi_2^* \bar{\Psi}_2 \bar{\Psi}_1^\dagger \bar{\Psi}_1 \right), \tag{2.8d}$$

$$\hat{H}_4 = \frac{1}{2} \sum_{j=1}^{2} g_j \int d\mathbf{r} \bar{\Psi}_j^\dagger \bar{\Psi}_j^\dagger \bar{\Psi}_j \bar{\Psi}_j + g_{12} \int d\mathbf{r} \bar{\Psi}_1^\dagger \bar{\Psi}_2^\dagger \bar{\Psi}_2 \bar{\Psi}_1, \tag{2.8e}$$

where $n_{cj} = |\Phi_j|^2$ is the condensed density of each component.

At zero temperature $T = 0$, almost all of the particles are in the condensate state, hence the noncondensed operator can be neglected ($\hat{\bar{\psi}}_j = 0$), and only the zeroth order $H^{(0)}$ term can be taken into account in equation (2.7). Therefore, the ground state of the system can be described by the following two coupled GP equations for the condensate wavefunctions $\Phi_j(\mathbf{r}, t)$ which can be derived through

$$i\hbar \frac{d\Phi_j}{dt} = \frac{d\mathcal{E}}{d\Phi_j^*}, \tag{2.9}$$

14
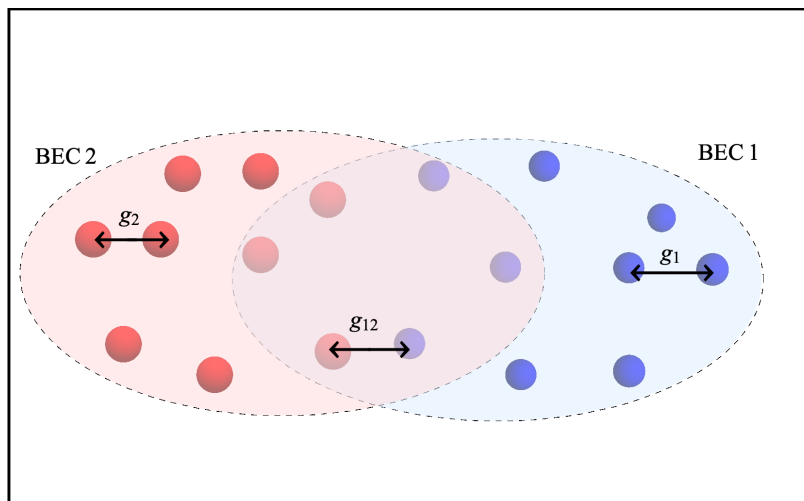
Figure 2.1: Schematic representation of a two-component BEC.

where

$$\mathcal{E} = \langle \hat{H} \rangle = \sum_{j=1}^{2} \int d\mathbf{r} \left(\Phi_j^* h_j^{sp} \Phi_j + \frac{g_j}{2} n_j^2 \right) + g_{12} \int d\mathbf{r} \, n_1 n_2, \qquad (2.10)$$

is the zero-temperature energy.

Inserting the energy (2.10) into equation (2.9), we get

$$i\hbar \frac{\partial \Phi_j(\mathbf{r}, t)}{\partial t} = \left[\frac{-\hbar^2}{2m} \nabla^2 + U(\mathbf{r}) + g_j |\Phi_j(\mathbf{r}, t)|^2 + g_{12} |\Phi_{3-j}(\mathbf{r}, t)|^2 \right] \Phi_j(\mathbf{r}, t). \qquad (2.11)$$

The GP equations (2.11) have widely employed to analyz the ground-state properties, collective excitations, phase transitions and topological defects of binary Bose mixtures at zero temperature (see for books and review [10, 11, 12]). Nevertheless, the GP equation is valid if the following criteria are satisfied:

1. The system is in the weakly interacting regime ($n_j a_j^3 \ll 1$) and at very low temperatures. Quantum and thermal depletion of the condensate are negligibly small.

2. The size of the system is much larger than the characteristic length scale given by the scattering length.

Note that GP equations (2.11) can also be derived in the framework of the Heisenberg picture in which the equation of motion of a general operator $\hat{\Psi}$ can be shown to obey $i\hbar \partial \hat{\Psi}_j / \partial t = [\hat{\Psi}, \hat{H}]$.

To go beyond the zero temperature discussion, we must additionally include the remaining contributions $\left(\hat{H}_3 + \hat{H}_4 \right)$ of equations (2.8) to the system Hamiltonian, one may use Wick's theorem for the noncondensate operators [9], which states that at equilibrium, an average over multiple operators can be approximated by sums of averages of pairwise contracted operators, i.e.

$$\left\langle \hat{\tilde{\Psi}}^\dagger \hat{\tilde{\Psi}}^\dagger \hat{\tilde{\Psi}} \hat{\Psi} \right\rangle = \left\langle \hat{\tilde{\Psi}}^\dagger \hat{\tilde{\Psi}}^\dagger \right\rangle \langle \hat{\Psi} \hat{\Psi} \rangle + 2 \langle \hat{\tilde{\Psi}}^\dagger \hat{\tilde{\Psi}} \rangle \langle \hat{\tilde{\Psi}}^\dagger \hat{\tilde{\Psi}} \rangle. \tag{2.12}$$

The above approximation maintains correlations of non-condensate operators only to quadratic order. One may thus also wish to approximate products of three noncondensate operators appearing in $\hat{H}_3$ by their corresponding quadratic form,

$$\begin{aligned}
\hat{\tilde{\Psi}}^\dagger \hat{\tilde{\Psi}}^\dagger \hat{\tilde{\Psi}} &= \left\langle \hat{\tilde{\Psi}}^\dagger \hat{\tilde{\Psi}}^\dagger \right\rangle \hat{\tilde{\Psi}} + 2 \hat{\tilde{\Psi}}^\dagger \langle \hat{\tilde{\Psi}}^\dagger \hat{\tilde{\Psi}} \rangle, \\
\hat{\tilde{\Psi}}^\dagger \hat{\tilde{\Psi}} \hat{\Psi} &= 2 \langle \hat{\tilde{\Psi}}^\dagger \hat{\tilde{\Psi}} \rangle \hat{\tilde{\Psi}} + \langle \hat{\Psi} \hat{\Psi} \rangle \hat{\tilde{\Psi}}^\dagger.
\end{aligned} \tag{2.13}$$

Since by construction $\langle \hat{\tilde{\Psi}} \rangle = \left\langle \hat{\tilde{\Psi}}^\dagger \right\rangle = 0$, the approximation of equation (2.13) implies that $\langle \hat{\tilde{\Psi}}^+ \hat{\tilde{\Psi}}^\dagger \hat{\tilde{\Psi}} \rangle = 0$. Therefore, the Hamiltonian (2.7) reduces to

$$\begin{aligned}
\hat{H} = \sum_{j=1}^{2} \int d\mathbf{r} \Bigg\{ &\Phi_j^* (h_j^{sp} + \frac{g_j}{2} n_{cj}) \Phi_j + \hat{\tilde{\Psi}}_j^\dagger \left(h_j^{sp} + 2 g_j n_j \right) \hat{\tilde{\Psi}}_j \\
&+ \frac{g_j}{2} \left[(\tilde{m}_j^* + \Phi_j^{*2}) \hat{\tilde{\Psi}}_j \hat{\tilde{\Psi}}_j + (\tilde{m}_j + \Phi_j^2) \hat{\tilde{\Psi}}_j^+ \hat{\tilde{\Psi}}_j^\dagger \right] \Bigg\} + g_{12} n_1 n_2,
\end{aligned} \tag{2.14}$$

16

where $\tilde{n}_j = \langle \hat{\tilde{\Psi}}_j^+ \hat{\tilde{\Psi}}_j \rangle$ is the noncondensed density and $\tilde{m} = \langle \hat{\tilde{\Psi}} \hat{\tilde{\Psi}} \rangle$ is often referred to as the pair anomalous average. The total density is given by $n_j = n_{cj} + \tilde{n}_j$.

The energy functional corresponding to the Hamiltonian (2.14) reads

$$
\mathcal{E} = \sum_{j=1}^{2} \left[\int d\mathbf{r} \left(\Phi_j^* h_j^{sp} \Phi_j + \hat{\tilde{\psi}}_j^\dagger h_j^{sp} \hat{\tilde{\psi}}_j \right) + \frac{g_j}{2} \int d\mathbf{r} \left(n_{cj}^2 + 4\tilde{n}_j n_{cj} + 2\tilde{n}_j^2 + |\tilde{m}_j|^2 \right. \right.
$$
$$
\left. \left. + \tilde{m}_j^* \Phi_j^2 + \tilde{m}_j \Phi_j^{*2} \right) \right] + g_{12} \int d\mathbf{r} \left(n_{c1} + \tilde{n}_1 \right) \left(n_{c2} + \tilde{n}_2 \right). \tag{2.15}
$$

Upon introducing the expression (2.15) into equations (2.9), one obtains the explicit extended coupled GP equations which govern the dynamics of binary BECs

$$
i\hbar \frac{d\Phi_j}{dt} = \left(h_j^{sp} + g_j n_j + g_{12} n_{3-j} + \delta\mu_{j\mathrm{LHY}} \right) \Phi_j, \tag{2.16}
$$

where

$$
\delta\mu_{j\mathrm{LHY}}(\mathbf{r})\Phi_j(\mathbf{r}) = g_j \left[\tilde{n}_j(\mathbf{r})\Phi_j(\mathbf{r}) + \tilde{m}_j(\mathbf{r})\Phi_j^*(\mathbf{r}) \right], \tag{2.17}
$$

is the relevant LHY term which can be calculated without any *ad-hoc* assumptions in contrast to the standard GGP equation of [44] due to the presence of the noncondensed and anomalous fluctuations. For $\tilde{n}_j = \tilde{m}_j = 0$, the GGP equations (2.16) reduce to the coupled GP equations (2.11).

Indeed, the HFB approximation, runs into trouble. The first problem is the destruction of the gaplessness of the HFB theory due to the inclusion of the anomalous density signaling that the theory does not satisfy the Hugenholtz-Pines theorem [126]. Secondly, the anomalous pair average which in general leads to a double counting of the interaction effects is ultraviolet divergent [127]. Physically this comes from the contact interaction potential, which treats collisions of different momenta with the same probability. The simplest way in calculation for trapped gases has been to neglect $\tilde{m}_j = 0$ in the above equations, which restores the symmetry and hence leads to

a gapless theory. This is often known as the Popov approximation [9] which unfortunately negelects many-body effects in the treatment of all interatomic interactions.

To go beyond Popov scheme and to self-consistently reinstate the gaplessness of the spectrum, one should renormalize the intraspecies coupling constants g_j following the procedure outlined in Refs.[9, 13, 128] for a single BEC. This gives

$$\bar{g}_j = g_j(1 + \tilde{m}_j/\phi_j^2). \tag{2.18}$$

The form of this equation is equivalent to the low momentum limit of the many-body T-matrix for a homogeneous system [128].

Despite the dilute nature of the system, the spatially dependent effective interaction $\bar{g}_j$ (2.18) may modify the static and the dynamics of the mixture. Furthermore, $\bar{g}_j$ have substantial implications for the stability condition. Hence, the renormalized extended coupled GP equations take the form:

$$i\hbar \frac{d\Phi_j}{dt} = \left[h_j^{sp} + \bar{g}_j n_{cj} + 2g_j \tilde{n}_j + g_{12} n_{3-j} \right] \Phi_j. \tag{2.19}$$

It is easy to check that equations (2.19) satisfy the energy and number conserving laws.

The static solutions can be readily determined via the transformation: $\Phi_j(\mathbf{r}, t) = \Phi_j(\mathbf{r}) \exp(-i\mu_j t/\hbar)$, where μ_j are chemical potentials related with each components. Substituting this transformation into (2.19) yields the time-independent GP equations:

$$\mu_j \Phi_j = \left[h_j^{sp} + \bar{g}_j n_{cj} + 2g_j \tilde{n}_j + g_{12} n_{3-j} \right] \Phi_j. \tag{2.20}$$

Here μ_j must be calculated self-consistently employing the normalization condition $N_j = \int n_j d\mathbf{r}$, where $N_j = N_{cj} + \tilde{N}_j$ is the single condensate total number of par-

ticles with $N_{cj} = \int n_{cj} d\mathbf{r}$ and $\tilde{N}_j = \int \tilde{n}_j d\mathbf{r}$ being respectively, the condensed and noncondensed number of particles in each component.

2.3   Miscible, immiscible and collapse mixture

As a starting point, it is useful to establish the stability condition. Working in the Thomas-Fermi (TF) approximation which consists in neglecting the kinetic terms in equations (2.19a) and (2.19b) and valid for large number of particles. The resulting equations for the condensed density distributions n_{c1} and n_{c2} are given by:

$$n_{c1} = \frac{\Delta}{\bar{g}_1(\Delta - 1)} \left[\mu_1 - U_1 - 2g_1\tilde{n}_1 - g_{12}\tilde{n}_2 - \frac{g_{12}}{\bar{g}_2} \left(\mu_2 - U_2 - 2g_2\tilde{n}_2 - g_{12}\tilde{n}_1 \right) \right],$$

$$(2.21)$$

$$n_{c2} = \frac{\Delta}{\bar{g}_2(\Delta - 1)} \left[\mu_2 - U_2 - 2g_2\tilde{n}_2 - g_{12}\tilde{n}_1 - \frac{g_{12}}{\bar{g}_1} \left(\mu_1 - U_1 - 2g_1\tilde{n}_1 - g_{12}\tilde{n}_2 \right) \right],$$

$$(2.22)$$

where $\Delta = \bar{g}_1\bar{g}_2/g_{12}^2$ is often known as the miscibility parameter. In our case the mixture can be miscible if $\Delta > 1$ or immiscible when $\Delta < 1$. The transition between the two regimes was previously observed in Bose-Bose mixtures in different spin states [129, 130], Bose-Bose mixtures of two Rb isotopes [23], and in heteronuclear Bose-Fermi mixtures [131, 132]. If $g_{12} = 0$ and one component vanishes (say $n_1 = 0$) in a certain space region, equations (2.21) and (2.22) simplify to the one-component TF equation, namely $n_{c2} = (\mu_2 - U_2 - 2g_2\tilde{n}_2)/\bar{g}_2$. For $\tilde{n}_j = \tilde{m}_j = 0$, they reduce to the usual TF equations at zero temperature. Inspection of equations (2.21) and (2.22) suggests that the stability of the mixture merely requires the conditions:

$$\bar{g}_1 > 0, \quad \bar{g}_2 > 0, \quad \text{and} \quad \Delta > 1. \tag{2.23}$$

In the limit $\tilde{m}_j/n_{cj} \ll 1$, the conditions (2.23) reduce to the standard stability conditions at zero temperature namely $g_1 g_2 > g_{12}^2$. For $\tilde{m}_j/n_{cj} > 1$, the system becomes strongly correlated. This means that at finite temperature, the stability criterion of the mixture requires the inequality $-1 < \tilde{m}_j/n_{cj} < 1$. If $\Delta < 1$ and $g_{12} < 0$, the gas is unstable whereas, for $g_{12} > 0$, the two components do not overlap with each other (separated solutions). One of the most important feature arising from our formula (2.23) is that when $\tilde{m}_j$ is large, the mixture undergoes a transition from miscible to immiscible phase.
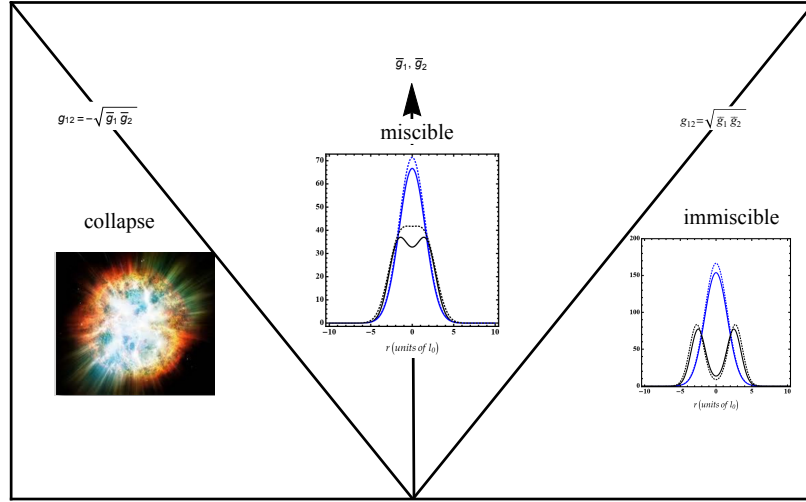
Figure 2.2: Phase diagram of a Bose-Bose mixture. The horizontal axis represents the renormalized interspecies scattering length, the vertical axis represents the intraspecies interactions on each condensate. Three different regimes are observed: miscibility, immisicbility and collapse. The miscible phase is bounded from the right and the left by the condition $|g_{12}| = \sqrt{\bar{g}_1 \bar{g}_2}$.

2.4 Collective excitations

The calculation of the elementary excitations and quantum fluctuations for Bose mixtures amounts to solving the Bogoluibov-de-Gennes equations. To do so, we linearize Eqs.(2.19) using the random-phase approximation (RPA) which consists of imposing small fluctuations of the condensates as:

$$\Phi_j(\mathbf{r}, t) = [\Phi_{0j}(\mathbf{r}) + \delta\Phi_j(\mathbf{r}, t)] \exp(-i\mu_j t/\hbar), \qquad (2.24)$$

where $\delta\Phi_j(\mathbf{r}, t) \ll \Phi_{0j}$ are small quantum fluctuations. Substituting Eq.(2.24) into Eqs.(2.19), we then obtain up to zeroth-order

$$\mu_j\Phi_{0j}(\mathbf{r}) = \left[h_j^{sp} + \bar{g}_j n_{cj} + 2g_j\tilde{n}_j + g_{12}n_{3-j}\right]\Phi_{0j}(\mathbf{r}). \qquad (2.25)$$

The first-order terms yield the HFB-RPA equations:

$$i\hbar\frac{\partial\delta\Phi_j}{\partial t} = \left[h_j^{sp} + 2\bar{g}_j n_{cj} + 2g_j\tilde{n}_j + g_{12}n_{3-j}\right]\delta\Phi_j + \bar{g}_j\Phi_{0j}^2\delta\Phi_j^*$$

$$+ g_{12}\Phi_{03-j}^*\Phi_{0j}\delta\Phi_{3-j} + g_{12}\Phi_{03-j}\Phi_{0j}\delta\Phi_{3-j}^*. \qquad (2.26)$$

Remarkably, equations (2.26) contain only the terms which describe the coupling to the condensate since all terms associated with fluctuations $\delta\tilde{n}$ and $\delta\tilde{m}$ are assumed to be not important [133]. In fact, this assumption is relevant to ensure the gaplessness of the spectrum. The obtained HFB-RPA equations can be regarded as a natural extension of those developed for a single component BEC [134]. If one neglects the anomalous density, equations (2.26) reduce to the Popov-RPA equations.

Writting the field fluctuations associated with the condensate in the form

$$\delta\Phi_j(\mathbf{r}, t) = \left[u_{kj}(\mathbf{r})e^{-i\varepsilon_k t/\hbar} + v_{kj}(\mathbf{r})e^{i\varepsilon_k t/\hbar}\right]e^{-i\mu_j t}, \qquad (2.27)$$

21

where ε_k is the Bogoliubov excitation energy, and $u_{kj}(\mathbf{r})$ and $v_{kj}(\mathbf{r})$ are the Bogoliubov quasiparticle functions constitute an orthonormal and complete set of functions with the relations $\int d\mathbf{r}\left[u_{kj}^2(\mathbf{r}) - v_{kj}^2(\mathbf{r})\right] = 1$. Upon introducing equation (2.27) into (2.26), we find for the second-order coupled HFB-de Gennes equations [135]:

$$
\begin{pmatrix}
\hat{\mathcal{L}}_j & \mathcal{M}_j & \mathcal{A}_j & \mathcal{B}_j \\
\mathcal{M}_j & \hat{\mathcal{L}}_j & \mathcal{B}_j & \mathcal{A}_j \\
\mathcal{A}_j & \mathcal{B}_j & \hat{\mathcal{L}}_j & \mathcal{M}_j \\
\mathcal{B}_j & \mathcal{A}_j & \mathcal{M}_j & \hat{\mathcal{L}}_j
\end{pmatrix}
\begin{pmatrix}
u_{jk}(\mathbf{r}) \\
v_{jk}(\mathbf{r}) \\
u_{(3-j)k}(\mathbf{r}) \\
v_{(3-j)k}(\mathbf{r})
\end{pmatrix}
= \varepsilon_k
\begin{pmatrix}
u_{jk}(\mathbf{r}) \\
-v_{jk}(\mathbf{r}) \\
u_{(3-j)k}(\mathbf{r}) \\
-v_{(3-j)k}(\mathbf{r})
\end{pmatrix},
\qquad (2.28)
$$

where $\hat{\mathcal{L}}_j = \hat{h}_j^{sp} + 2\bar{g}_j n_{cj} + 2g_j \tilde{n}_j + g_{12} n_{3-j} - \mu_j$, $\mathcal{M}_j = \bar{g}_j \Phi_{0j}^2$, $\mathcal{A}_j = g_{12}\Phi_{03-j}^*\Phi_{0j}$, and $\mathcal{B}_j = g_{12}\Phi_{03-j}\Phi_{0j}$. The solutions of full HFB-de Gennes equations for trapped Bose mixtures can be obtained numerically.

The thermal cloud and the anomalous density can be determined in terms of the quasiparticle amplitudes, $u_{jk}(\mathbf{r})$, $v_{jk}(\mathbf{r})$, and quasiparticle energies ε_{jk} via the transformation :

$$
\hat{\bar{\psi}}_j(\mathbf{r}) = \sum_k [u_{jk}(\mathbf{r})\hat{b}_{jk} + v_{jk}(\mathbf{r})\hat{b}_{jk}^\dagger].
\qquad (2.29)
$$

This gives

$$
\tilde{n}_j(\mathbf{r}) = \left\langle \hat{\bar{\psi}}_j^\dagger(\mathbf{r})\hat{\bar{\psi}}_j(\mathbf{r}) \right\rangle = \sum_k \left[v_{jk}^2(\mathbf{r}) + \left(u_{jk}^2(\mathbf{r}) + v_{jk}^2(\mathbf{r})\right) N_{jk} \right],
\qquad (2.30)
$$

and

$$
\tilde{m}_j = -\langle \hat{\bar{\psi}}_j(\mathbf{r})\hat{\bar{\psi}}_j(\mathbf{r})\rangle = -\sum_k \left[u_{jk}(\mathbf{r})v_{jk}(\mathbf{r})\left(2N_{jk} + 1\right) \right],
\qquad (2.31)
$$

where $N_{jk} = \left[\exp\left(\varepsilon_{jk}/T\right) - 1\right]^{-1}$ are occupation numbers for the excitations. The renormalization (2.18) renders the GP equations (2.16) gapless but leaves the anomalous density divergent. So, one has to renormalize the anomalous density to remove

this ultraviolet divergence. This can be seen, in a homogeneous mixtures (section 2.5).

Equations (2.19), (2.30) and (2.31) are appealing since they permit us to study the density profiles, the collective excitations, and the behavior of the thermal cloud and the pair anomalous density of Bose-Bose atomic mixtures at any temperature.

For the remainder of the thesis we turn our attention to the homogeneous Bose mixture.

2.5   Homogeneous mixtures

We concentrate here on the elementary excitations of a homogeneous mixed Bose gas, where $V_j(\mathbf{r}) = 0$. Keep in mind that the wavefunctions are real-valued i.e. $\Phi_{0j} = \Phi_{0j}^* = \sqrt{n_{cj}}$, and $\Phi_{0\,3-j} = \Phi_{0\,3-j}^* = \sqrt{n_{c3-j}}$ and the $u_{jk}(\mathbf{r}) = u_{jk}e^{i\mathbf{k}\cdot\mathbf{r}}$ and $v_{jk}(\mathbf{r}) = v_{jk}e^{i\mathbf{k}\cdot\mathbf{r}}$. Within this, the chemical potentials turn out to be given as

$$\mu_j = \bar{g}_j n_{cj} + 2g_j \tilde{n}_j + g_{12} n_{3-j}. \tag{2.32}$$

Inserting equation (2.32) into (2.28), we obtain the second-order coupled HFB-Bogoluibov-de-Gennes equations for uniform Bose mixtures :

$$\varepsilon_k u_{jk} = \left(E_{kj} + 2\bar{g}_j|\Phi_j|^2 + 2g_j\tilde{n}_j\right)u_{jk} + g_j n_j v_{jk} + g_{12}\sqrt{n_j n_{3-j}}(u_{jk} + v_{jk}), \tag{2.33}$$

$$-\varepsilon_k v_{jk} = \left(E_{kj} + 2\bar{g}_j|\Phi_j|^2 + 2g_j\tilde{n}_j\right)v_{jk} + g_j n_j u_{jk} + g_{12}\sqrt{n_j n_{3-j}}(u_{jk} + v_{jk}), \tag{2.34}$$

where $E_{kj} = \hbar^2 k^2/2m_j$ is the free-particle energy. For $g_{12} = 0$, equations (2.33) and (2.34) coincide with the finite temperature second-order equations obtained by Shi and Griffin using diagrammatic methods [9] and with the finite temperature time-dependent mean-field scheme proposed by Giorgini [133]. At zero temperature they

correspond to the well-known second-order Beliaev's results [136] discussed in a single component Bose condensed gas over six decades ago, while at high temperature our second-order coupled HFB-de Gennes equations reproduce those derived by Fedichev and Shlyapnikov [137] employing Green's function perturbation scheme.

The solution of the above HFB-Bogoluibov-de-Gennes equations (2.33) and (2.34) leads for the Bogoliubov quasiparticle amplitudes:

$$u_{kj}, v_{kj} = \frac{1}{2} \left(\sqrt{\frac{\varepsilon_{k\pm}}{E_{kj}}} \pm \sqrt{\frac{E_{kj}}{\varepsilon_{kj}}} \right). \tag{2.35}$$

Once these quantities have been determined, the gapless Bogoliubov excitations spectrum composed of two branches are obtained from the following expressions:

$$\varepsilon_{k\pm}^2 = \frac{1}{2} \left(\varepsilon_{k1}^2 + \varepsilon_{k2}^2 \right) \pm \sqrt{\frac{1}{4} \left(\varepsilon_{k1}^2 - \varepsilon_{k2}^2 \right)^2 + 16 E_{k1} E_{k2} g_{12}^2 n_{c1} n_{c2}}, \tag{2.36}$$

where $\varepsilon_{kj} = \sqrt{E_{kj}^2 + 2 E_{kj} \bar{g}_j n_{cj}}$ are the Bogoliubov spectra for the individual components. The presence of the interspecies interactions g_{12} gives rise to hybridize the two Bogoliubov modes namely : the highest energy branch ε_{k+}, known as the hard mode, corresponds to the spin excitations and lowest energy branch ε_{k-} is known as the soft branch and corresponds to the density excitations [12]. For $m_1 = m_2$ and for a trivial case, such as $g_{12} = 0$, the two excitation branches (2.36) take the form of the usual single-component Bogoliubov spectrum. Obviously for $\tilde{n} = \tilde{m} = 0$, we recover the standard spectra describing Bose mixtures without quantum fluctuations [98].

In the limit $k \to 0$, we have $\varepsilon_{kj} = \hbar c_j k$ where $c_j = \sqrt{\bar{g}_j n_{cj}/m_j}$ is the sound velocity of a single condensate. The total dispersion is phonon-like in this limit

$$\varepsilon_{k\pm} = \hbar c_\pm k, \tag{2.37}$$

24

where the sound velocities $c_\pm$ are

$$c_\pm^2 = \frac{1}{2}\left[c_1^2 + c_2^2 \pm \sqrt{(c_1^2 - c_2^2)^2 + 4\Delta^{-1}c_1^2 c_2^2}\right].$$ (2.38)

Remarkably, the sound velocity $c_\pm \to 0$ as $T \to T_c$ since $n_{cj} = \tilde{m}_j = 0$ near the transition, which means that the phonons in the HFB theory are the soft modes of the Bose-condensed mixture. For $g_{12}^2 > \bar{g}_1 \bar{g}_2$, the spectrum (2.49) becomes unstable and thus, the two condensates spatially separate. As we will see in the next chapters, if this mechanical instability is counterbalanced, it could lead to the formation of self-bound solutions.

2.6 Quantum and thermal fluctuations

Inserting the definitions (2.35) into equations (2.30) and (2.31), and using the identity $2N(x)+1 = \coth(x/2)$, we can rewrite the condensate depletion and the anomalous in terms of parameter $I_{k\pm} = \coth^2(\varepsilon_{k\pm}/2T)$ which represents the variance of the number of noncondensed particles [13, 37]

$$\tilde{n}_\pm = \frac{1}{2}\int \frac{d\mathbf{k}}{(2\pi)^3}\left[\frac{E_k + \mu_\pm}{\varepsilon_{k\pm}}\sqrt{I_{k\pm}} - 1\right],$$ (2.39)

and

$$\tilde{m}_\pm = -\frac{1}{2}\int \frac{d\mathbf{k}}{(2\pi)^3}\frac{\mu_\pm}{\varepsilon_{k\pm}}\sqrt{I_{k\pm}}.$$ (2.40)

If one uses this integral directly by summing over all states, we find that the anomalous density suffers from the ultraviolet divergence from large k contributions. This difficulty is due to the use of short-range contact potential which is valid only for

small momenta. To circumvent this problem, we should renormalize the coupling constants and introduce the Beliaev-type second-order corrections [136, 74]

$$g_j(\mathbf{k}) = g_j + g_j^2 \int \frac{d\mathbf{k}}{(2\pi)^3} \frac{1}{2E_k}, \quad \text{and} \quad g_{12}(\mathbf{k}) = g_{12} + g_{12}^2 \int \frac{d\mathbf{k}}{(2\pi)^3} \frac{1}{2E_k}. \tag{2.41}$$

After the subtraction of the ultraviolet divergent part, the renormalized anomalous density takes the form:

$$\tilde{m} = -\int \frac{d\mathbf{k}}{(2\pi)^3} \left[\frac{1}{\varepsilon_k} - \frac{n_j^2 g_j^2}{2E_k} - \frac{n_1 n_2 g_{12}^2}{2E_k} \right]. \tag{2.42}$$

The HFB equations (2.39) and (2.40) are coupled with an useful equation linking the normal and anomalous densities [37, 119]

$$I_\pm = (2\tilde{n}_\pm + 1)^2 - 4|\tilde{m}_\pm|^2. \tag{2.43}$$

For a noninteracting Bose gas where the anomalous density vanishes, $I_{kj} = \coth^2(E_{kj}/2T)$. Equation (2.43) clearly shows that the anomalous density is not negligible even at zero temperature $(I \to 1)$, contrary to what has been argued in the literature. Hence, $\tilde{m}$ is crucial for the stability of Bose gases. It also allows us to determine in a very convenient manner the critical temperatures of the mixture.

2.7 Equation of state

The knowledge of the noncondensed and anomalous densities allows one to calculate in useful manner the ground-state energy of the system including the LHY corrections. In the frame of our formalism, it can be written as:

$$E = E_0 + E_{\text{LHY}}, \tag{2.44}$$

where

$$E_0 = \frac{g_j}{2} \sum_j (n_{cj}^2 + 4n_{cj}\tilde{n}_j + 2\tilde{n}_j^2 + |\tilde{m}_j|^2 + 2n_{cj}\tilde{m}_j) + g_{12}n_1 n_2, \qquad (2.45)$$

is the mean-field energy, and

$$E_{\mathrm{LHY}} = \sum_{\mathbf{k}} \sum_{\pm} \varepsilon_{\pm k} v_{\pm k}^2, \qquad (2.46)$$

accounts for the LHY quantum corrections. It is ultraviolet divergent and necessitates to be regularized. Using again the renormalization (2.41), the LHY energy takes the explicit form [44, 98, 37],

$$E_{\mathrm{LHY}} = \frac{1}{2} \sum_{\mathbf{k}} \left[\varepsilon_{+k} + \varepsilon_{-k} - \sum_{j=1}^{2} \left(E_{jk} + g_j n_{cj} - \frac{n_{cj}^2 g_j^2}{2E_{jk}} \right) + n_{c1} n_{c2} g_{12}^2 \sum_{j=1}^{2} \frac{2}{E_{jk}} \right]. \qquad (2.47)$$

The HFB formalism provides also useful expression for the free energy of the system:

$$F = E + T \int \frac{d^d k}{(2\pi)^d} \ln \left(\frac{2}{\sqrt{I_{k\pm}} + 1} \right). \qquad (2.48)$$

The minimization of both E and F with respect to the density permits us to check the existence of the self-bound droplet at zero and finite temperatures, respectively as we shall see in next chapters.

2.8   Homonuclear Bose mixtures

For qualitative estimates, we mainly focus in this section on the case of equal masses $m_1 = m_2 = m$ which experimentally corresponds to a homonuclear mixture. We restrict ourselves to first-order in fluctuations which means that $\tilde{m}_j/n_{cj} \ll 1$ and $\tilde{n}_j/n_{cj} \ll 1$.

The Bogoliubov spectum (2.36) reduces to

$$\varepsilon_{k+} = \sqrt{E_k^2 + 2E_k\mu_+}, \qquad \varepsilon_{k-} = \sqrt{E_k^2 + 2E_k\mu_-}, \tag{2.49}$$

where

$$\mu_\pm = \frac{g_1 n_{c1}}{2} f_\pm(\Delta, \alpha), \tag{2.50}$$

where $f_\pm(\Delta, \alpha) = 1 + \alpha \pm \sqrt{(1-\alpha)^2 + 4\Delta^{-1}\alpha}$ and $\alpha = g_2 n_{c2}/(g_1 n_{c1})$. In figure 2.3 the spin and density branches are sketched. Crossing the stability condition $\Delta < 1$, the density branche becomes imaginary meaning that a mechanical instability is occured.
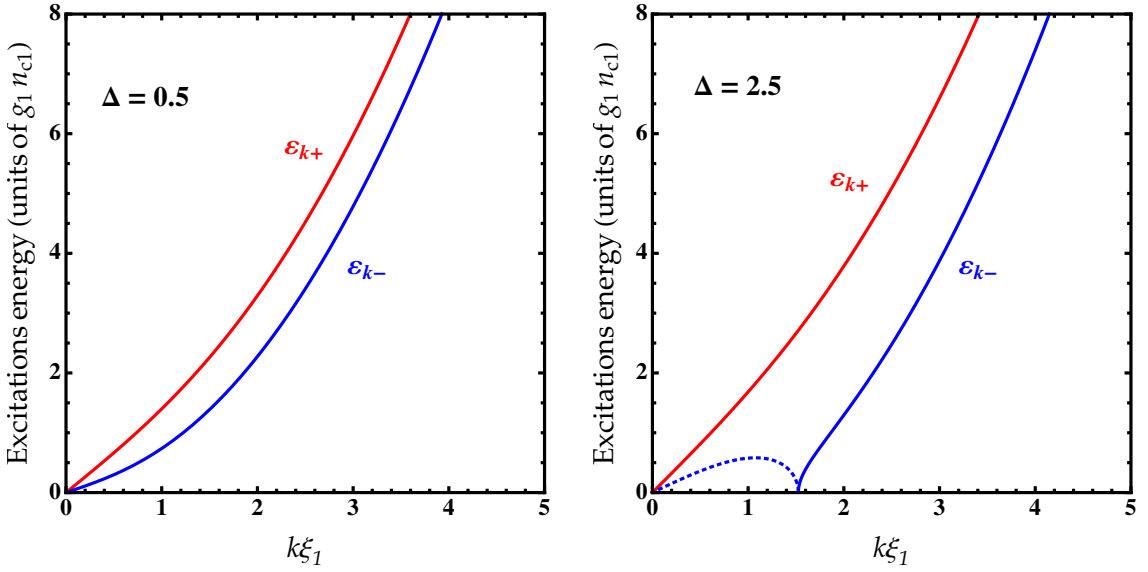
Figure 2.3: Excitation spectra $\varepsilon_{k\pm}$ from (2.49) as a function of $k\xi_1$ for $\alpha = 1$. Here $\xi = \hbar/\sqrt{mn_1 g_1}$ is the healing length associated to first component.

At $T = 0$, the total depletion $\tilde{n} = \tilde{n}_1 + \tilde{n}_2$ can be calculated via the integral (2.39) [37]

$$\tilde{n} = \frac{2\sqrt{2}}{3} n_{c1} \sqrt{\frac{n_{c1} a_1^3}{\pi}} \sum_\pm f_\pm^{3/2}(\Delta, \alpha). \tag{2.51}$$

28

For $\tilde{m}_1 = \tilde{n}_1 = 0$ the depletion (2.51) is formally similar to that obtained by Tommasini et al. [34] using the Bogoliubov theory. For $g_{12} = 0$, one recovers the results of a single component BEC, $\tilde{n}_1^0 = (8/3)n_{c1}\sqrt{n_{c1}a_1^3/\pi}$. The noncondensed fraction is proportional to Δ and α signaling that the number of excited atoms increases with Δ and α as displayed in figure 2.4.

After renomalization, the integration over k of equation (2.42) becomes trivial and we finally obtain the following formula for the total anomalous density [37] $\tilde{m} = \tilde{m}_1 + \tilde{m}_2$:

$$\tilde{m} = 2\sqrt{2}\,n_{c1}\sqrt{\frac{n_{c1}a_1^3}{\pi}}\sum_{\pm} f_{\pm}^{3/2}(\Delta, \alpha). \tag{2.52}$$

In the absence of the interspecies interactions equation (2.52) reduces to $\tilde{m}_1^0 = 8n_{c1}\sqrt{n_{c1}a_1^3/\pi}$ which is the anomalous density of an individual BEC [13]. As anticipated above, equation (2.52) shows that $\tilde{m}$ is larger than $\tilde{n}$ similarly to the case of a single component. This indicates that the anomalous density is significant even at zero temperature in Bose-Bose mixtures. We see also from equation (2.52) that $\tilde{m}$ is increasing with Δ. If the interspecies and intraspecies interactions were strong enough, the pair anomalous density becomes important results in a large fraction of the total atoms would occupy the excited states.

One should stress that the same results (2.52) can be found using the dimensional regularization [13, 138, 139, 140] which follows from perturbation theory of scattering. It gives asymptotically exact results at weak interactions and in the limit $\tilde{m}_j/n_c \ll 1$ (for more details, see Appendix A of [13]).

At temperatures $T \ll g_1 n_{c1}$, the main contribution to integrals (2.39) and (2.40) comes from the long-wavelength region where the Bogoliubov the excitations (2.49)
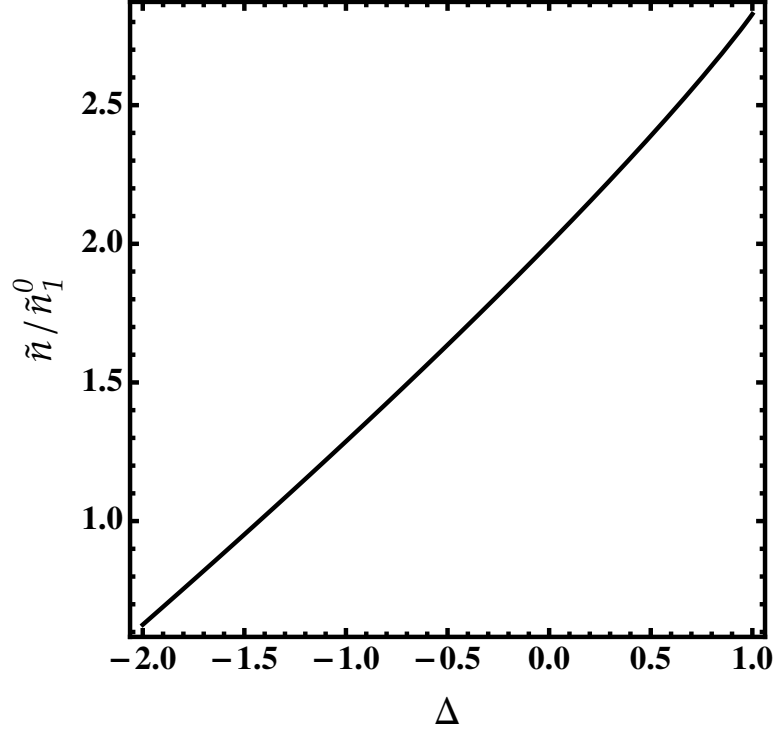
Figure 2.4: Condensate depletion from equation (2.51) as a function of Δ for $\alpha = 1$ and $n_{c1}a^3 = 0.001$.

are sound waves. Then the use of the integral $\int_0^\infty x^{2j-1}[\coth(\alpha x)-1]dx = \pi^{2j} \left| B_{2j} \right| /2j\alpha^{2j}$[58], where B_{2j} are the Bernoulli number, allows us to obtain the following expressions for the thermal contribution of the noncondensed and anomalous densities [37]:

$$\tilde{n}_{th} = |\tilde{m}_{th}| = \frac{2\sqrt{2}}{3}n_{c1}\sqrt{\frac{n_{c1}a^3}{\pi}} \left(\frac{\pi T}{n_{c1}g_1} \right)^2 \sum_{\pm} f_{\pm}^{-1/2}(\Delta, \alpha). \qquad (2.53)$$

Equation (2.53) shows clearly that $\tilde{n}$ and $\tilde{m}$ are of the same order of magnitude at low temperature and only their signs are opposite. A comparaison between equations (2.51), (2.52) and (2.53) shows that at $T \ll g_j n_{cj}$, thermal fluctuations are smaller than the quantum fluctuations.

Notice that, at $T \gg g_j n_{cj}$ where the main contribution to integrals (2.39) and

30

(2.40) comes from the single particle excitations, there is copious evidence that $\tilde{n}_j$ become identical to the noncondensed density of an ideal Bose gas. This implies that corrections to all thermodynamic quantities are closer to the values obtained for an ideal Bose gas. However, the anomalous density being proportional to the condensed density, tend to zero together and hence, their contributions become negligeably small [13, 141, 9].

Under the above assumptions ($\tilde{m}_j/n_{cj} \ll 1$ and $\tilde{n}_j/n_{cj} \ll 1$), the mean-field energy (2.45) becomes

$$E_0 = (g_j/2) \sum_j n_{cj}^2 + g_{12} n_1 n_2. \tag{2.54}$$

The corrections to the ground-state energy can be computed through (2.47). This gives [37]:

$$\frac{E_{\mathrm{LHY}}}{V} = \frac{16 g_1 \sqrt{a_1^3/\pi}}{15\sqrt{2}} n_{c1}^{5/2} \sum_{\pm} f_{\pm}^{5/2}(\Delta, \alpha). \tag{2.55}$$

This is the well-known first beyond mean-field correction to the ground-state energy, the so-called LHY energy derived by Lee, Huang and Yang in the 50's [45]. The origin of such LHY corrections is the zero point motion of the Bogoliubov excitations in the BEC. This is why they are of quantum nature [44]. For $g_{12} = 0$, the energy reduces to that of a single BEC $E_1^0/V = (64/15) g_1 n_{c1}^2 \sqrt{n_{c1} a_1^3/\pi}$. For $n \approx n_c$ and $g_{12} = 0$, the LHY energy is proportional to $(gn)^{5/2}$, and thus for small gas parameters $na^3 \ll 1$, the LHY energy is really small.

At temperatures $T \ll g_1 n_{c1}$ where the main contribution to equation (6.13) comes from the phonon region, the evaluation of the thermal contribution of the free energy
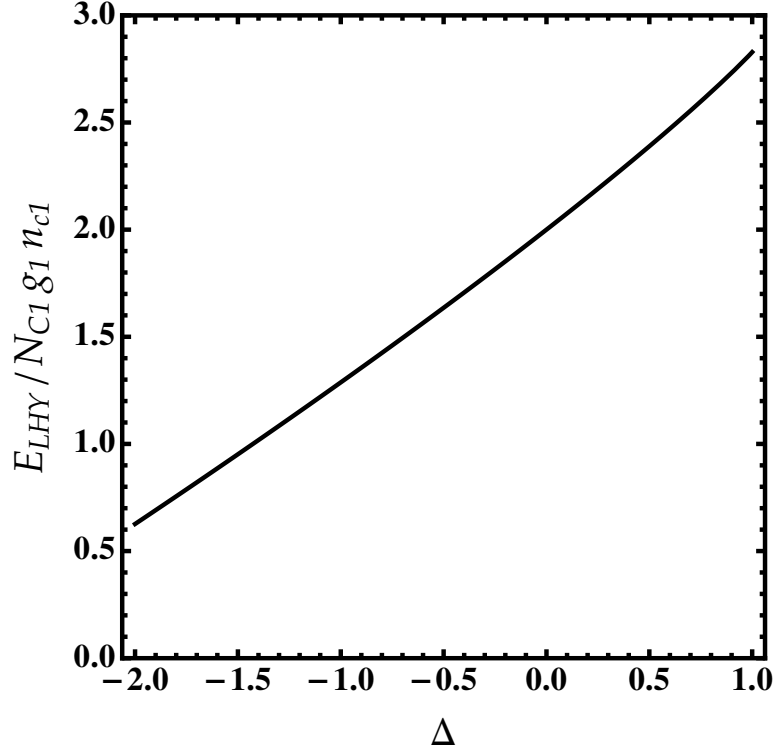
Figure 2.5: LHY-corrected energy from Eq.(2.55) as a function of Δ for $\alpha = 1$ and $n_c a^3 = 0.001$.

yields the famous T^4-law [37]

$$\frac{F}{V} = \frac{E}{V} - \frac{16 g_1 \sqrt{a_1^3/\pi}}{15\sqrt{2}} n_{c1}^{5/2} \sum_{\pm} \left[\frac{1}{2\sqrt{2}} f_{\pm}^{-3/2}(\Delta, \alpha) \left(\frac{\pi T}{g_1 n_{c1}} \right)^4 \right], \qquad (2.56)$$

here we employed the identity $\int_0^\infty dx x^2 \ln[2/(\coth(x/2) + 1)] = -\pi^4/45$. In the limit of lower density $n \to 0$, the thermal corrections to the free energy (2.56) diverge as $n^{-3/2}$ and vanish at zero temperature. A similar formula has been derived in Ref.[76] using the beyond LHY theory, based on the calculation of second-order terms in the Bogoliubov phonon modes.

In conclusion, the presence of quantum fluctuation in Bose mixtures where the mean-field contribution can be tuned close to zero allows beyond mean-field effects to be appeared. The ground-state of the mixture is modified for $\Delta < 0$, or equivalently

32

$g_{12} < -\sqrt{\bar{g}_1 \bar{g}_2}$ and the collapse at the mean-field level can be halted. This will be explained in detail in next chapters.

Chapter 3

Overview of quantum liquid droplets

3.1 Introduction

Self-bound droplets are ubiquitous in nature and formed through a balance of attractive and repulsive forces. They appear in various systems ranging from classical fluids, such as liquid water in normal conditions, to quantum many-body systems, such as atomic nuclei [142], liquid helium [143], photon fluid (liquid light) [144], dipolar BEC [46, 47, 48] and Bose mixtures [44, 56, 57, 58, 59]. In the case of quantum droplets of ultracold bosonic mixtures, whose stability originates from the interplay between the interspecies attractive mean-field energy and the repulsive beyond mean-field corrections due to the LHY quantum fluctuations. The stabilization mechanism of such an exotic state is based on tuning the interspecies interaction, by means of Feshbach resonances, in order to keep only a weak interspecies attraction which tends to cause

a system to collapse. The quantum LHY repulsion balances the mean-field attraction and stabilizes the system against collapse, the mixture can then exist as a droplet and remain bound even in the absence of an external trapping. Other stabilization mechanisms have been proposed to produce self-bound droplets including three-body correlations [145, 55], and dynamical stabilization using Rabi oscillations between two states [146].

In this chapter we present a brief review of basic theoretical model which is based on the GGP equation, describes the formation of self-bound liquid droplets in an ensemble of bosonic mixtures. The conditions underlying the formation of self-bound states in binary BECs have been introduced. We then focus on the experimental realization of this interesting kind of matter. Finally, we discuss the main properties of the liquid-like droplet and its potential applications.

3.2 Theoretical description

In this section we will use the results previously shown in chapter 2 in the case of a Bose-Bose mixture at zero temperature without higher-order quantum effects i.e. $\bar{g}_j = g_j$.

The regime of interest corresponds to repulsive intraspecies interaction $g_1 > 0$ and $g_2 > 0$ and attractive interspecies interaction $g_{12} < 0$. In such an unstable mixture, the mean-field energy is negative. Thus, it is useful to introduce an effective scattering length for the mixture $\delta a = a_{12} + \sqrt{a_1 a_2}$, or equivalently the quantity

$$\delta g = g_{12} + \sqrt{g_1 g_2}, \tag{3.1}$$

which is becomes negative close to the collapse regime, $\delta g < 0$. This describes the
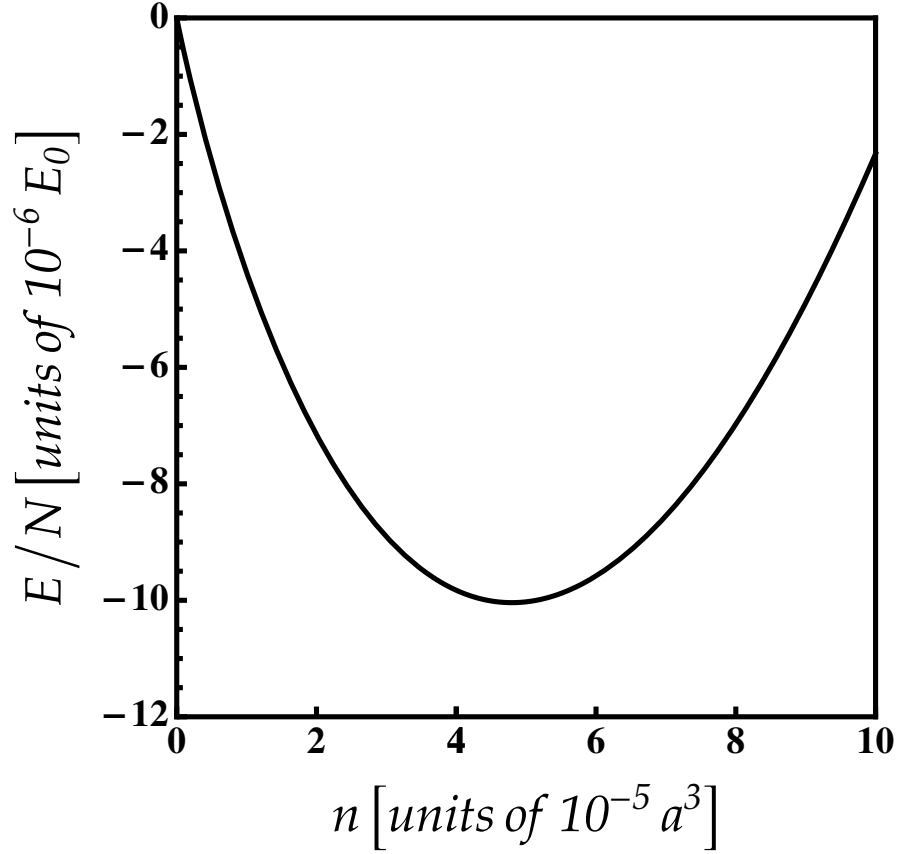
Figure 3.1: Ground-state energy (3.7) as a function of the density for $a_{12}/a_0 = -1.1$.

deviations with respect to g_{12}. We can express the mean-field energy (2.54) in terms of this parameter

$$E_0 = \frac{1}{2} \left(\sqrt{g_1} n_1 - \sqrt{g_2} n_2 \right)^2 + \delta g n_1 n_2. \tag{3.2}$$

Assuming now that the densities of the two clouds satisfy the condition $n_2 = \sqrt{g_1/g_2} n_1 \equiv \sqrt{g_1/g_2} n$, the energy (3.2) becomes

$$E_0 = \delta g \sqrt{g_1/g_2} n^2. \tag{3.3}$$

The LHY energy term for a homonuclear mixture at $T = 0$ can be given from (2.55)

as by setting $\tilde{n}_j = \tilde{m}_j = 0$ and $n_{cj} = n_j$:

$$\frac{E_{\text{LHY}}}{V} = \frac{8m^{3/2}}{15\pi^2\hbar^3}(g_1 n_1)^{5/2} \sum_{\pm} f_{\pm}(\Delta, \alpha)^{5/2}. \tag{3.4}$$

In the mean-field unstable regime, $g_{12} + \sqrt{g_1 g_2} < 0$, the term with the function f_- is negative, adding an imaginary term to the LHY energy. In the original work of Petrov [44], this problem is cured by neglecting the small δg corrections (i.e. $\delta g \ll g$). Setting, just for the LHY term, $g_{12} = \sqrt{g_1 g_2}$ and supposing that the two species are prepared with the same density distribution ($n_1 = n_2$), the LHY energy turns out to be given as:

$$\frac{E_{\text{LHY}}}{V} = \frac{8m^{3/2}}{15\pi^2\hbar^3}(g\,n)^{5/2} f_+(\Delta, 1)^{5/2}. \tag{3.5}$$

So, the total energy reads:

$$E = E_0 + E_{\text{LHY}} = \delta g\sqrt{g_1/g_2}n^2 + V\frac{8m^{3/2}}{15\pi^2\hbar^3}(g\,n)^{5/2} f_+^{5/2}(\Delta, 1). \tag{3.6}$$

In order to obtain a deeper insight about the scaling of both the mean-field and LHY contributions, let us consider the symmetric case where $g_2 = g_1 = g$. In terms of the δg, g and n, we can rewrite equation (3.6) as

$$E = \delta g n^2 + V\frac{8m^{3/2}}{15\pi^2\hbar^3}(g\,n)^{5/2} f_+^{5/2}(g_{12}^2/g^2, 1). \tag{3.7}$$

This form permits us to estimate the different scaling of both the mean-field and the LHY terms and their dependence on the interaction strength. We cearly see that the LHY term presented in equation (3.7) depends only on intraspecies interaction g while the mean-field is proportional to δg. This means that if we explore the regime close to the collapse point of a Bose-Bose mixture ($\delta g = 0$) we can find a situation where the mean-field energy is small while keeping the LHY term sizeable. Furthermore, the

two terms have a different dependence on the density n. For $\delta g < 0$, the attractive mean-field term $E_0 \propto n^2$ is compensated by the repulsive LHY energy $E_{\text{LHY}} \propto n^{5/2}$ which arrests the collapse and stabilizes the system. This will give rise to a self-bound quantum liquid droplet.

In order to check the formation of such a droplet phase, we plot the ground-state energy in units of $E_0 = \hbar^2/ma^2$ as a function of the density for $a_{12}/a = -1.1$. Figure 3.1 shows that the energy exhibits a minimum at a finite density corresponding to a self-bound droplet state.

The equilibrium density of the droplet can be obtained by minimizing the energy with respect to the density. This yields [44]

$$n_{j\text{eq}} = \frac{25\pi}{1024} \frac{|\delta a|^2}{a_1 a_2 \sqrt{a_j} \left(\sqrt{a_1} + \sqrt{a_2} \right)^5}. \tag{3.8}$$

For the sepcial case where $g_1 = g_2 = g$, $n_1 = n_2 = n/2$, the equilibrium density (3.8) reduces to:

$$n_{\text{eq}} = \frac{25\pi}{16384} \left(1 + \frac{a_{12}}{a} \right)^2 a^{-3}, \tag{3.9}$$

its behavior in terms of the interpsecices interaction, a_{12}/a, is displayed in figure (3.2). We observe that n_{eq} is decreasing with decreasing $|a_{12}/a|$.

3.2.1   Generalized GP equation

In the miscible phase and close to the collapse point, we can describe the system with an effective single component GGP equation. This latter enables us to study the density profile and the lowlying excitations of the droplet.

Following the method outlined by Petrov [44], we rescale the wavefunction of each
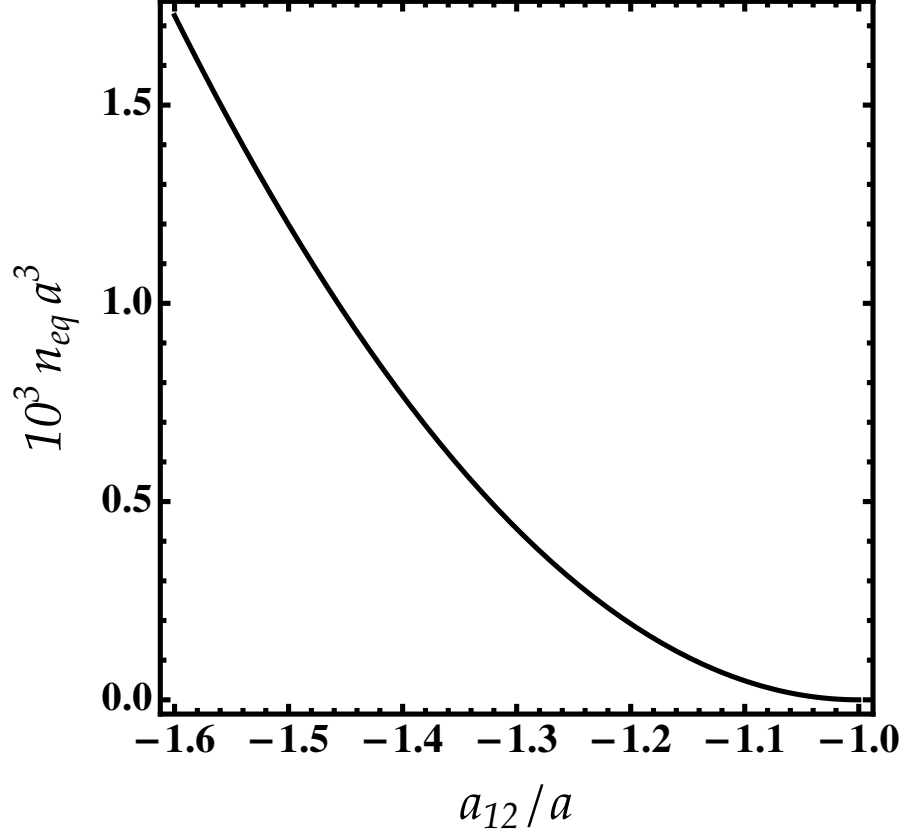
Figure 3.2: Equilibrium density of the droplet from equation (3.9) as a function of a_{12}/a.

species as:

$$\Phi(r,t) = \sqrt{n_0}\phi(r,t), \tag{3.10}$$

where $\phi(r,t)$ is a scalar wavefunction common to both species. It is convenient to introduce the dimensionless parameters : $\tilde{N} = N/(n_0\xi^3)$, $\tilde{r} = r/\xi$, and $\tilde{t} = t/\tau$, where

$$\xi = \sqrt{6\hbar^2/(m|\delta g|n_0)}, \tag{3.11}$$

and

$$\tau = 6\hbar/(|\delta g|n_0), \tag{3.12}$$

are respectively, the extended healing length of the droplet and the rescaled time. For $\hbar = m = 1$, the energy functional associated to the equation of state (3.7) can be written as:

$$\tilde{\mathcal{E}}(\phi, \phi^*) = \frac{1}{2} \left| \nabla_{\tilde{r}}^2 \phi \right|^2 - \frac{3}{2} |\phi|^4 + |\phi|^5, \tag{3.13}$$

The wavefuction of the ground-state can be obtained by solving the following extended GP equation in the dimensionless form :

$$\mu\phi(\tilde{r}) = \left(-\frac{1}{2}\nabla^2 - 3\left|\phi(\tilde{r})\right|^2 + \frac{5}{2}\left|\phi(\tilde{r})\right|^3 \right)\phi(\tilde{r}), \tag{3.14}$$

which is commonly used framework to describe the stationary and dynamical aspects of quantum droplets at zero temperature [44]. It includes the effect of quantum fluctuations to leading order within the local density approximation. The chemical potential is fixed by the normalization condition: $\tilde{N} = \int |\phi|^2 \, d^3\tilde{r}$ is related to the actual atom number via

$$N = n_0 \xi^3 \tilde{N}. \tag{3.15}$$

Some examples of the ground-state wavefunctions obtained for different values of $\tilde{N}$ are reported in figure 3.3. For small $\tilde{N}$ the shape of the wave-function is similar to a gaussian while, for large $\tilde{N}$, the ground state of the mixture is a spherical droplet which displays a flat-top shape indicating a saturation density in the bulk.

3.2.2   Gaussian Ansatz

An alternative way to derive the equilibrium properties of the droplet is to use a gaussian ansatz for the wave-function of the ground state. In this approximation we
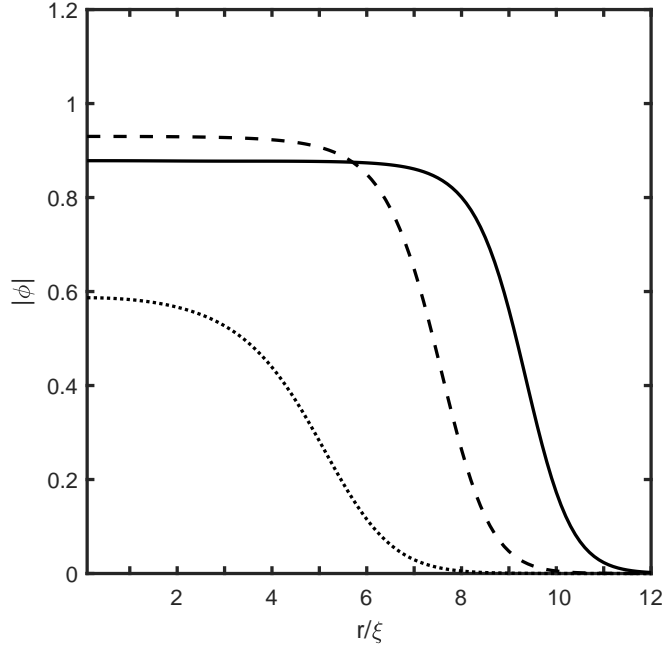
Figure 3.3: Droplet wavefunction versus radial coordinate for $\tilde{N} = \tilde{N}_c \approx 18.65$ (dotted), $\tilde{N} = 500$ (Dashed), and $\tilde{N} = 3000$ (solid) [44].

can write the density of the system as:

$$n(\tilde{r}) = \frac{\tilde{N}}{2\sqrt{2}\pi^{3/2}\sigma^3}e^{-\tilde{r}^2/(2\sigma^2)}, \tag{3.16}$$

where σ is the droplet width.

Assuming that the associated wavefunction is $\phi(\mathbf{r}, t) = \sqrt{n(\mathbf{r}, t)}$ without considering phase terms which are not relevant in the study of the equilibrium properties of the system. Inserting (3.16) into Eq.(3.13) and intergrating over $\mathbf{r}$, one finds for the energy functional:

$$\tilde{E} = \int d\mathbf{r}\tilde{\mathcal{E}}(\phi, \phi^*) = \frac{3\tilde{N}}{4\sigma^2} - \frac{3\tilde{N}^2}{4\sqrt{2}\pi^{3/2}\sigma^3} + \frac{2}{5}\frac{\tilde{N}^{5/2}}{\pi^{9/4}\sigma^{9/2}}. \tag{3.17}$$

In figure 3.4 we show the minima in energy for a stable droplet (blue) and
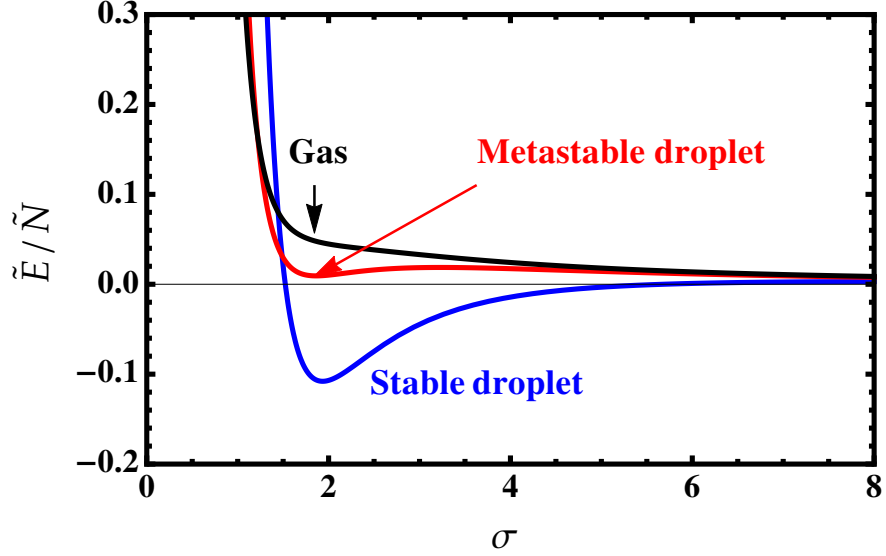
Figure 3.4: Droplet minima for three different values of $\tilde{N}$. For large atom number $\tilde{N} > 22.55$, the droplet is stable (blue line). Close to the critical atom number, $18.65 < \tilde{N} < 22.55$, the droplet becomes metastable (red line). Finally for low atom number $\tilde{N} < 18.65$, the droplet dissociates into a gas [44].

metastable droplet (red). Below critical atom number the minimum in energy disappears and there is a liquid-to-gas phase transition.

3.2.3   Collective excitations

The excitation spectrum of quantum droplets is among their most intriguing and unusual characteristics.in order to research the small-amplitude excitations, Petrov solves the BdG equation derived from the linearization of the GGP equation (3.14). In this approach, the energies of the droplet's collective exciations, such as the monopole, quadrupole, and oscillations with increasing angular momenta, may be calculated. So, the spectrum of the droplet's surface modes (ripplons) is obtained in the limit of large
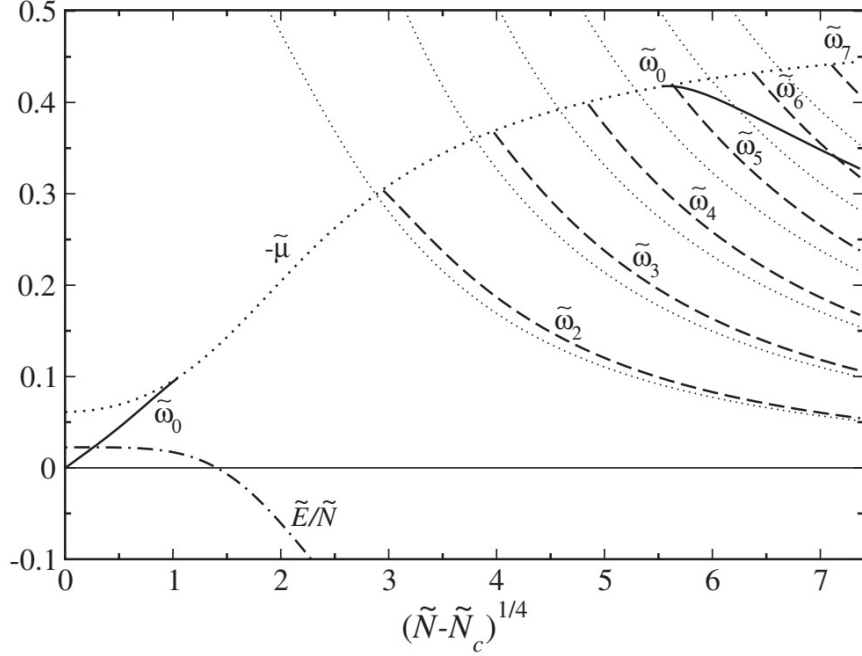
Figure 3.5: The dash-dotted line corresponds to the energy per particle $\tilde{E}/\bar{N}$ analogously to the one reported in Fig.3.4. The thick dotted line represent $-\tilde{\mu}$, i.e. the particle emission threshold. The solid line is the monopole mode ω_0, while the dashed are the higher angular momentum modes ω_l. The thin dotted lines are the corresponding modes calculated with the surface modes approximation of (3.18). All these quantities are plotted as a function of $\left(\tilde{N} - \tilde{N}_C\right)^{1/4}$. Figure taken from [44].

N.

$$\tilde{\omega}_l = \sqrt{(4\pi/3)l(l-1)(l+2)\tilde{\sigma}/\tilde{N}}, \tag{3.18}$$

where angular momentum is represented by $l > 0$. The dipolar mode, or $l = 1$, denotes a displacement of the droplet's center of mass, so $\omega_1 = 0$. Since it is a classical conclusion that is invalid in the limit of an incompressible droplet, the $l = 0$ mode, which represents the monopole mode, cannot be derived using equation (3.18). The thin- dotted lines in figure (3.5) represent the modes derived using equation (3.18).

3.3 Experimental realization of a mixture droplet
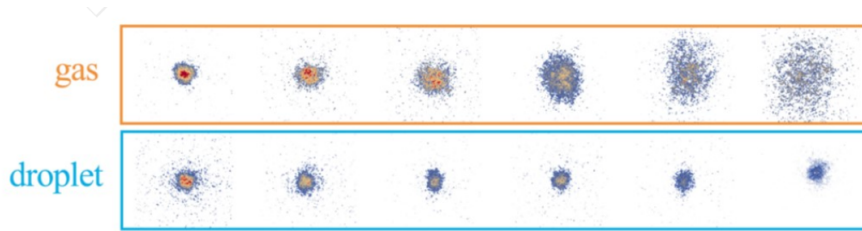
Figure 3.6: Self-bound droplets in the absence of an external trapping potential can be imaged experimentally. The densities of two such systems are shown here. When the mean-field energy of a BoseBose mixture is repulsive (top row), it results in a gas phase, and the droplet expands over time. When the mean-field energy is attractive (bottom row), the size of the self-bound droplet remains constant over time, although its density, shown in false color, decays due to three-body losses. (Adapted from [https://quicproject.wordpress.com/2018/03/07/self-bound-liquid-droplets-in-free-space/]).

3.3.1 Droplet in homonuclear mixtures of ^{39}K

In this subsection we briefly summarize the main experimental steps for achieving potassium mixture droplets [56, 22].

1. The experiment starts in a chamber with a high vapor pressure of natural potassium. A cold atomic beam is generated from the background pressure using a 2D Magneto-Optical Trap (MOT).

2. The atoms are trapped in a 3D MOT and then successively cooled below the Doppler limit to a few tens of μK.

3. Gray optical molasses on the D1-line are used to obtain efficient sub-Doppler cooling.

4. The atoms are prepared in $|F = 2, m_F = 2\rangle$ by optical pumping and captured in a magnetic quadrupole trap provided by a couple of anti-Helmotz movable coils.

5. Radio-frequency evaporation on the hyperfine transition leads to a phase-space density.

6. The atoms are transferred to a hybrid trap (optical dipole trap beam plus a weak quadrupole field) and subsequently to a crossed optical dipole trap and evaporated to BEC with negligible non-condensed part (smaller than 10% of the total atom number). If required a Feshbach field is used to control the interactions during the final evaporation stage. After the creation of a BEC, and by increase the value of the magnetic field up to $\simeq 55$G turning off the magnetic curvature used during the evaporation [22].

7. Finally, the system is characterized using absorption imaging after time of flight or in situ phase contrast imaging.

3.3.2 Droplet in heteronuclear mixtures of ^{41}K-^{87}Rb

Here we present the main steps involved in producing ^{41}K-^{87}Rb mixture.

After a first cooling stage in a two-species magneto-optical trap, both ^{41}K and ^{87}Rb in the low-field-seeking state $|F = 2, m_F = 2\rangle$, are optically pumped and then loaded in an hybrid potential, consisting of a magnetic quadrupole plus an optical dipole
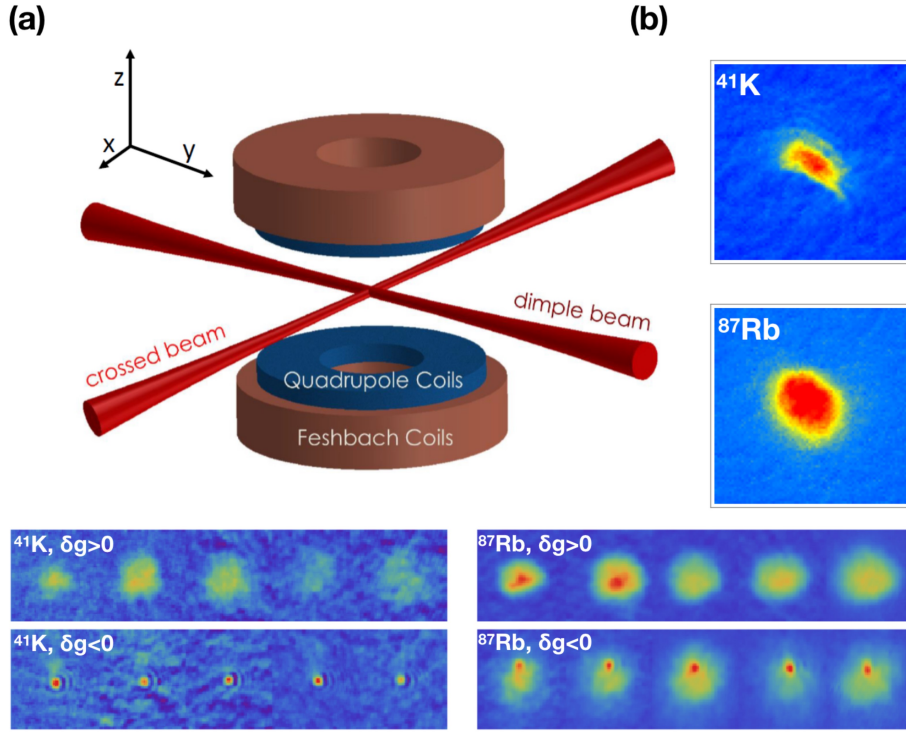
Figure 3.7: Top panel (a) Schematics of the experiment, showing the optical dipole trap beams, quadrupole and Feshbach coils. (b) Absorption images of the binary BECs. Bottom panel: Self-bound droplets for different time-of-flight expansion and for different values of a_{12}. Top row corresponds to $a_{12} \simeq -18a_0 (\delta g > 0)$. Bottom row corresponds to $a_{12} \simeq -85a_0 (\delta g < 0)$. Figures taken from [148].

trap [148]. In such an hybrid potential ^{87}Rb is first magnetically and then optically evaporated, while ^{41}K is almost sympathetically cooled by elastic collisions with ^{87}Rb. The cooling sequence is ended with a degenerate mixture in the pure optical trap[148]. At this stage, the mixture is transfered into the $|F = 1, m_F = 1\rangle$ state and thus, drived into its absolute ground-state, where easily accessible Feshbach resonances enable for tuning the interspecies scattering length a_{12} [148]. Schematics of the experiment are depicted in figure 3.7 (top). Finally, the evolution of the attractive ^{41}K-^{87}Rb mixture is studied in free space, after removing the trapping potential, the droplet is then held

against gravity via a magnetic levitation[148]. Absorption images of ^{41}K and ^{87}Rb are shown in figure 3.7 (bottom).

3.4 Quantum properties

In general, the investigation of quantum droplets forming in ultracold atomic systems could be a useful tool to understand complex quantum systems beyond the mean-field paradigm. The most interesting features of these quantum liquid droplets are:

1. **Self-bound quantum objects:** quantum droplets remain self-bound (confined on a finite volume) even without any external trap and solely by quantum effects, due to the interplay of attractive and repulsive forces in the system.

2. **Ultradilute systems:** in the quantum droplets the atoms are so far away from each other that they have ultralow density (a lower density than air). As consequence of such a low density proeprties is that the quantum depletion remains weak, so the LHY approximation remains valid. This in contrast to atomic nuclei [142] and liquid helium [143] droplets which are dense and strongly interacting many-body systems.

3. **Surface effects:** in the droplet, kinetic energy acts as a surface tension, contributing an additional energy that depends on the density gradient. The energy related to the surface is proportional to its area $\propto V^{2/3}$. In the limit of infinite system, the surface effect is not important.

4. **Constant density:** quantum droplets are characterized by a constant density, meaning that adding atoms just makes a droplet wider. The stabilization

mechanism due to quantum fluctuations prevents a runaway implosion [44]. Intriguingly, it is predicted that by adjusting the number of atoms or interparticle interactions producing a novel, unexcitable object that awaits experimental confirmation.

5. **Self evaporation:** there exists indeed a regime where droplets are predicted to be zero temperature objects, meaning that they cannot live in an excited state, but they are able to dissipate energy by expelling atoms, a phenomenon called self evaporation. The Bose droplet then may automatically lose its thermal energy upon releasing the most energetic particles and reach exactly zero temperature. This peculiar mechanism could pave the way to a possible use of the quantum droplet as a coolant for other system.

6. **Liquid-like properties:** despite the droplets are extremely dilute, they present liquid-like properties, closely analogous to those of classical liquids. When increasing the atom number, the ground-state wavefunction reaches a saturation density, so that it develops a bulk with uniform density and very weak compressibility.

7. **Supersolids:** supersolid are a fundamental quantum phase of matter atoms are arranged in a crystalline pattern while at the same time behaving like a superfluid with no friction, no resistance. In dipolar BECs, the combination of the roton instability and quantum stabilization leads under proper conditions to a phase transition from the single quantum droplet phase to a density-modulated supersolid properties, due to the coexistence of stripe modulation and phase coherence [66, 67, 68]. Whereas, in binary BEC droplets, it has been found

that a first-order phase transition from a self-bound supersolid stripe phase to a zero-minimum droplet state of the Bose gas occurs as a function of the Rabi coupling strength [69].

3.5 Applications

Since quantum droplets occur only in very specific circumstances, they raise some exciting prospects and present potential applications. Understanding self-bound quantum droplets is essential for future technologies, such as gravitational wave detectors and precise clocks. It has been even suggested that self-bound droplets could be used to test quantum gravity. The investigation of quantum droplets as a new form of quantum matter with exotic properties is a particularly powerful platform for research in microgravity. The dilutness of quantum liquid droplets make them an ideal testbed for better understanding quantum many-body systems, and understanding the characteristics they share with liquid helium, stars neutrons, black holes, supersolid, superglass, and other complex systems. Additionally, a profound study of quantum droplets will provide essential new insights into the fundamental nature of the interplay between few- and many-body interactions. Ultracold self-bound droplets are promising candidates for studying entanglement, and proposals for a quantum computer capable of simulating aspects of atomic physics and cosmology. They are also important for inspiring new materials as well as novel superconductors which leads to a real revolution for quantum electronic devices.

Chapter 4

Effects of higher-order quantum fluctuations on symmetric self-bound droplets

4.1 Introduction

Quantum fluctuations which are crucially tied to Heisenberg's uncertainty principle, often associated with a change in the energy of the system. They can alter virtually all aspects of matter leading to the emergence of novel phase transitions such as quantum liquid droplets, supersolids, superglasses.

In this chapter, we will investigate the influence of higher-order quantum fluctuations upon quantum droplets of symmetric Bose-Bose mixtures using the self-consistent HFB theory presented in chapter 2. This model which we developed to remove the handicaps of the standard Bogoliubov prescription [44], can self-consistently

evaluate the quantum and thermal fluctuations exhibited by weakly-interacting binary BECs [37]. In the case of dipolar droplets, the HFB theory is capable of producing excellent predictions for the condensate, the depletion, the pair correlation function, the critical number of particles, and the ground-state energy that have been measured experimentally and with QMC [50].

We derive useful analytical results for the ground-state energy and the equilibrium density that extend naturally the seminal equations of Petrov [44]. Explicit expressions connecting normal and anomalous correlations to the droplet equilibrium density are also obtained for the first time to the best of our knowledge. We show that our theory not only provides fascinating results but also captures genuine higher-order quantum effects predicted from recent DMC simulations [88]. Our study is extended to the regime of relatively strong interactions. We reveal that such higher-order quantum corrections become more pronounced for large values of the interspecies interaction. On the other hand, we calculate the density profiles and the collective modes of the droplet. Our calculations are based on the GGP equation which will be derived in a self-consistent manner from our HFB formalism taking into account higher-order quantum corrections under the local density approximation.

We show that the inclusion of the condensed density and the pairing is essential, in order to have a consistent description of the quanutm droplet.

4.2   Quantum fluctuations effects

Let us consider a homonuclear Bose-Bose mixture (i.e $m_1 = m_2$) with equal repulsive intraspecies interactions (i.e., $g_1 = g_2 = g > 0$) and attractive interspecies interactions

$(g_{12} < 0)$. In this case, we have equal population $n_1 = n_2 = n/2$, $\tilde{n}_1 = \tilde{n}_2 = \tilde{n}/2$, and $\tilde{m}_1 = \tilde{m}_2 = \tilde{m}/2$ inside a volume V. The ground-state energy (2.44) can be rewritten in the following dimensionless form [78]:

$$\frac{E}{NE_0} = \pi \left(\frac{\delta a}{a}\right)_+ (na^3) + \frac{32\sqrt{\pi}}{15} (na^3)^{3/2} \left(1 + \frac{\tilde{m} - \tilde{n}}{n}\right)^{5/2} \sum_\pm \left(\frac{\delta a}{a}\right)_\pm^{5/2}, \quad (4.1)$$

where $E_0 = \hbar^2/ma^2$, and $(\delta a/a)_\pm = 1 \pm (a_{12}/a)$. Equation (4.1) extends and unifies various EoS in the existing literature. For $(\delta a/a)_+ < 0$, the mean-field theory energy furnishes a term $\propto n^2$ leading to a collapse of a homogeneous state towards bright soliton formation. The higher-order LHY corrections furnish an additional repulsive terms $\propto n^\ell$, compensating the attractive mean-field term, enabling quantum and thermal fluctuations to stabilize mixture droplets against collapse.

We solve iteratively the energy (4.1) up to the second-order in $\tilde{n}$ and $\tilde{m}$. Our results are compared with recent DMC data [88] and theoretical analysis [44, 77]. Figures 4.1 (a) and (b) show that our findings are in excellent agreement with the DMC simulations [88], and improve upon the conventional Bogoliubov and the pairing predictions previously reported in [44, 77] whatever the value of a_{12}. This indicates the importance of the beyond LHY quantum corrections.

To gain further insights into the stabilization mechanism, we analyze the density dependence of the energy per particle in the strongly interacting regime, i.e. $|a_{12}| \gg a$. Figure 4.2 clearly shows that higher-order quantum fluctuations become more prominent for relatively large interspecies interactions. This is indeed understandable since both the normal and anomalous fluctuations originate themselves from the interaction [79]. For $a_{12}/a < -1.1$, effects of fluctuations higher than first-order are not important.
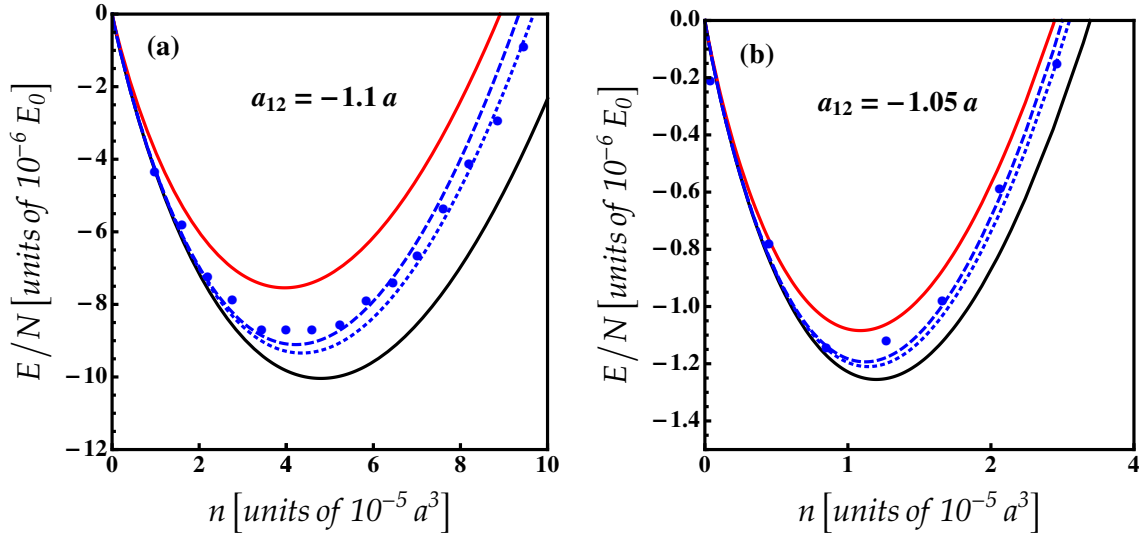
Figure 4.1: (a) Ground-state energy from Eq.(4.1) as a function of the density for $a_{12}/a = -1.1$. (b) Ground-state energy as a function of the density for $a_{12}/a = -10$. Red lines correspond to the pairing theory [77]. Blue dashed lines correspond to our results up to first-order corrections of quantum fluctuations. Blue dotted lines correspond to our results up to second-order corrections of quantum fluctuations. Black solid lines correspond to the Petrov's predictions [44]. Circles represent the DMC results of [88].

Figure 4.3 depicts that as interspecies attraction gets larger the energy decreases (depth of the local minimum increases) indicating that a stable droplet still survives even for strongly interacting regime[79]. One can expect that this behavior persists even when a_{12} crosses the Feshbach resonance [77].

Noteworthy, strong interactions and higher-order fluctuations do not considerably affect the equilibrium density of the self-bound droplet.

The equilibrium density of the droplet can be obtained by minimizing the energy with respect to the density [44]. Using the identity $(1+a_{12}/a)^{j/2}+(1-a_{12}/a)^{j/2} = 2^{j/2}$,
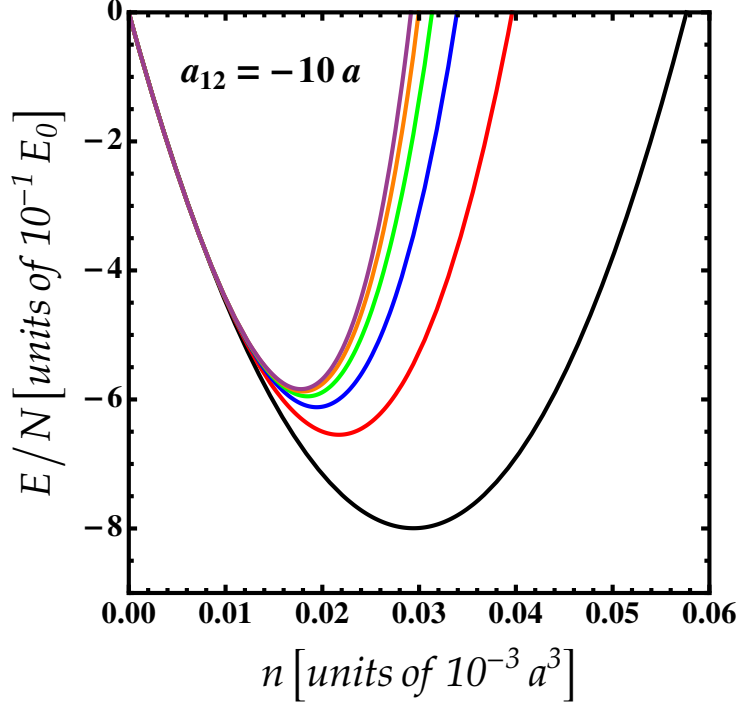
Figure 4.2: Ground-state energy from Eq.(4.1) as a function of the density for $a_{12}/a = -10$. Black line: zeroth-order corrections. Red line: first-order corrections. Blue line: second-order corrections. Green line: third-order corrections. Orange line: fourth-order corrections. Purpule line: fifth-order corrections.

we immediately get [78]

$$\frac{n_{\text{eq}}}{n_0} = \frac{0.0576}{(\delta a/a)_+^2} \left[18 - 25 \left(\delta a/a\right)_+ - 6\sqrt{9 - 25 \left(\delta a/a\right)_+} \right]. \tag{4.2}$$

This equation differs by the term $[0.0576/ \left(\delta a_+/a\right)^2][18 - 25 \left(\delta a_+/a\right) - 6\sqrt{9 - 25 \left(\delta a_+/a\right)}]$ from the equilibrium density $n_0 a^3 = (25\pi/16384) \left(\delta a_+/a\right)^2$ predicted by Petrov Eq.(3.9).

In Figures 4.4 and 4.5 we plot our predictions for the equilibrium density and compare the results with the DMC simulation points [88] and the existing previous theoretical models [44, 77]. Figure 4.4 shows that our theoretical results based on the HFB theory are in good agreement with the DMC simulation practically in the whole
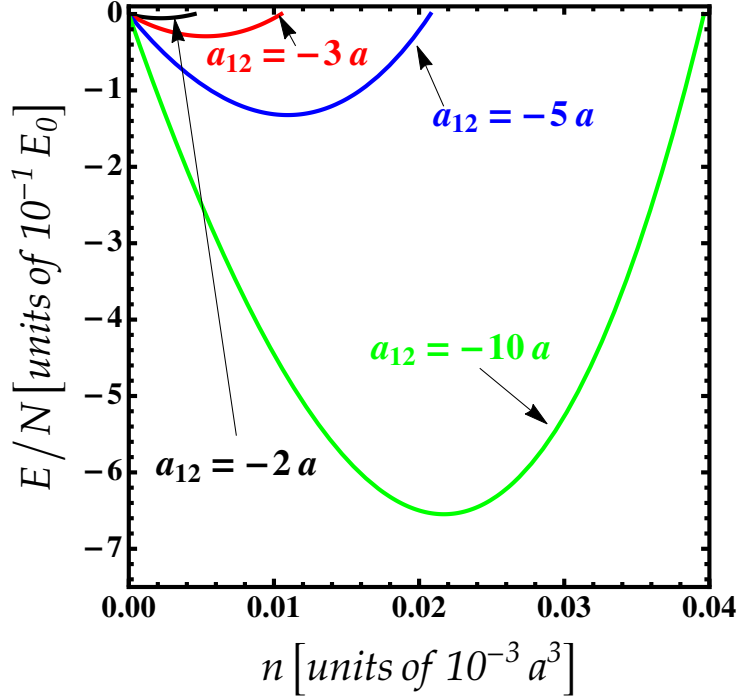
Figure 4.3: Ground-state energy from Eq.(4.1) up to second-order corrections as a function of the density for different values of interspecies.

the range of interactions. However, for the large value of $|a_{12}/a|$, the ratio n_{eq}/n_0 assessed by our theory diverges from that of the Bogoliubov approach [44] and the pairing theory [77] (see figure 4.5). One might argue that quantum fluctuations are responsible for such an increase in our equilibrium density.

We now focus ourselves to calculate the noncondensate and anomalous densities in the equilibrium phase. One can rewrite the noncondensate and anomalous densities of the droplet in terms of the equilbruim denisty up to first-order [78]:

$$\tilde{n}_{\text{eq}} = \frac{2\sqrt{2}}{3} n_{\text{eq}} \sqrt{\frac{a^3 n_{\text{eq}}}{\pi}} \sum_{\pm} \left(\frac{\delta a}{a} \right)^{3/2}_{\pm}, \tag{4.3}$$
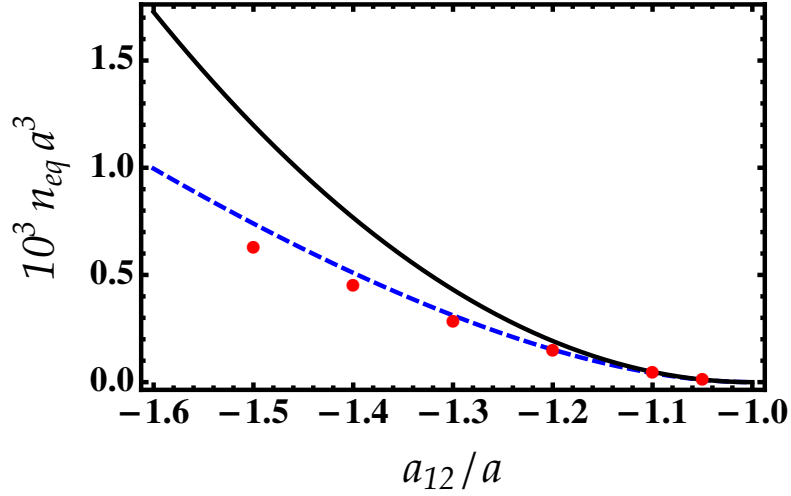
Figure 4.4: Equilibrium density of the droplet as a function of a_{12}/a. Black solid lines correspond to Petrov's equilibruim density [44]. Blue dashed lines correspond to our results from Eq. (4.2). Circles correspond to DMC data [88].

and

$$\tilde{m}_{\text{eq}} = 2\sqrt{2}\, n_{\text{eq}} \sqrt{\frac{a^3 n_{eq}}{\pi}} \sum_{\pm} \left(\frac{\delta a}{a} \right)_{\pm}^{3/2}. \tag{4.4}$$

To the best of our knowledge, these quantities have never been determined in the literature. Remarkably, equations (4.3) and (4.4) show that the anomalous density of the droplet is larger than the noncondensed density specifically for large $|a_{12}/a|$ like in the case of an ordinary BEC. We see from figure 4.6 that $\tilde{n}_{\text{eq}}$ and $\tilde{m}_{\text{eq}}$ increase with increasing the ratio $|a_{12}/a|$ which is indeed natural since both quantities arise from interactions.
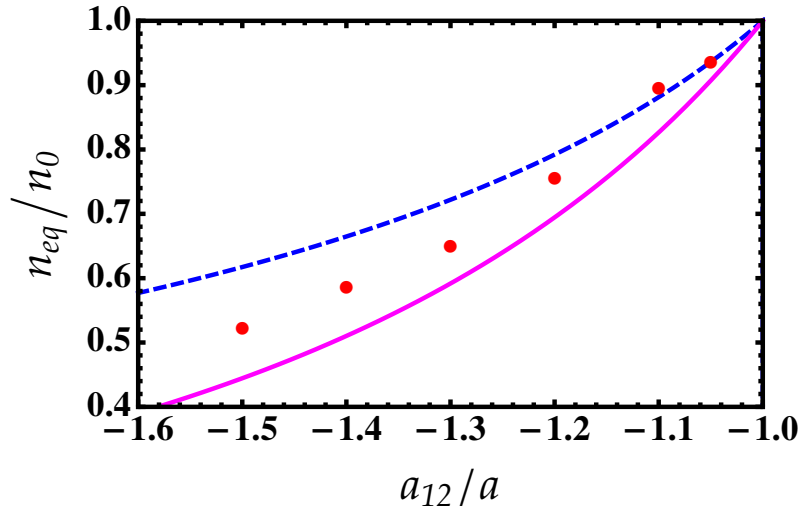
Figure 4.5: Equilibrium density in units of n_0, as a function of a_{12}/a. Blue dashed lines correspond to our results from Eq. (4.2). Magenta lines correspond to pairing theory of [77]. Circles correspond to DMC data [88].

4.3 Density profiles

Our main aim in this section is to discuss the effects of higher-order quantum corrections on the structural shape and on the collective modes of the self-bound droplet. W then derive the GGP equation which can be obtained directly from our HFB formalism. It permits us to study both the equilibrium and the dynamics of self-bound droplets in a selfconsistent way.

To facilitate the numerical and analytical workload, it is convenient to introduce the rescaled (dimensionless) wavefunction, number fo particles, coordinate and time as defined in equations (3.10)-(3.12) namely: $\Phi(r,t) = \sqrt{n_0}\phi(r,t)$, where $\phi(r,t)$ is a scalar wavefunction common to both species, $\tilde{N} = N/(n_0\xi^3)$, $\tilde{r} = r/\xi$, and $\tilde{t} = t/\tau$, where $\xi = \sqrt{6\hbar^2/(m|\delta g|n_0)}$, and $\tau = 6\hbar/(|\delta g|n_0)$ [44].

The functional energy associated to the equation of state (5.6) can be written in
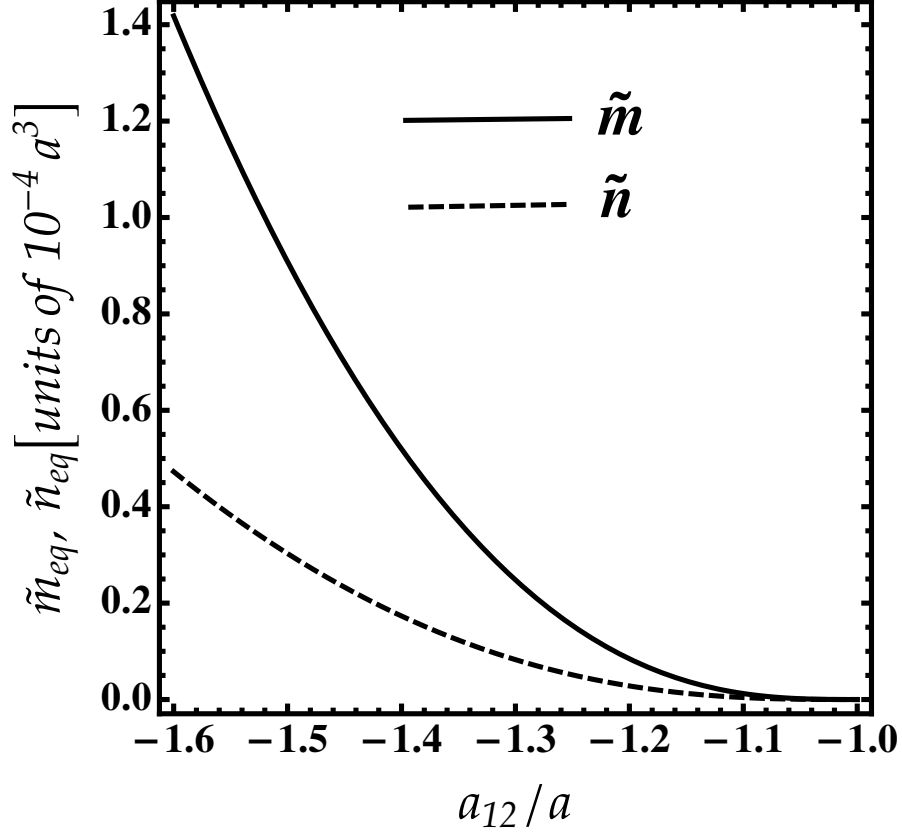
Figure 4.6: Anomalous and noncondensed densities of the self-bound droplet state from Eqs.(4.3) and (4.4) as a function of a_{12}/a.

the following dimensionless form:

$$\mathcal{E}\left(\phi, \phi^*\right) = \frac{1}{2}|\nabla\phi|^2 - \frac{3}{2}|\phi|^4 + \alpha|\phi|^5(1-|\phi|)^{5/2}, \tag{4.5}$$

where $\alpha = (4\sqrt{2}/3)(\delta g/g)_+^{3/2}\sqrt{a^3 n_0/\pi}$. The corresponding GGP equation can be derived using $i\partial\phi/\partial\tilde{t} = \partial\mathcal{E}/\partial\phi^*$. This yields [78]

$$i\frac{\partial\phi}{\partial\tilde{t}} = \left[-\frac{1}{2}\Delta_{\tilde{\mathbf{r}}} - 3|\phi|^2 + \frac{5}{2}[1+\alpha|\phi|(1+\alpha|\phi|)^{3/2}]^{5/2}|\phi|^3\right]\phi, \tag{4.6}$$

Equation (4.6) is appealing since it obviously contains higher-order quantum corrections. It is valid when the spatial variations of the condensate density are small

over the extended healing length, ξ, validating a description of a locally homogeneous system. Another important point is that our GGP equation (4.6) is known to provide an adequate description of droplets in the limit of large systems associated with high-particle densities, and in the weakly interacting case at both zero and finite temperatures. Similar equation has been derived by Ota et *al.* [76] using the beyond mean-field corrections to the phonon modes of the mixture based on the Bogoliubov theory. For $\alpha = 0$, one recovers the Petrov's generalized GPE [44]. The stationary solutions is obtained from equation (4.6) by substituting $\phi(\mathbf{r}, t) = \phi(\mathbf{r})e^{-i\tilde{\mu}t}$, where the chemical potential $\tilde{\mu}$ is fixed by the normalization condition $\tilde{N} = \int d\tilde{\mathbf{r}} |\phi|^{\mathbf{2}}$.

4.3.1 Numerical method

The nonlinear differential equation (4.6) does not have analytic solution and hence requires a numerical simulation. Stationary ground-state solutions are reached by imaginary time evolution ($\tilde{\tau} = i\tilde{t}$) [10, 76] of equation (4.6) using a split step Fourier method. The method was proved to be a quite powerful numerical tool for solving similar problems. It is efficient in particular for for small nonlinearities, since it retains the near-integrable structure of the problem.

A Gaussian wavefunction is set as an initial state in imaginary-time propagation in order to ensure an easy convergence. The boundary condition implies that the wavefunction and its first derivative vanish at the boundary. A small space step, $\Delta r = 0.01$, is needed to find out the possible collapse of the self-bound state when its size becomes very small [147]. For $N = N_{\text{cr}}$, the contributions by the effective mean-field attraction and the quantum fluctuations are the same in magnitude, and
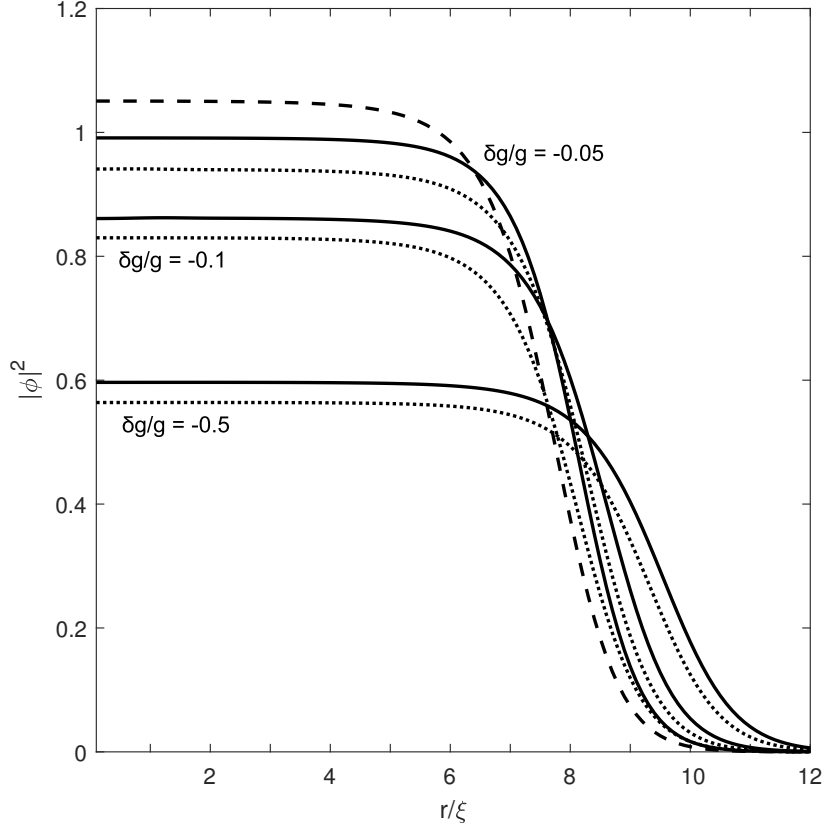
Figure 4.7: Density profile of the self-bound droplet obtained at zero temperature for different values of interaction strength $\delta g/g$, and $\tilde{N} = 3000$. Solid lines: Our results. Dashed lines: Petrov's results [44]. Dotted lines: Findings of Ref.[76].

the droplet evaporates quickly. The self-evaporation process manifestsmanifests itself as a decrease in peak density [47].

The results of the mentioned numerical method are captured in figure 4.7. It is clearly seen that as the interaction strength $|\delta g/g|$ increases, the central density decreases and the size of the droplet enlarges in agreement with the findings of [76]. This may provoke a shift in the critical number compared to the universal results of Ref.[44].

4.4   Collective modes

Collective modes play a crucial role for probing many-body effects in ultradilute self-bound droplets. Experimentally, collective excitations can be accurately measured through in-situ or time-of-flight absorption imaging [10]. They can be analytically explored employing a Gaussian ansatz

$$\phi(r) = A \exp\left[-\left(\frac{1}{2\sigma^2} + i\beta\right)r^2\right],\qquad(4.7)$$

where $A = \sqrt{\tilde{N}/(\pi^{3/2}\sigma^3)}$ is the normalization factor, σ and β are the variational parameters standing for the width and the phase of the condensate, respectively.

The Lagrangian density reads

$$\mathcal{L} = \frac{i}{2}\left(\phi^*\frac{\partial\phi}{\partial\tilde{t}} - \phi\frac{\partial\phi^*}{\partial\tilde{t}}\right) - \mathcal{E}(\phi, \phi^*).\qquad(4.8)$$

Replacing the ansatz (4.7) into the Lagrangian density in equation (4.8), we derive the Lagrangian $L = \int d^3r\mathcal{L}$ [78]:

$$L = \left[-2\tilde{N}\left(\sigma\dot{\beta} - 2\sigma^2\beta^2\right) + \frac{\tilde{N}}{2\sigma^2} - \frac{\sqrt{2}}{3\pi^{3/2}}\frac{\tilde{N}}{\sigma^3} - \frac{8\sqrt{2/5}}{27\pi^{9/4}}\frac{\tilde{N}^{3/2}}{\sigma^{9/2}} - \frac{4\sqrt{2/5}}{18\pi^3}\frac{\tilde{N}}{\sigma^6}\alpha\right].\qquad(4.9)$$

Given the vector of variational parameters $\mathbf{U}$, the Euler-Lagrange equations are computed from equation (4.9) via $\frac{d}{dt}\frac{dL}{d\dot{\mathbf{U}}} - \frac{dL}{d\mathbf{U}} = 0$. Accordingly, the phase of the droplet can be written as [78]:

$$\beta = \frac{\dot{\sigma}}{2\sigma},\qquad(4.10)$$

and the dynamics of the width reads

$$\ddot{\sigma} = -\frac{dV_{\text{eff}}(\sigma)}{d\sigma},\qquad(4.11)$$

61

where the effective potential is given by:

$$V_{\text{eff}}(\sigma) = -\frac{\tilde{N}}{2\sigma^2} + \frac{\sqrt{2}}{3\pi^{3/2}}\frac{\tilde{N}}{\sigma^3} + \frac{8\sqrt{2/5}}{27\pi^{9/4}}\frac{\tilde{N}^{3/2}}{\sigma^{9/2}} + \frac{4\sqrt{2/5}}{18\pi^3}\frac{\tilde{N}}{\sigma^6}\alpha. \tag{4.12}$$

The equilibrium widths σ_0 are calculated by minimizing the potential $V_{\text{eff}}(\sigma)$. Frequencies of the low-lying collective modes are determined by linearizing equation (4.12) around the equilibrium solutions. The breathing modes can be found by inserting the decomposition $\sigma(t) = \sigma_0 + \delta\sigma(t)$ (with $\delta\sigma(t) = \delta\sigma\, e^{i\omega t}$ and $\delta\sigma \ll \sigma_0$) into equation (4.12) and expanding the effective potential into a Taylor series. This yields

$$V_{\text{eff}}(\sigma_0, \delta\sigma) = V_{\text{eff}}(\sigma_0) + \begin{pmatrix} \delta\sigma \end{pmatrix} \begin{pmatrix} A_1 \\ A_2 \end{pmatrix} \begin{pmatrix} \delta\sigma \end{pmatrix}, \tag{4.13}$$

where

$$A_1 = 1 - \frac{6}{\sigma_0^4} + \frac{3\tilde{N}}{\sigma_0^5} + \frac{6\tilde{N}^{3/2}}{\sigma_0^{13/2}},$$

$$A_2 = +\frac{\tilde{N}}{\sigma_0^5} + \frac{15\tilde{N}^{3/2}}{8\sigma_0^{14/2}} - \frac{\tilde{N}^{-1/2}\alpha}{8\sigma_0^{3/2}}.$$

The coupled set of differential equations (4.11) can be rewritten in a matrix form:

$$\begin{pmatrix} \delta\ddot{\sigma} \end{pmatrix} + \begin{pmatrix} \delta\sigma \end{pmatrix} \begin{pmatrix} A_1 \\ A_2 \end{pmatrix} \begin{pmatrix} \delta\sigma \end{pmatrix} = 0. \tag{4.14}$$

Inserting the ansatz $\delta\sigma_i(t) = \delta\sigma_i \exp(i\omega t)$ in equations (4.14), we obtain for the collective modes [78]:

$$\omega_\pm^2 = \frac{A_1 + A_2 \pm \sqrt{(A_1 - A_2)^2}}{2}. \tag{4.15}$$

As shown in figure 4.8, the interaction strength $|\delta g/g|$ tends to increase the frequency of the breathing modes. Another important remark is that higher-order effects in the breathing modes are substantial [78].
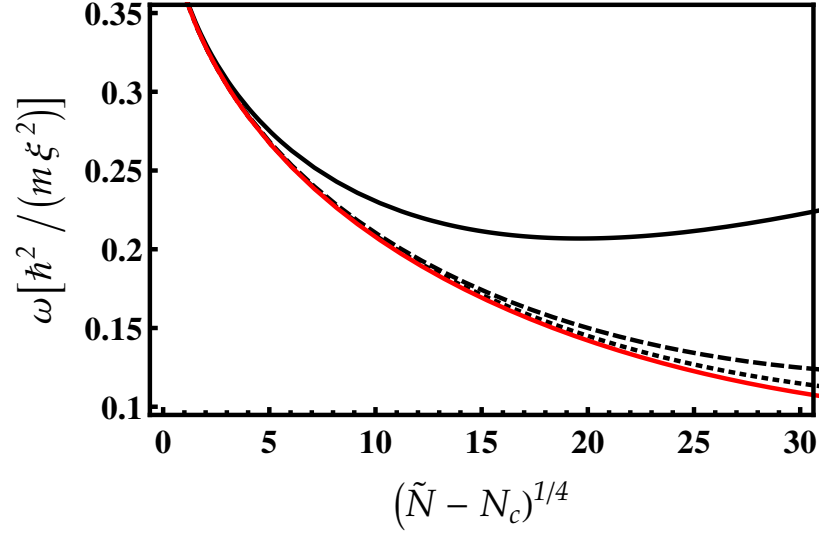
Figure 4.8: Frequencies of low-lying collective excitation modes as a function of the total atom number in units of $\tilde{N}$. Thick red line corresponding to the calculation of [44]. Black our result in the present of higher order fluctuation. Dotted line: our results for $\delta g/g = 0.05$. Dashed line: our results for $\delta g/g = 0.1$. Black solid line: our results for $\delta g/g = 0.5$.

In the next chapter we extend our results to the heteronuclear droplets for a direct comparison with recent QMC data.

Chapter 5

Dilute self-bound droplets in a heteronuclear Bose-Bose mixture

The observation of heteronuclear quantum droplets in an attractive bosonic mixture of ^{41}K-^{87}Rb and ^{23}Na-^{87}Rb has been reported most recently in [59, 60, 148]. Their properties have been also studied using DMC method and Density Functional Theory (DFT) [88]. In contrast to the homonuclear droplets, the heteronuclear self-bound liquids are very dilute since they are characterized by lower densities. They are stable long-lived structures (about three times longer than the lifetime of ^{39}K droplets). The longer lifetime and the lower three-body recombination of this exotic liquid mixture allows to observe more complex phenomena such as the self-evaporation of the droplet [44], the characterization of the incompressible regime [59], and the creation of larger droplets [88].

In this chapter we study the properties of free space self-bound quantum liquid droplets in heteronuclear Bose-Bose mixtures of ^{41}K-^{87}Rb [59], beyond the LHY de-
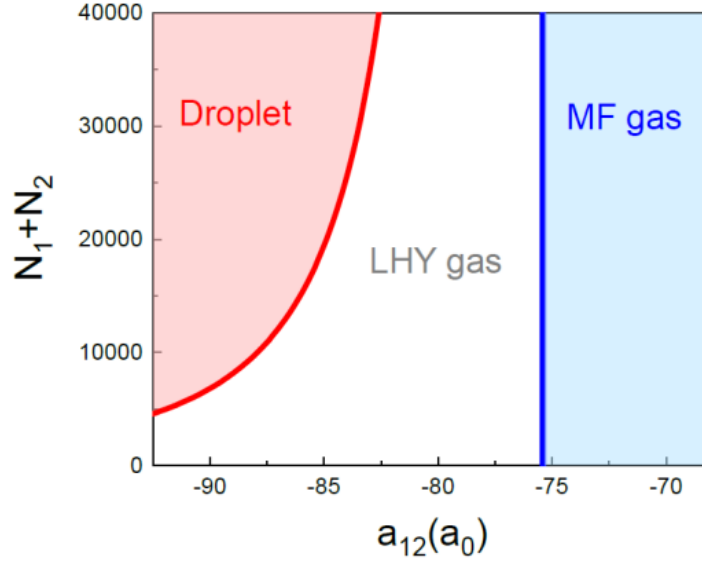
Figure 5.1: Phase diagram for the ^{41} K $- ^{87}$Rb mixture, in free space. For $a_{12} > a_{12}$ the gas is stable within the mean-field (MF) theory (the blue solid line represents the critical scattering length $a_{12} = -75.4a_0$). For $a_{12} < a_{12}$, the mean-field energy is balanced by the LHY term, giving birth to a LHY gas. For a sufficiently large atom number (the red solid line stands for the critical curve N_{cr}) and strong interactions, self-bound droplets can be formed. Figure taken from [148].

scription using our HFB theory described in preceding chapters.

A stability phase diagram of attractive of ^{41}K-^{87}Rb mixture in free space as a function of the interspecies scattering length a_{12} is shown in figure 5.1. For $\delta g > 0$, the gas is stable at the mean-field level, while for $\delta g < 0$, beyond the mean-field threshold for collapse, the mixture is stabilized by quantum fluctuations. If the number of particles is below N_{cr}, the system is a so-called LHY gas, while above N_{cr} a droplet forms [148].

We calculate in particular the ground-state energy, the equilibrium density, the surface tension, and the critical number of particles and compare them with available

DMC and DFT data. It is found that our results excellently agree with the predictions of DMC and DFT simulations [88] revealing the pertinence of our theory in capturing higher-order quantum correlations effects.

5.1 Model

We consider a homogeneous heteronuclear two-component BECs with masses m_1 and m_2 in a volume V and a total number of bosons $N = N_1 + N_2$. We recall that the energy of the system per unit volume including higher-order quantum fluctuations can be calculated through equation (2.44). Following the method outlined in [98, 149], we obtain for LHY-corrected energy:

$$\frac{E_{\text{LHY}}}{V} = \frac{16g_1\sqrt{a_1^3/\pi}}{15\sqrt{2}} n_1^{5/2} \left(1 + \frac{\tilde{m}_1 - \tilde{n}_1}{n_1}\right)^{5/2} \overline{f}\left(\frac{m_2}{m_1}, \frac{g_{12}^2}{\bar{g}_1 \bar{g}_2}, \frac{\bar{g}_2 n_{c2}}{\bar{g}_1 n_{c1}}\right), \qquad (5.1)$$

where $\overline{f}(z = m_2/m_1, x = g_{12}^2/\bar{g}_1\bar{g}_2, y = \bar{g}_2 n_{c2}/\bar{g}_1 n_{c1}) > 1$ is a dimensionless function. For homonuclear mixtures, $z = 1$, the function $\overline{f}$ reduces to $\overline{f}(1, x, y) = f^{5/2}(1, x, y) = \sum_{\pm} \left[1 + y \pm \sqrt{(1-y)^2 + 4xy}\right]^{5/2}/4\sqrt{2}$ found in Chapter 4. For $\tilde{m}_j = 0$ and $n_c \approx n$, one can reporduce the early Larsen's formula [98]. In the heteronuclear case, a simple analytical expression for $\overline{f}(z, x, y)$ is not accessible. According to Refs.[44, 150], in the region where $x \sim 1$ (i.e. $\overline{f}$ is weakly dependent on x), the expression of the dimensionless function $\overline{f}$ is given by :

$$\overline{f}(z, x, y) = \frac{15}{32} \int_0^\infty k^2 \mathcal{F}(k, z, x, y) dk, \qquad (5.2)$$

where

$$\mathcal{F}(k, z, x, y) =$$

$$\sqrt{\sqrt{\frac{1}{2}\left[k^2\left(1+\frac{y}{z}\right)+\frac{1}{4}\,k^4\left(1+\frac{1}{z^2}\right)\right]+\left[\frac{1}{4}\left[\left(k^2+\frac{1}{4}k^4\right)-\left(\frac{y}{z}k^2+\frac{1}{4z^2}k^4\right)\right]^2+x\frac{y}{z}k^4\right]^{1/2}}}$$

$$+\sqrt{\frac{1}{2}\left[k^2\left(1+\frac{y}{z}\right)+\frac{1}{4}-k^4\left(1+\frac{1}{z^2}\right)\right]-\left[\frac{1}{4}\left[\left(k^2+\frac{1}{4}k^4\right)-\left(\frac{y}{z}k^2+\frac{1}{4z^2}k^4\right)\right]^2+x\frac{y}{z}k^4\right]^{1/2}}$$

$$-\frac{1+z}{2z}k^2-(1+y)+\frac{1}{k^2}\left[1+y^2z+4xy\frac{z}{1+z}\right]. \tag{5.3}$$

The result of the numerical integration of equation (5.2) for the case of ^{41}K-^{87}Rb
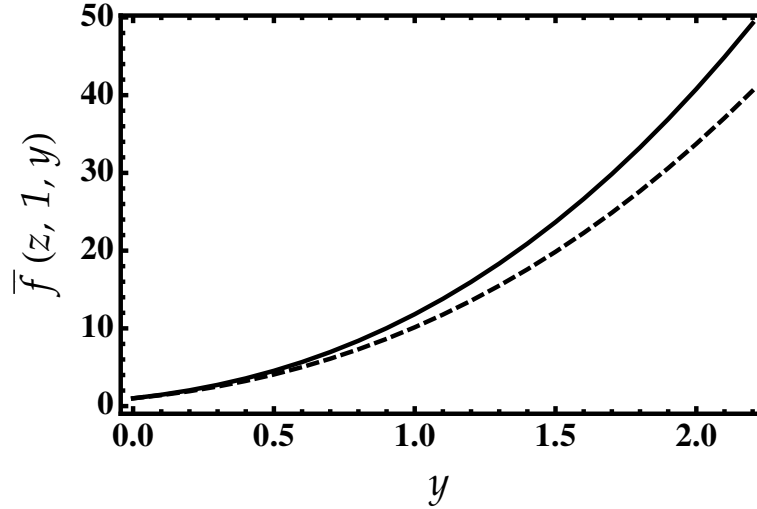
Figure 5.2: The dimensionless function $\overline{f}$ from equation (5.3) for ^{41}K-^{87}Rb mixture ($z \simeq 2.1$) and $x \sim 1$. Solid line: our predictions. Dashed line: without higher-order corrections.

mixture ($z \simeq 2.1$) with and without higher-order corrections is displayed in figure 5.2. We see that the higher-order fluctuations may increase the function $\overline{f}$ in particular for large y leading to enhance the ground-state energy and the other thermodynamic quantities. This gives rise to affect the properties of the droplet as we will see in next

sections.

At zero temperature, the noncondensed $\tilde{n} = \sum_{\pm}\sum_{\mathbf{k}} v_{\pm k}^2$ and the anomalous $\tilde{m} = \sum_{\pm}\sum_{\mathbf{k}} u_{\pm k}v_{\pm k}$ densities are given by:

$$\tilde{n} = \frac{2\sqrt{2}}{3} n_1 \sqrt{\frac{n_1 a_1^3}{\pi}} \left(1 + \frac{\tilde{m}_1 - \tilde{n}_1}{n_1}\right)^{3/2} \overline{\overline{f}}(z, x, y), \tag{5.4}$$

and

$$\tilde{m} = 2\sqrt{2}\, n_1 \sqrt{\frac{n_1 a_1^3}{\pi}} \left(1 + \frac{\tilde{m}_1 - \tilde{n}_1}{n_1}\right)^{3/2} \overline{\overline{f}}(z, x, y), \tag{5.5}$$

where $\mathcal{U}(z, x, y) > 1$ is a dimensionless function. For $z = 1$, it simplifies to $\overline{\overline{f}}(1, x, y) = f^{3/2}(1, x, y) = \sum_{\pm} \left[1 + y \pm \sqrt{(1 - y)^2 + 4xy}\right]^{3/2}/2\sqrt{2}$ [37].

Equations (5.1)-(5.5) are self-consistent that can be solved by iteration and whose solutions directly provide the desired corrections to the ground-state energy and fluctuations of the droplet.

From now on, we consider the case of a mixture of the hyperfine state $|F = 1, m_F = 1\rangle$ of ^{41} K as component 1, and the hyperfine state $|F = 1, m_F = 1\rangle$ of ^{87}Rb as component 2 [59]. The scattering parameters describing the intra-species repulsion are fixed and their values are equal to $a_1 = 65a_0$ [151], and $a_2 = 100.4a_0$ [152]. Experimentally, the interspcies interaction a_{12} varies from $-80a_0$ to $-95a_0$ [59]. Lengths are measured in units of the Bohr radius a_0, while energies are expressed in Hartree (1Ha = 27.2eV). Moreover, ^{41} K is denoted as the first species and it is labelled by the index 1 , while ^{87}Rb is the second species, labelled by the index 2 .
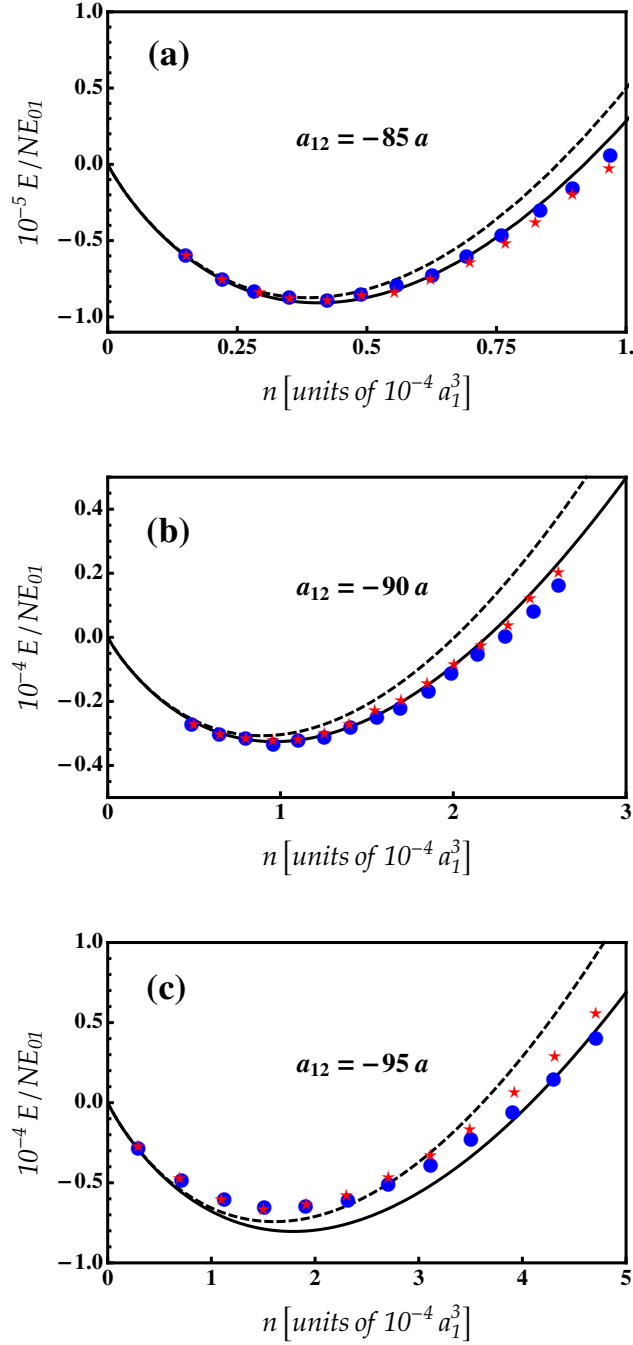
Figure 5.3: Ground-state energy $E/(NE_{01})$ as a function of the density (na_1^3) for different values of a_{12}. (a) $a_{12} = -85a_0$, (b) $a_{12} = -90a_0$, and (c) $a_{12} = -95a_0$. Dashed lines correspond to the standard Bogoliubov theory [44]. Solid lines correspond to our results up to first-order corrections of quantum fluctuations. Circles represent the DMC results corresponding to the POT-I model [88]. Stars represent the DMC results corresponding to POT-II model [88]. Here $E_{01} = \hbar^2/2m_1a_1^2$.

69

5.2 Bulk properties

In this section we analyze the bulk properties of ^{41}K-^{87}Rb mixture in the droplet regime.

5.2.1 Ground-state energy

According to the Petrov's theory [44], the stability of the mixture against fluctuations requires the condition: $n_2/n_1 = \sqrt{\bar{g}_1/\bar{g}_2}$. Therefore, the energy functional becomes effectively single-component, and can be written in terms of the total density $n = n_1 + n_2$ as:

$$\frac{E}{N} = \frac{2\pi\hbar^2 \left[2a_1 z + a_{12}\sqrt{\frac{a_1}{a_2}}z\,(1+z)\right]}{m_2 \left(\sqrt{\frac{a_1}{a_2}}z + 1\right)^2} n^2 + \frac{256\sqrt{\pi}\hbar^2 a_1^{5/2}}{15 m_1} \left(\frac{1 + z^{1/10}\sqrt{a_2/a_1}}{1 + \sqrt{\frac{a_1}{a_2}z}}\right)^{5/2} n^{5/2}$$

$$\times \left(1 + \frac{\tilde{m} - \tilde{n}}{n}\right)^{5/2}. \tag{5.6}$$

In figure 5.3 we plot the energy (5.6) and compare it with recent DMC data [88] and theoretical prediction for different values of the interspcies interactions a_{12}. DMC simulations were performed with two models of the interaction potential called POT-I and POT-II, which satisfy both scattering parameters, namely: the s-wave scattering length a and the effective range r_{eff}. This latter can be estimated from the knowledge of the Van der Waals coefficient, C_6 (for more details we refer the reader to Ref.[88]). We see that our findings agree with the theoretical predictions [44] at densities smaller than the equilibrium density, revealing the universality of our theory in such a regime. Whereas, they down-shift from the Bogoliubov results [44] at relatively higher densities due to the inclusion of the anomalous correlations (pairing effects) [13]. On the

other hand, our HFB predictions are in excellent agreement with the DMC simulations [88] for the three values of a_{12}. This proves the relevance of the beyond LHY stabilization of quantum liquid droplets in heteronuclear Bose mixtures.

5.2.2 Equilibrium density
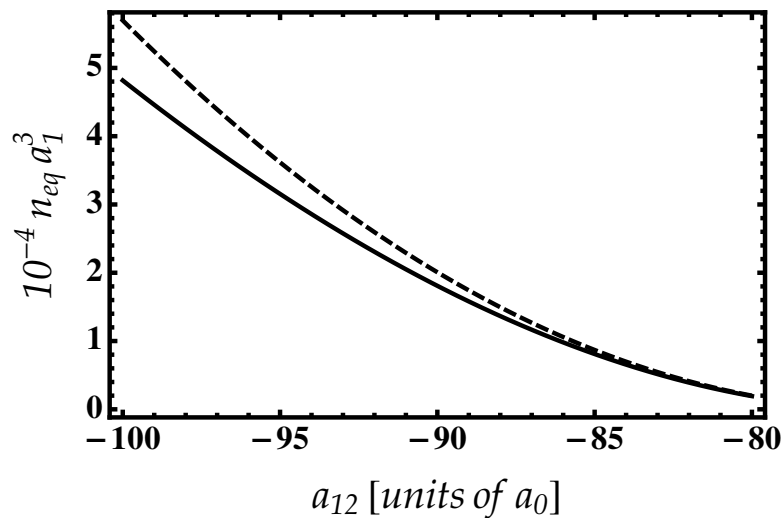
Figure 5.4: Equilibrium density of the self-bound droplet n_{eq} as a function of the interspecies scattering length a_{12}/a_0. Solid lines correspond to our results from Eq. (5.7). Dashed lines correspond to the theory of Ref.[44].

The equilibrium density of the droplet can be obtained by minimizing the energy. For analytical tractability, we retain only first-order in $\tilde{n}$ and $\tilde{m}$. This yields:

$$n_{\mathrm{eq}} = \frac{25\pi}{4096 a_1^3} \left[\frac{2 + a_{12}/a_1 \sqrt{\frac{a_1}{a_2}} z (1 + z^{-1})}{\left(\sqrt{\frac{a_1}{a_2}} z + 1 \right) f(z, 1, \sqrt{\bar{g}_2/\bar{g}_1})} \right]^2 . \tag{5.7}$$

The behavior of the equilibrium density is displayed in Fig.5.4. We see that our results improve those obtained from the standard Bogoliubov approach. Another important

remark is that beyond a certain critical value of a_{12}, the equilibrium density tends to zero and hence, the liquid evaporates. The reason is that the interspecies interactions are not strong enough to balance the LHY repulsion even they are attractive therefore, the droplet cannot preserve its self-bound character.

5.2.3 Compressibility

Another interesting thermodynamic property that we can get is the compressibility, which measures the relative change of volume as a consequence of a pressure variation at constant temperature. The inverse of the compressibility is defned as:

$$\kappa^{-1} = -V \frac{\partial P\,(n_1, n_2)}{\partial V} = -V \sum_{i=1,2} \frac{\partial n_i}{\partial V} \frac{\partial P}{\partial n_i} = \sum_{i=1,2} n_i \frac{\partial P}{\partial n_i}, \tag{5.8}$$

where the pressure is defined as: $P = -E + \sum_j n_j (\partial E / \partial n_j)$.

Computing the derivatives of the total pressure

$$\begin{aligned}
\frac{\partial P}{\partial n_1} &= g_1 n_1 + g_{12} n_2 + n_1 \frac{\partial^2 E_{\mathrm{LHY}}}{\partial n_1^2} + n_2 \frac{\partial^2 E_{\mathrm{LHY}}}{\partial n_1 \partial n_2}, \\
\frac{\partial P}{\partial n_2} &= g_2 n_2 + g_{12} n_1 + n_1 \frac{\partial^2 E_{\mathrm{LHY}}}{\partial n_1 \partial n_2} + n_2 \frac{\partial^2 E_{\mathrm{LHY}}}{\partial n_2^2},
\end{aligned} \tag{5.9}$$

and exploiting equation (5.1)

$$\begin{aligned}
\frac{\partial^2 E_{\mathrm{LHY}}}{\partial n_1^2} &= \frac{16 g_1 \sqrt{a_1^3/\pi}}{15\sqrt{2}} \left(1 + \frac{\tilde{m}_1 - \tilde{n}_1}{n_1}\right)^{5/2} \left[\frac{15}{4} n_1^{1/2} \overline{f} + 5 n_1^{3/2} \frac{\partial \overline{f}}{\partial n_1} + n_1^{5/2} \frac{\partial \overline{f}^2}{\partial n_1^2}\right], \\
\frac{\partial^2 E_{\mathrm{LHY}}}{\partial n_2^2} &= \frac{16 g_1 \sqrt{a_1^3/\pi}}{15\sqrt{2}} \left(1 + \frac{\tilde{m}_1 - \tilde{n}_1}{n_1}\right)^{5/2} \left[n_1^{5/2} \frac{\partial \overline{f}^2}{\partial n_2^2}\right], \\
\frac{\partial^2 E_{\mathrm{LHY}}}{\partial n_1 \partial n_2} &= \frac{16 g_1 \sqrt{a_1^3/\pi}}{15\sqrt{2}} \left(1 + \frac{\tilde{m}_1 - \tilde{n}_1}{n_1}\right)^{5/2} \left[n_1^{3/2} \frac{\partial \overline{f}}{\partial n_2} + n_1^{5/2} \frac{\partial \overline{f}}{\partial n_1 \partial n_2}\right],
\end{aligned} \tag{5.10}$$

one finds for the inverse compresibility of an homogeneous Bose-Bose mixture with the addition of the higher-order corrections:

$$\kappa^{-1} = \left(g_1 n_1^2 + g_2 n_2^2 + 2 g_{12} n_1 n_2 + \frac{15}{4} E_{\mathrm{LHY}}\right)^{-1}, \tag{5.11}$$

where n_1 and n_2 are the equilibrium densities of the homogeneous system computed in the previous subsection and E_{LHY} is given by equation (5.6).

As is seen form figure 5.5, the inverse compressibility κ^{-1} is higher compared to that predicted from the standard Bogoliubov theory [44] due to relatively smaller values of effective ranges in a ^{41}K-^{87}Rb mixture [88] on the one hand, and owing to the higher-order quantum effects on the other. This makes our results in good agreement with the QMC-based functional POT-I of Ref.[88].
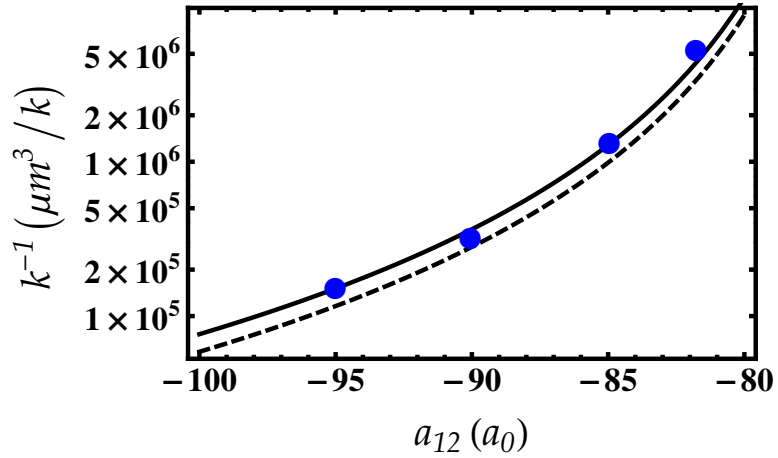
Figure 5.5: Inverse compressibility κ^{-1} as a function of the interspecies scattering length a_{12}/a_0 in the self-bound droplet regime. Solid lines corresponds to our HFB results up to first-order corrections. Dashed lines correspond to the standard Bogoliubov theory of [44]. Circles represent the QMC results corresponding to the POT-I model [88]

5.3 Surface tension

The surface tension is a relevant parameter in a liquid droplet that governs its existence, stability, and equilibrium shape. The appearance of self-bound droplets in bosonic mixtures implies the existence of a surface and a surface tension associated to it. The surface tension of the planar interface consists of assuming an infinite homogeneous system along the xy-plane and we study the density profile along the z-axis (i.e. use a slab geometry) [88]. Given the liquid-like nature of this self-bound droplet, we rewrite the energy density E of the mixture in terms of density n_1 using the assumption $n_2/n_1 = \sqrt{g_1/g_2}$ [44]:

$$E = \alpha \frac{\left(\nabla \sqrt{n_1}\right)^2}{n_1} + \beta n_1^2 + \gamma n_1^{5/2}(1 + \lambda \sqrt{n_1})^{5/2}, \tag{5.12}$$

where

$$\alpha = (\hbar^2/8m_1^2)\left(1 + z^{-1}\sqrt{g_1/g_2}\right),$$

$$\beta = g_1 + g_{12}\sqrt{g_1/g_2},$$

$$\gamma = \frac{8}{15\pi^2}\left(\frac{m_1}{\hbar^2}\right)^{3/2} g_1^{5/2} f\left(z, 1, \frac{\bar{g}_2}{\bar{g}_1}\right),$$

$$\lambda = 1 + \frac{4}{3\sqrt{\pi}}\left(\frac{1 + \sqrt{a_2 z^{-1}/a_1}}{1 + \sqrt{a_2 z^{-1}/a_1}}\right)^{3/2}.$$

The surface tension of the planar interface represented by the energy functional (5.12) can be evaluated using the integral [88, 153]

$$\sigma = 2\int_0^{n_{\text{eq}}} dn_1 \sqrt{\alpha(\beta n_1 + \gamma n_1^{3/2}(1 + \lambda \sqrt{n_1})^{5/2} - \mu_0)}, \tag{5.13}$$

where $\mu_0 = \beta n_{n_{\text{eq}}} + \gamma n_{n_{\text{eq}}}^{3/2}(1 + \lambda \sqrt{n_{n_{\text{eq}}}})^{5/2}$ is the chemical potential of a droplet in the equilibrium, evaluated at the equilibrium density n_{eq}.

The corresponding density profile can be obtained via:

$$z = z_0 + \int_{n_{eq}/2}^{n} dn' h(n'), \qquad (5.14)$$

where

$$h(n) = -\sqrt{\frac{\alpha}{n}(\beta n^2 + \gamma n^{5/2}(1 + \lambda\sqrt{n})^{5/2} - \mu_0 n)},$$

with $n \in [0, n_{eq}]$. Here the minus sign indicates that density profile is decreasing from bulk to vacuum.

Evidently, equations (5.13) and (5.14) for the surface tension and the density profile extend naturally those of Refs.[88, 153]. The results of their numerical integration are shown in figures 5.6 and 5.7.
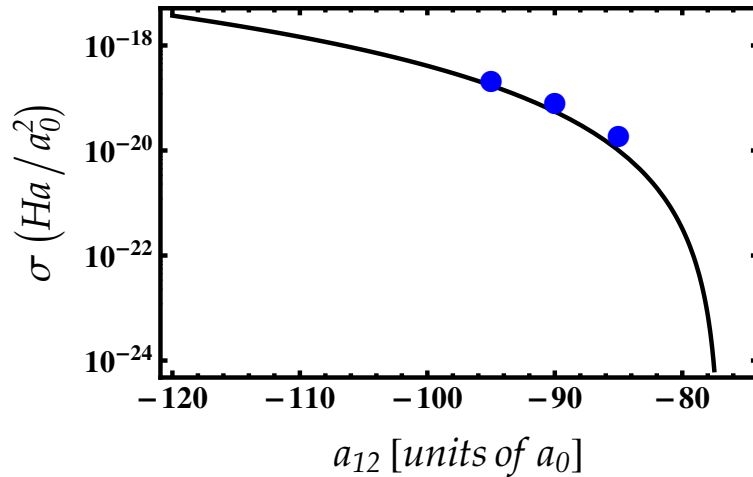
Figure 5.6: Surface tension (on the logarithmic scale) as a function of the interspecies scattering length a_{12}/a_0. Solid line corresponds to our results. Circles represent the QMC results corresponding to the POT-I model [88].

Figure 5.6 illustrates the comparison between the obtained surface tension (5.13) and the QMC-based functional POT-I of Ref.[88]. The surface tension axis is on

the logarithmic scale in order to well emphasize its rate of change as a function of the interspecies interactions. We observe that our findings agree well with QMC calculations [88] in the whole range of a_{12}/a_0.

The density profiles (5.14) for different values of a_{12} are reported in Fig.5.7. We see that the presence of the higher-order effects leads to decrease the density of the droplet as foreseen above.

5.4 Critical number of atoms

In a dilute quantum liquid the density gradient at the surface acts as a surface tension that enters the GGP equation in the kinetic energy terms. If the surface tension shifts the total energy from negative to positive, then the system cannot be self-bound anymore and the ground-state is a gas: the kinetic energy can thus drive to a liquid-to-gas phase transition. As a result, not all values of the total number of atoms N are allowed for droplet formation: small droplets with N lower than a critical value N_{cr} are unstable. So, to determine the critical number of atoms N_{cr} for a given value of a_{12}, we can use a variational method. The assumed density profile of the first component of the mixture is of the form:

$$n_1(r) = \frac{N_1}{\pi^{3/2}\sigma^3} e^{-\frac{r^2}{\sigma^2}}, \tag{5.15}$$

where the variance σ plays the role of variational parameter. This ansatz describes a so-called "surface" droplet, since the density profile feels a dominant contribution from surface rather than from the bulk region that is not extended in space: this represents a good approximation of what happens near the evaporation threshold.
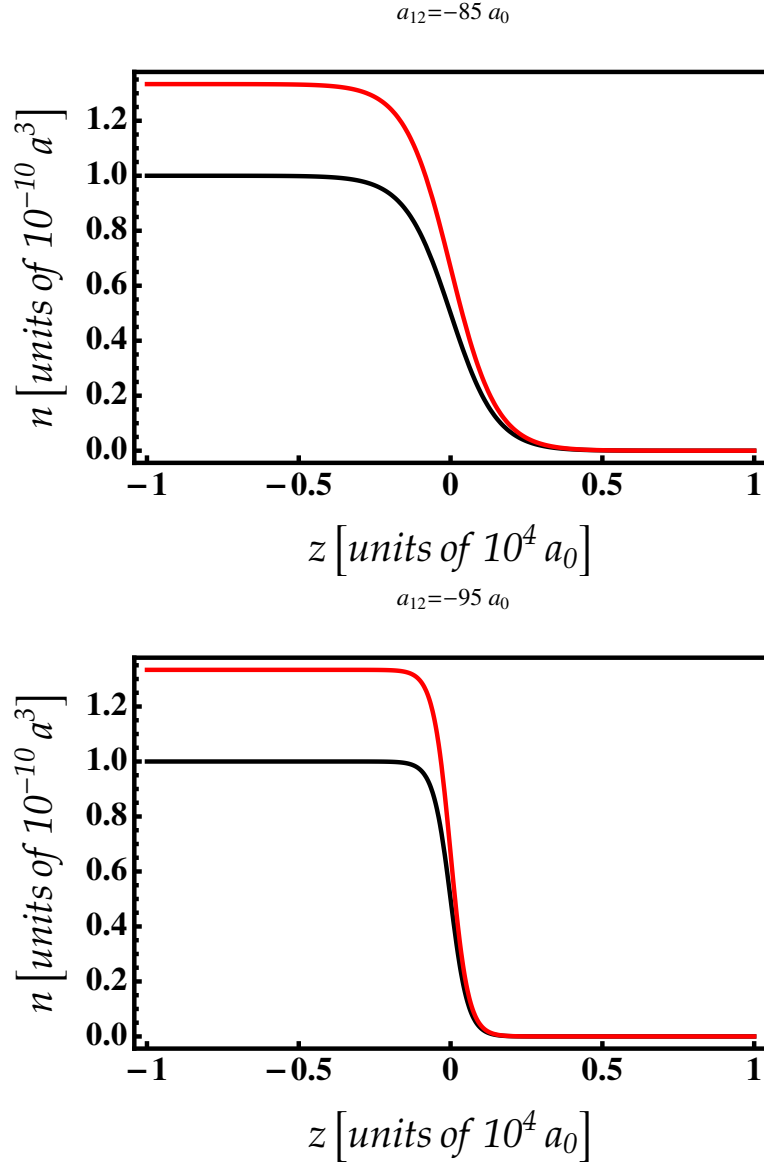
Figure 5.7: Density profile along the z-direction (a) $a_{12} = -85a_0$, (b) $a_{12} = -95a_0$. Red lines: our predictions. Black lines: standard results without higher-order corrections.

Inserting the ansatz (5.15) into equation (5.12), the effective single-component energy per particle turns out to be given:

$$\frac{E}{N_1} = \frac{6\alpha}{\sigma^2} + \frac{\beta}{(2\pi)^{3/2}}\frac{N_1}{\sigma^3} + \int dr\gamma n_1^{5/2}(1+\lambda\sqrt{n_1})^{5/2}. \qquad (5.16)$$

For a fixed value of a_{12}, we are interested in the pair of parameters $(\sigma_0, N_{1,\mathrm{cr}})$ for which the conditions $\partial(E/N_1)/\partial\sigma = 0$ (for a minimum) and $E/N_1 = 0$ (gives the line separating stable droplets with negative total energy from unstable ones with positive energy) must be fulfilled [88].
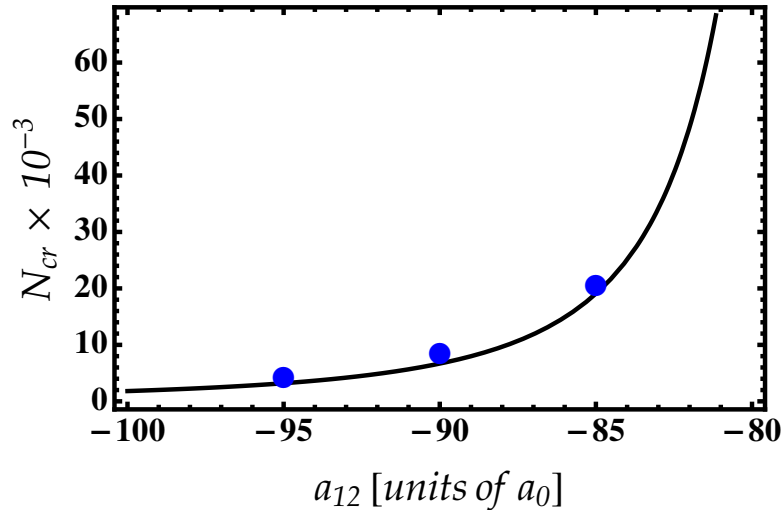
Figure 5.8: Critical atom number N_{cr} as a function of the interspecies scattering length a_{12}/a_0. Solid line corresponds to our results. Circles represent the QMC results corresponding to the POT-I model [88].

In the presence of higher-order fluctuations, the above system cannot be solved analytically. Therefore, we solve it numerically with respect to σ, for the critical total number of atoms $N_{\mathrm{cr}} = N_{1,\mathrm{cr}}\left(1 + \sqrt{\bar{g}_1/\bar{g}_2}\right)$. We then compare our results with the QMC data of [88]. Figure 5.8 shows that the critical atom number obtained from

our HFB theory is in perfect agreement with the QMC simulations of [88] due to the effects of higher-order quantum correlations.

Chapter 6

Self-bound droplets at finite temperature

6.1 Introduction

The finite-temperature properties of quantum liquid droplets in both dipolar BECs and binary Bose mixtures remains largely unexplored owing to the intriguing self-evaporation feature of quantum droplets. Dipolar quantum droplets at finite temperature have been recently analyzed in the presence of a harmonic trap potential [75, 74]. For self-bound droplets in dual BECs, the bulk properties (of an infinitely large droplet) at finite temperature have been discussed most recently [76, 77, 78, 73, 49, 72, 79]. A finite-temperature phase diagram as a function of the number of particles has been determined recently for ultradilute droplets in a mixture of BECs [154].

As a self-bound object, the energy of single-particle/collective excitations is bounded

from above by the particle-emission threshold making the droplet automatically lose its thermal energy and hence reach zero temperature [44]. The experimental observation of this is still challenging. It has been argued that the self-evaporation efficiency of Bose droplets at low temperature can be considerably reduced similarly to the case of helium nano-droplets [155]. Therefore, the experimentally observed binary liquid mixtures might have a low but nonzero temperature in the realistic time-scale of experiments [56, 57, 22].

In this chapter, we study the finite-temperature structure and collective excitations of both homonuclear and heteronuclear self-bound Bose droplets utilizing our time-dependent HFB theory presented in previous chapters. We compute in particular the free energy, the critical temperature and precisely determine the thermal equilibrium density of the droplet. We then derive a finite-temperature GGP equation in a self-consistent fashion from our formalism taking into account higher-order quantum and thermal corrections under the local density approximation. The density profiles and the collective oscillations are also calculated for different values of temperature by numerically and variationally solving the developed GGP equation. We find that the droplet destabilizes when the temperature becomes slightly larger than the ground-state energy of the droplet, in good agreement with recent results inferred from the macroscopic approach [76] and the pairing theory [77].

For the heteronuclear droplet, it is pointed out that the self-bound droplet remains robust even for relatively large thermal fluctuations in contrast to the homonuclear case. This might lead to a possible long-lived droplet. For sufficiently large thermal fluctuations, the droplet becomes unstable and eventually destroys.

6.2 Homonuclear self-bound droplets

6.3 Bulk properties

Let now discuss how the temperature affects the stability of a homonuclear symmetric self-bound droplet in a binary Bose-Bose mixture with attractive interspecies interactions on the verge of mean-field collapse. The free energy functional can be computed from equation (2.56). In terms of the small parameter of the theory $na^3 \ll 1$, it could take the form [78]

$$\frac{F}{NE_0} = \frac{E}{NE_0} - \frac{8\sqrt{\pi}}{675}(na^3)^{1/6}\left(1 + \frac{\tilde{m} - \tilde{n}}{n}\right)^{-3/2}\sum_{\pm}\left(\frac{\delta a}{a}\right)_{\pm}^{-3/2}\left(\frac{T}{E_0}\right)^4, \qquad (6.1)$$

where E is given in equation (4.1). In the limit of lower density $n \to 0$, the thermal corrections to the free energy diverge as $n^{-3/2}$ and vanish at zero temperature. A similar formula has been derived in Ref.[76] using the beyond-LHY theory, based on the calculation of second-order terms in the Bogoliubov phonon modes. At $T = 0$ and for $\tilde{m} = \tilde{n} = 0$, the free energy (6.1) reproduces the analytical expression for the ground-state energy [44]. The lowest thermal approximation ($\tilde{m} = \tilde{n} = 0$) implies that F reduces to its standard form (i.e. without higherorder corrections).

The iterative solutions of equation (6.1) up to second-order for several values of temperature and interspecies interactions are shown in figure 6.1. We see that below a certain critical temperature $T < T_c \simeq 1.3 \times 10^{-4}E_0$, the free energy exhibits a local maximum which corresponds to an unstable droplet, and a local minimum supporting a higher density stable self-bound solution. The two solutions disappear at the critical temperature ($T = T_c \simeq 1.3E_0$) at which the thermal fluctuations compensate the repulsive quantum fluctuations indicating that the liquid-like droplet

starts to evaporate. This value is greater by $\sim 23\%$ than the threshold temperature obtained in Refs.[77, 76] owing to the higher-order beyond-LHY corrections. At higher temperatures ($T \simeq 1.5 \times 10^{-4} E_0$), the self-bound droplet is completely evaporated due to the strong thermal fluctuations. Another important remark is that the higher-order correlations may lead shift the critical temperature.
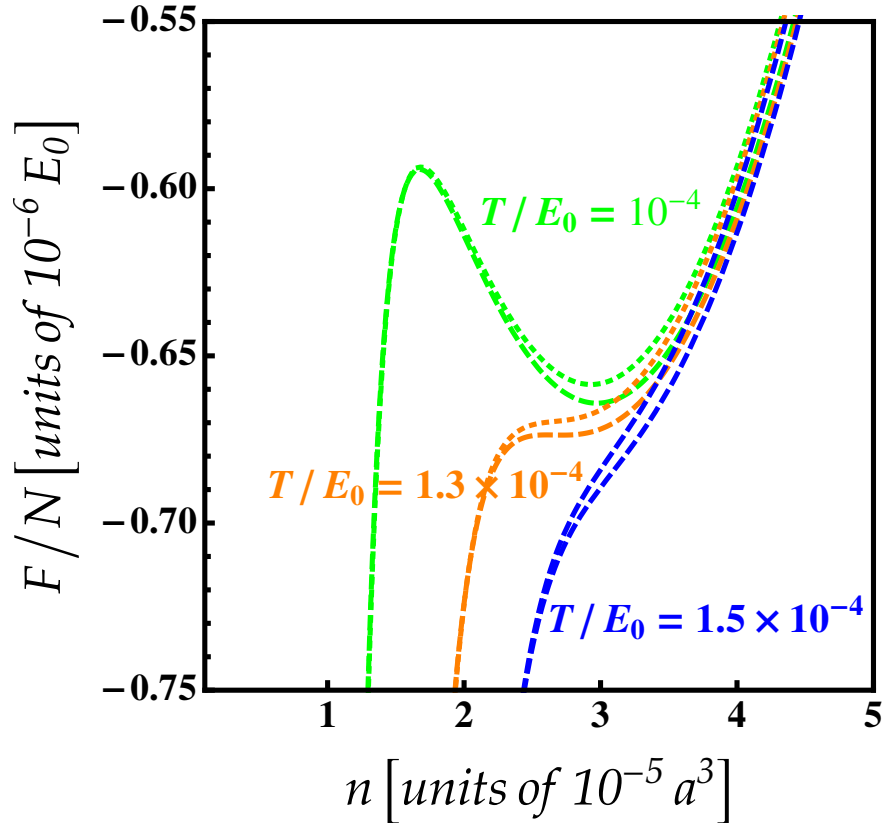
Figure 6.1: Free energy as a function of the density for $a_{12} = -1.1a$ at different values of temperature. Dashed lines are our results up to first-order in $\tilde{m}$ and $\tilde{n}$. Solid lines are our results up to the second-order in $\tilde{m}$ and $\tilde{n}$.

A useful analytical expression for the critical temperature above which the droplet destabilizes can be extracted by minimizing the free energy (6.1) with respect to the

density. This yields

$$\frac{T_c}{E_0} = 0.0114 \left(\frac{\delta a}{a}\right)_+^2 \left[72 + 25 \left(\frac{\delta a}{a}\right)_+\right]^{1/4}. \tag{6.2}$$
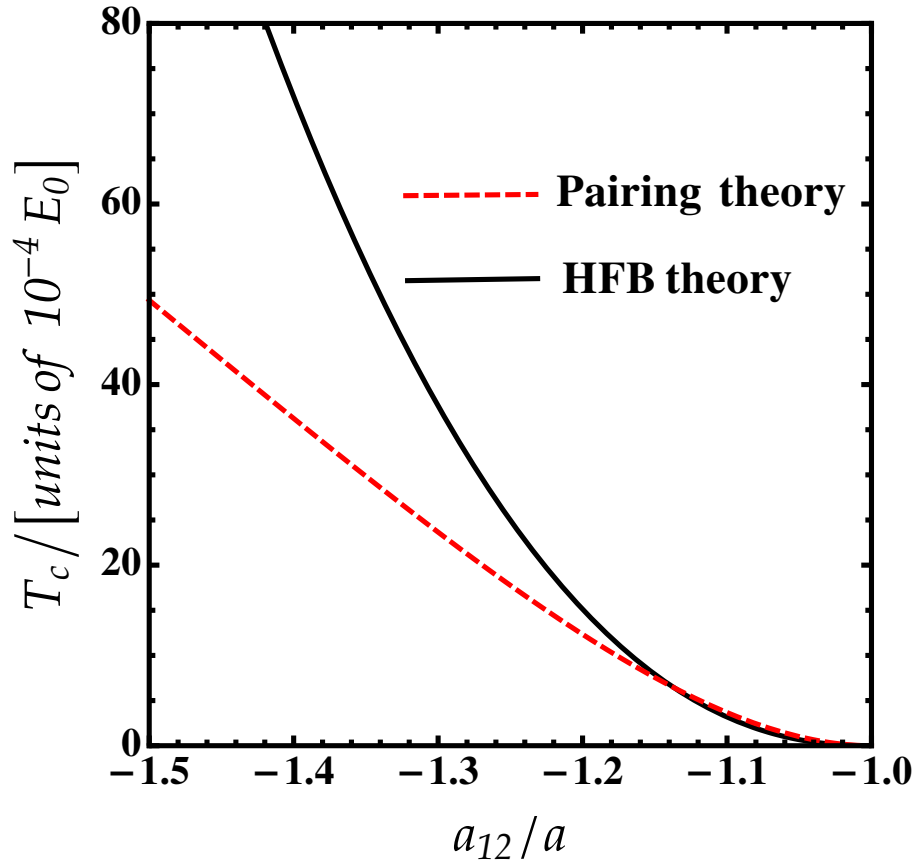
Figure 6.2: Critical temperature T_c of a droplet as a function of the interspecies interaction strength a_{12}/a.

In figure 6.2 we plot the critical temperature from Eq.(6.2) and compare it with the results of Ref.[77]. We observe that T_c decreases with decreasing the ratio $|a_{12}/a|$. Our findings agree with the pairing preditions only for small $|a_{12}/a|$ and then both theories diverge from each other on account of the higher-order contribution of the anomalous correlations.
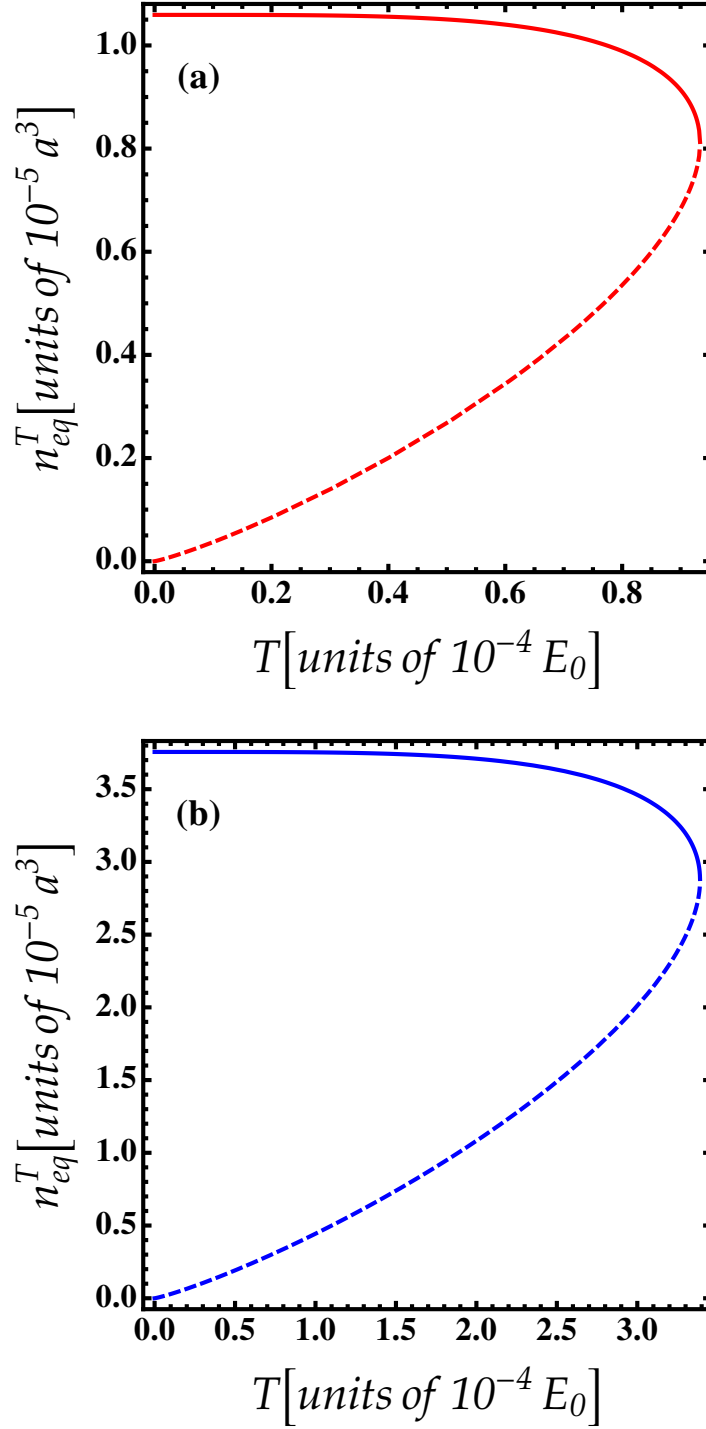
Figure 6.3: Thermal equilibrium density n_{eq}^T as a function of the temperature for (a) $a_{12} = -1.05a$ and (b) $a_{12} = -1.1a$. The dashed lines correspond to the unphysical solution, in which the droplet becomes mechanically unstable with $\partial F / \partial n < 0$.

In figure 6.3 we show the temperature dependence of the thermal equilibrium density for two values of interspecies interaction strength $a_{12} = -1.05a$ and $a_{12} = -1.1a$. We distinct in general two solutions for n_{eq}^T when the temperature gets higher. The first one (dashed lines) corresponds to the unphysical solution, in which the droplet becomes mechanically unstable, and hence should be ignored. It is clearly visible from the upper branch (stable solutions) that the thermal equilibrium density slightly lowers with temperature. Therefore, it exhibits a relatively weak temperature dependence near the critical region. For example for $a_{12} = -1.05a$ and at $T \leq 7 \times 10^{-5}E_0$, n_{eq}^T remains almost unchanged by the increase in temperature in good agreement with the result of the pairing theory [77]. The same behavior holds true for $a_{12} = -1.1a$ but with different values of T.

6.3.1 Finite-temperature generalized GP equation

To address the finite-temperature properties of a finite-size Bose droplet, we derive the finite-temperature version of the extended GP equation. Using the rescaled quantities defined in chapters 3 and 4, and upon inserting expressions of $\tilde{m}$ and $\tilde{n}$ up to the second-order, we obtain for the dimensionless free energy functional

$$\mathcal{F}(\phi, \phi^*) = \frac{1}{2}|\nabla \phi|^2 - \frac{3}{2}|\phi|^4 + \alpha|\phi|^5(1 - |\phi|)^{5/2} + \alpha^{\mathrm{T}}|\phi|, \qquad (6.3)$$

where $\alpha^{\mathrm{T}} = -(4/9)\sqrt{a^3 n_0/\pi}(\delta g/g)_+^{-1/2}(T/4a^3 n_0 E_0)^2$. Employing again variational equation $i\partial\phi/\partial t = \partial\mathcal{F}/\partial\phi^*$, we get the following finite-temperature GGP equation [78]:

$$i\frac{d\phi}{d\tilde{t}} = \left\{-\frac{1}{2}\Delta_{\tilde{\mathbf{r}}} - 3|\phi|^2 + \frac{5}{2}[1 + \alpha|\phi|(1 + \alpha|\phi|)^{3/2}]^{5/2}|\phi|^3 + \frac{5}{2}\alpha^{\mathrm{T}}|\phi|^{-1}\right\}\phi, \qquad (6.4)$$

For $\alpha^{\mathrm{T}} = 0$, equation (6.4) reduces to equation (4.6) derived in chapter 4. For $\alpha = \alpha^{\mathrm{T}} = 0$, one recovers the standard dimensionless GGP equation used earlier by Petrov [44].

6.3.2   Density profiles
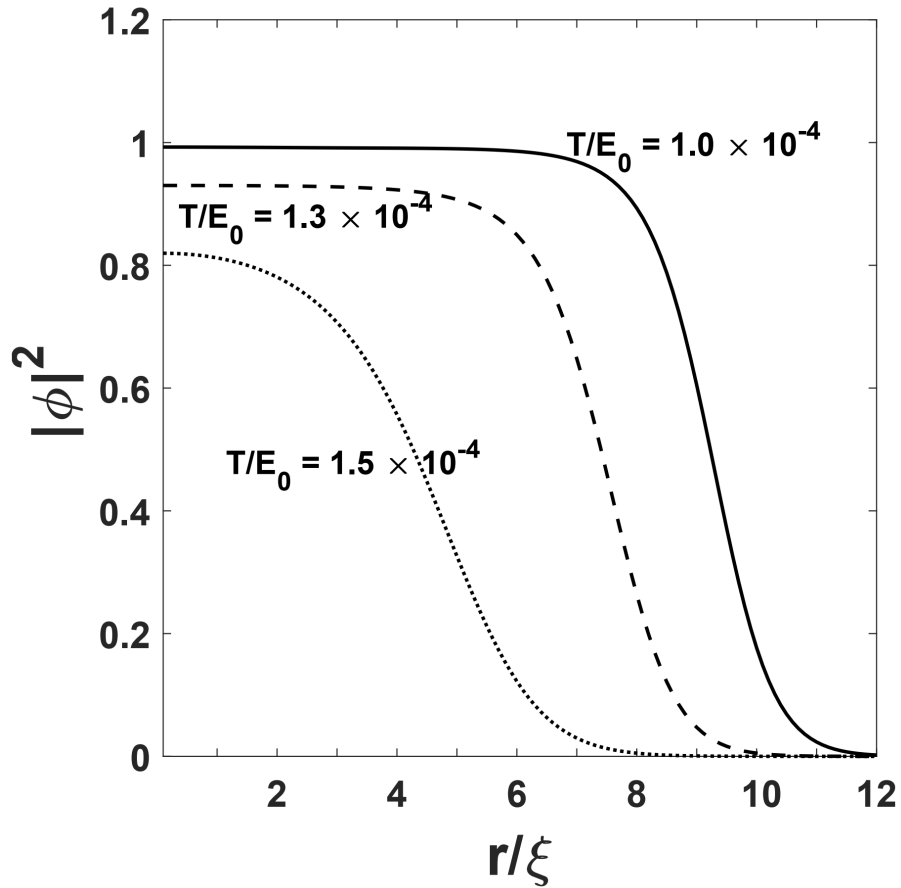
Figure 6.4: Density profile of the self-bound droplet at different values of temperature for $g_{12}/g = -1.1$.

We solve numerically the stationnary equation (6.4) employing the same imaginary time propagation technique described in chapter 4. The corresponding results are

captured in figure 6.4. It is readily seen that the droplet exhibits a flat-top profile at the equilibrium (i.e. at $T < T_c$). As the temperature increases, a dramatic change in the shape of the spatial density profile is observed where the condesate is Gaussian-like shape at $T \geq T_c$. This signals the evaporation of the droplet to the gas state as is foreseen above.

6.3.3 Collective modes

To calculate analytically the collective modes of the self-bound droplet at finite temperature, we employ the variational method aforementioned in Chapter 4. The extended Lagrangian density can be written as:

$$\mathcal{L} = \frac{i}{2} \left(\phi^* \frac{\partial \phi}{\partial \tilde{t}} - \phi \frac{\partial \phi^*}{\partial \tilde{t}} \right) - \mathcal{F}(\phi, \phi^*). \tag{6.5}$$

Inserting the Gaussian ansatz (4.7) into equation (6.5). Subsequent integration over the space variable $L = \int d^3 r \mathcal{L}$ yields the finite-temperature Lagrangian

$$L = \left[-2\tilde{N}(\sigma\dot{\beta} - 2\sigma^2\beta^2) + \frac{\tilde{N}}{2\sigma^2} - \frac{\sqrt{2}}{3\pi^{3/2}}\frac{\tilde{N}}{\sigma^3} - \frac{8\sqrt{2/5}}{27\pi^{9/4}}\frac{\tilde{N}^{3/2}}{\sigma^{9/2}} - \frac{4\sqrt{2/5}}{18\pi^3}\frac{\tilde{N}}{\sigma^6}\alpha \right.$$
$$\left. - \frac{4\sqrt{2}\sigma^2}{3\pi^3}\alpha^T \right]. \tag{6.6}$$

The Euler-Lagrange equations $\frac{d}{dt}\frac{dL}{d\dot{U}} - \frac{dL}{dU} = 0$ gives the following system:

$$\beta = \frac{\dot{\sigma}}{2\sigma}, \tag{6.7}$$

and

$$\ddot{\sigma} = -\frac{dV_{\text{eff}}(\sigma)}{d\sigma}, \tag{6.8}$$

where the effective potential is given by:

$$V_{\text{eff}}(\sigma) = -\frac{\tilde{N}}{2\sigma^2} + \frac{\sqrt{2}}{3\pi^{3/2}}\frac{\tilde{N}}{\sigma^3} + \frac{8\sqrt{2/5}}{27\pi^{9/4}}\frac{\tilde{N}^{3/2}}{\sigma^{9/2}} + \frac{4\sqrt{2/5}}{18\pi^3}\frac{\tilde{N}}{\sigma^6}\alpha + \frac{4\sqrt{2}\sigma^2}{3\pi^3}\alpha^T. \tag{6.9}$$

88

The breathing modes can be found by inserting the decomposition $\sigma(t) = \sigma + \delta\sigma(t)$ (with $\delta\sigma(t) = \delta\sigma\, e^{i\omega t}$ and $\delta\sigma \ll \sigma$) into equation (6.9) and expanding the effective potential into a Taylor series.

Frequencies of the low-lying collective modes are determined by linearizing equation (6.9) around the equilibrium positions. We then insert the decomposition $\sigma = \sigma_0 + \delta\sigma$ into equation (6.9) and expand the effective potential into a Taylor series, we get

$$V_{\text{eff}}(\sigma_0, \delta\sigma) = V_{\text{eff}}(\sigma_0) + \begin{pmatrix} \delta\sigma \end{pmatrix} \begin{pmatrix} A_1^T \\ A_2^T \end{pmatrix} \begin{pmatrix} \delta\sigma \end{pmatrix}, \tag{6.10}$$

where

$$A_1^T = 1 - \frac{6}{\sigma_0^4} + \frac{3\tilde{N}}{\sigma_0^5} + \frac{6\tilde{N}^{3/2}\alpha}{\sigma_0^{3/2}} + \frac{6\tilde{N}\alpha^T\sigma_0^{1/2}}{3\sqrt{2}},$$

$$A_2^T = +\frac{\tilde{N}}{\sigma_0^5} + \frac{15\tilde{N}^{3/2}}{8\sigma_0^{14/2}} - \frac{\tilde{N}^{-1/2}\alpha}{8\sigma_0^{3/2}} + \frac{6\tilde{N}\alpha^T\sigma_0^{1/2}}{3\sqrt{2}}.$$

The coupled set of differential equations (4.11) can be rewritten in matrix form:

$$\begin{pmatrix} \delta\ddot{\sigma} \end{pmatrix} + \begin{pmatrix} \delta\sigma \end{pmatrix} \begin{pmatrix} A_1^T \\ A_2^T \end{pmatrix} \begin{pmatrix} \delta\sigma \end{pmatrix} = 0. \tag{6.11}$$

Substituting the ansatz $\delta\sigma(t) = \delta\sigma \exp(i\omega t)$ into equation (6.11), the collective modes turn out to be given as:

$$\omega_\pm^2 = \frac{A_1^T + A_2^T \pm \sqrt{(A_1^T - A_2^T)^2}}{2}. \tag{6.12}$$

Figure 6.5 depicts that both temperature and interactions $|\delta g/g|$ tend to increase the frequency of the breathing modes. Another important remark is that higher-order effects in the breathing modes are substantial.
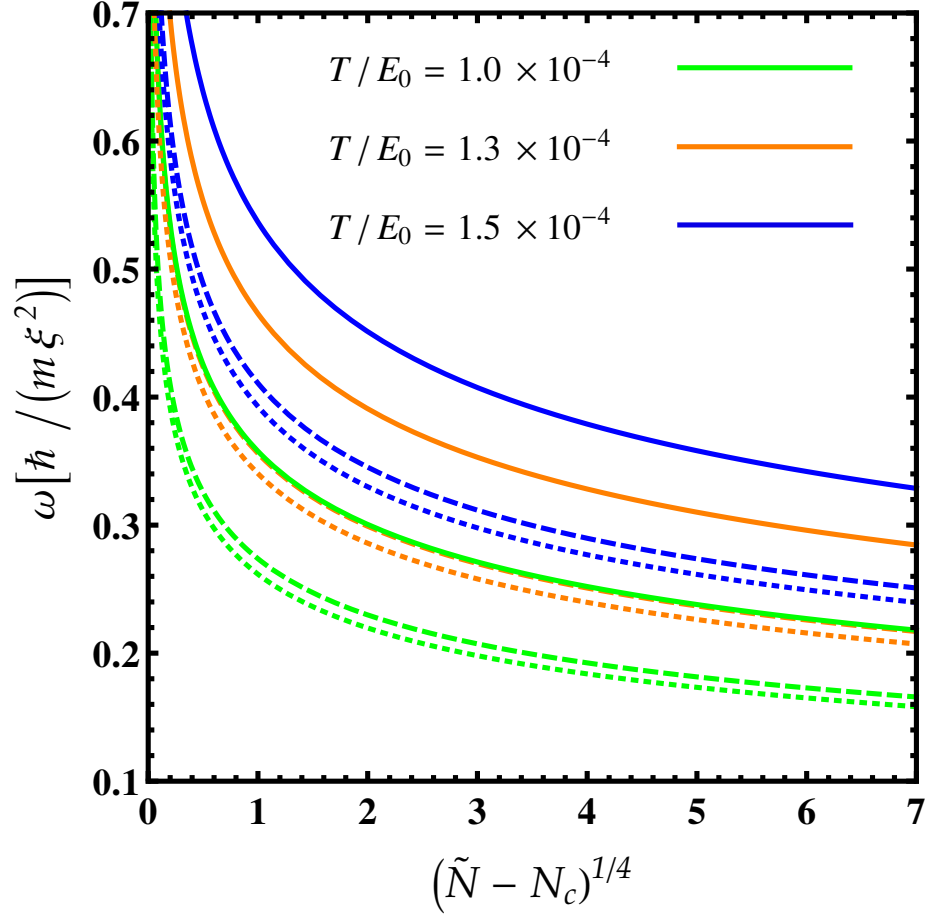
Figure 6.5: Frequencies of low-lying collective excitation modes as a function of the total atom number in units of $\tilde{N}$. Dotted line: $\delta g/g = -0.05$, dashed line: $\delta g/g = -0.1$, solid line: $\delta g/g = -0.5$.

6.4 Heteronuclear self-bound droplets

6.4.1 Thermal destabilization

We remind that in the frame of the HFB formalism, the free energy can be given as [73, 78]:

$$F = E + \frac{T}{2\pi^2} \int k^2 dk \sum_{\pm} \ln \left(\frac{2}{\sqrt{I_{k\pm} + 1}} \right), \qquad (6.13)$$

where $I_{k\pm} = \coth^2 \left(\varepsilon_{k\pm}/2T \right)$. At low temperature, the main contribution to integral (6.13) comes from the phonon branch. This yields

$$\frac{F}{V} = \frac{E}{V} - \frac{\pi^2}{90} \frac{T^4}{\hbar^3} \sum_{\pm} \frac{1}{c_{s\pm}^3}, \qquad (6.14)$$

which can be rewritten as:

$$\frac{F}{N} = \frac{E}{N} - \frac{\sqrt{2} m_1^{3/2} (g_1 n_1)^{5/2}}{45\pi^2 \hbar^3} \left(1 + \frac{\tilde{m}_1 - \tilde{n}_1}{n_1} \right)^{-3/2} \overline{f}(z, x, y)^{-1/2} \left(\frac{\pi T}{g_1 n_1} \right)^4, \qquad (6.15)$$

where the function $\overline{f}(z, x, y)$ is defined in equation (5.2) and the energy E/N is given in equation (5.6).

The presence of the normal and anomalous fluctuations in Eq.(6.15) not only ensures the convergence of the free energy but also provides higher-order corrections which may shift the critical temperature of the self-bound droplet.

The minimization of the free energy up to second-order with respect to the density is shown in Fig.6.7. We see that below a certain critical temperature $T < T_c \simeq 1.7 E_{01}$, the free energy features a local maximum, corresponding to the formation of an unstable droplet, and a local minimum supporting a higher density stable self-bound solution. The two solutions disappear at the critical temperature $(T = T_c \simeq 1.7 E_{01})$, indicating that the liquid-like droplet starts to dissolve. Importantly, this critical
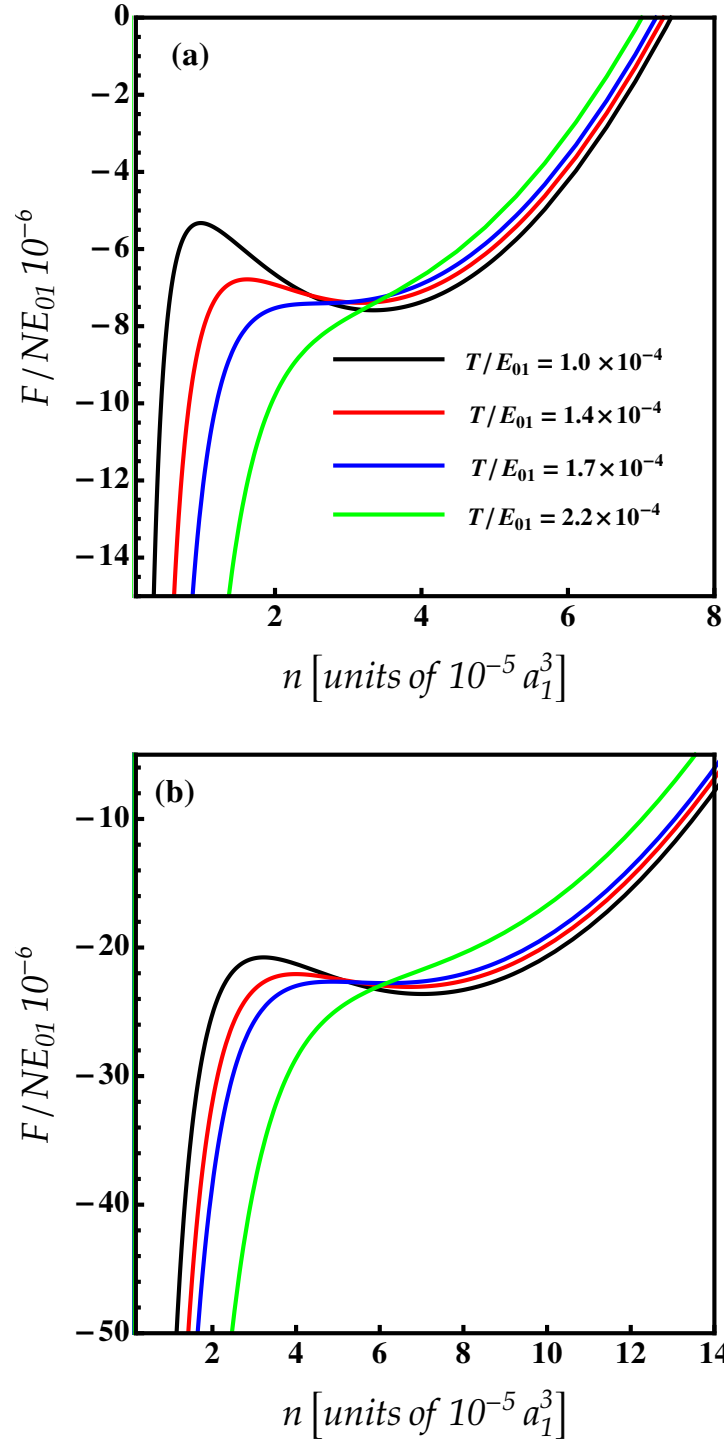
Figure 6.6: Free energy as a function of the density (na_1^3) at different values of temperature T/E_{01} for $a_{12} = -85a_0$ (a) and $a_{12} = -90a_0$ (b).
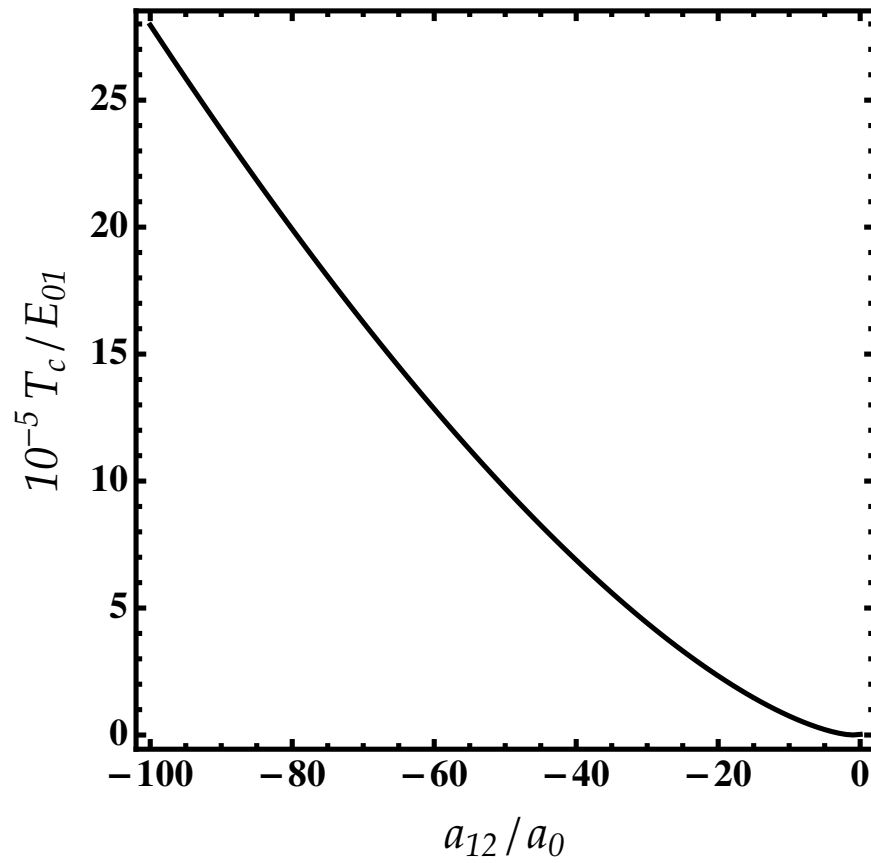
Figure 6.7: Critical temperature as a function of a_{12}/a_0.

temperature is higher than that predicted for the homonuclear droplet where T_c is somehow comparable with ground-state energy of the liquid (as is seen in figure 6.1), giving rise to the formation of long-lived droplets. This fascinating feature enables the observation of the self-evaporation mechanism. Augmenting further the temperature $(T > T_c)$, the self-bound state becomes unstable and then completely evaporates eventually.

Likewise the homonuclear case, the critical temperature T_c of self-bound state in an heteronuclear mixture is also decreasing with the interspecies interactions as shown in figure 6.7.

It is worth stressing that the experimental measurement of the predicted thermal effects of a self-bound droplet is a demanding task due to the lack of efficient thermometry at low temperatures [154].

Chapter 7

General Conclusion and outlook

7.1 Summary

In this thesis we investigated effects of higher-order quantum corrections on the properties of ultradilute self-bound droplets in both homonuclear and heteronuclear Bose-Bose mixtures using the HFB theory. This latter includes, without any subsidiary approximation, beyond mean-field corrections in the form of the LHY term. We studied the stability of such an exotic state of matter and provided an adequate treatment of its excitations and structure.

We first addressed the effects higher-order quantum corrections on the properties of a self-bound droplet in a symmetric homonuclear mixture. We derived useful formulas for the ground-state energy, the free energy, the thermal equilibrium, the normal and anomalous densities, and the critical temperature of the self-bound droplet. Our predictions have been tested against DMC data and the existing theoretical results, and excellent agreement is found revealing that higher-order effects play a key role in

the stabilization and the robustness of the droplet state. Using the HFB equation, we evaluated stationary density profiles and collective excitations of the self-bound droplet, which are important features in the experimental observation.

Furthermore, we employed our HFB equations in order to handle the bulk and surface properties of quantum droplets in a heteronuclear Bose-Bose mixture of ^{41}K-^{87}Rb in the presence of higher-order quantum and thermal corrections. We computed in particular the ground-state energy, the droplet equilibrium density, the surface tension, and the critical number of particles. Our results have been compared with recent predictions of DMC simulation and the DFT method and excellent agreement is found. The density profile of the droplet along the radial direction has been examined by means of a variational approach and a numerical scheme.

On the other hand, we discussed in this thesis the stabilization mechanism of homonuclear and heteronuclear self-quantum droplets at finite temperature. The minimization of the free energy with respect to the density reveals that the self-bound droplet evaporates itself once the temperature is above a critical value. We showed that the inclusion of higher-order quantum and thermal corrections may shift the density profiles and frequencies of the breathing oscillations. Our calculations are based on the finite-temperature GGP equation. The density profiles have been determined by numercially solving the static GGP equation, while the frequencies of the breathing modes have been obtained variationally. Our findings unveil also that a robust heteronuclear droplet can survive even for relatively large temperature compared to the homonuclear self-bound droplets. To the best of our knowledge, this study provides the first comprehensive assessment of finite-temperature effects on the gound-state properties of ultradilute heteronuclear droplet in free space.

All in all, the results acquired from this thesis could uncover valuable insights and support future experiments for many interesting phenomena such as the self-evaporation, larger droplets, superfluidity and supersolidity in self-bound droplets.

7.2   Outlook

Understanding quantum fluctuations in the self-bound droplets would open new prospects for the possible exploitation of useful entangled states and quantum information. On the other hand, the HFB theory presented in this thesis can be extended for gases of doubly-dipolar condensates, which show a rich ground-state physics of supersolids and incoherent droplet arrays.

The existence of superfluidity in quantum droplets is one of the most important open question. Since it is formed in binary BECs, one would expect that the quantum droplet keeps its superfluid character in particular in the presence of higher-order fluctuations. These latter which stem from the anomalous correlations are primordial for the occurrence of the superfluidity even for ordinary BECs [13].

In the future we plan to investigate effects of thermal and quantum flcutuations on the superfluid-supersolid quantum phase transition in dipolar and binary Bose gases. Supersolid is a fundamental phase of matter that mixes the properties of superfluids and crystals (i.e. periodic density modulation) [157, 158, 159, 160, 161, 162], and represents a set of quantum droplets that are closely connected such that the common wave function phase is preserved.

Another promising avenue which constitutes the main thrust of our future program is the investigation of droplet molecules. Such intriguing structures are bound states

of two or more individual droplets, whose existence and stability are determined by the separation and phase shift between the constituents. The physical mechanisms as well as the properties of these composite objects are different from those of usual soliton molecules.

Bibliography

[1] S.N.Bose, Z.phys. **26**, 178 (1924).

[2] A. Einstein. Zur quantentheorie des idealen gases. Sitzungsber. Preuss. Akad. Wiss., Bericht. **3**, 18 (1925).

[3] M.H. Anderson, J.R. Ensher, M.R. Matthews C.E. Wieman, E.A. Cornell, Science **269**, 198 (1995).

[4] K.B. Davis, M.O. Mewes, M. R. Andrews, N.J. Van Druten, D.S. Durfee, D.M. Kurn, W. Ketterle, Phys. Rev. Lett. **75**, 3969 (1995).

[5] C. C. Bradley, C. A. Sackett, J. J. Tollett, and R. G. Hulet, Phys. Rev. Lett. **75**, 1687 (1996).

[6] S. Chu, Rev. Mod. Phys. **70**, 685 (1998).

[7] C. N. Cohen-Tannoudji, Rev. Mod. Phys. **70**, 707 (1998).

[8] W. D. Phillips, Rev. Mod. Phys. **70**, 707 (1998).

[9] H. Shi and A. Griffin, Physics Reports. **304**, 1 (1998).

[10] F. Dalfovo, S. Giorgini, L. P. Pitaevskii, and S. Stringari, Rev.Mod. Phys. **71**, 463 (1999).

[11] L. Pitaevskii and S. Stringari, Bose-Einstein Condensation, (Oxford University Press, 2003).

[12] C. J. Pethick and H. Smith, Bose-Einstein Condensation in Dilute Gases, (second edition, Cambridge University Press, 2008).

[13] A. Boudjemâa, Degenerate Bose Gas at Finite Temperatures, (Lambert Academic Publishing, Saarbrücken, Germany, 2017).

[14] T. Lahaye et al., Rep. Prog. Phys. **72**, 126401 (2009).

[15] M. A. Baranov, Physics Reports **464**, 71 (2008).

[16] L.D. Carr, D. DeMille, R.V. Krems, and J. Ye, New. J. of Phys. **11**, 055049 (2009).

[17] M.A. Baranov, M. Delmonte, G. Pupillo, and P. Zoller, Chemical Reviews, **112**, 5012 (2012).

[18] C. J. Myatt, E. A. Burt, R. W. Ghrist, E. A. Cornell, and C. E. Wieman, Phys. Rev. Lett.**78**, 586 (1997).

[19] D. S. Hall, M. R. Matthews, J. R. Ensher, C. E. Wieman, and E. A. Cornell, Phys. Rev. Lett. **81**, 1539 (1998).

[20] P. Maddaloni, M. Modugno, C. Fort, F. Minardi, and M. Inguscio, Phys. Rev. Lett. **85**, 2413 (2000).

[21] C. R. Cabrera, L. Tanzi, J. Sanz, B. Naylor, P. Thomas, P. Cheiney, L. Tarruell, Science **359**, 301 (2018); P. Cheiney, C. R. Cabrera, J. Sanz, B. Naylor, L. Tanzi, and L. Tarruell; inarXiv: 1710.11079v1 (2017).

[22] G. Semeghini, G. Ferioli, L. Masi, C. Mazzinghi, L. Wolswijk, F.Minardi, M. Modugno, G. Modugno, M. Inguscio, and M. Fattori, arXiv:1710.10890v1 (2017).

[23] S. B. Papp, J. M. Pino, and C. E.Wieman, Phys. Rev. Lett. **101**, 040402 (2008).

[24] S. Sugawa, R. Yamazaki, S. Taie, and Y. Takahashi, Phys. Rev. A **84**, 011610 (2011).

[25] G. Modugno, M. Modugno, F. Riboli, G. Roati, and M. Inguscio, Phys. Rev. Lett. **89**, 190404 (2002); G. Thalhammer, G. Barontini, L. De Sarlo, J. Catani, F.Minardi, and M. Inguscio, ibid. **100**, 210402 (2008).

[26] D. J. McCarron, H.W. Cho, D. L. Jenkin, M. P. Köppinger, and S. L. Cornish, Phys. Rev. A **84**, 011603 (2011).

[27] A. D. Lercher, T. Takekoshi, M. Debatin, B. Schuster, R.Rameshan, F. Ferlaino, R. Grimm, and H.-C. Nägerl, Eur. Phys. J. D **65**, 3 (2011).

[28] B. Pasquiou, A. Bayerle, S. M. Tzanova, S. Stellmer, J. Szczepkowski, M. Parigger, R. Grimm, and F. Schreck, Phys. Rev. A **88**, 023601 (2013).

[29] L. Wacker, N. B. Jorgensen, D. Birkmose, R. Horchani, W.Ertmer, C. Klempt, N. Winter, J. Sherson, and J. J. Arlt, Phys. Rev. A **92**, 053602 (2015).

[30] F. Wang, X. Li, D. Xiong, and D. Wang, J. Phys. B **49**, 015302 (2016).

[31] I. Ferrier-Barbut, M. Delehaye, S. Laurent, A. T. Grier, M. Pierce, B. S. Rem, F. Chevy, and C. Salomon, Science **345**, 1035 (2014).

[32] Tin-Lun Ho and V. B. Shenoy, Phys. Rev. Lett. **77**, 3276 (1996).

[33] B. D. Esry, C. H. Greene, J. P. Burke, and J. L. Bohn, Phys. Rev. Lett. **78**, 3594 (1997).

[34] H. Pu and N. P. Bigelow, Phys. Rev. Lett. **80**, 1130 (1998).

[35] K-L. Lee, N. B. Jorgensen, I-K. Liu, L. Wacker, J. Arlt, and N. P. Proukakis, Phys. Rev. A **94**, 013602 (2016).

[36] A. Roy and D. Angom, Phys. Rev. A **92**,011601(R) (2015).

[37] A. Boudjemâa, Phys. Rev. A **97**, 033627 (2018).

[38] M. Ota, S. Giorgini, and S. Stringari, Phys. Rev. Lett. **123**, 075301 (2019).

[39] P.G. Kevrekidis, H. Nistazakis, D.J. Frantzeskakis, Boris A. Malomed, R. Carretero-González, Eur. Phys. J. D: At. Mol. Opt. Phys., **28**, 2, (2004).

[40] K. Kasamatsu, M. Tsubota, M. Ueda, Int. J. Mod. Phys. B **19**, 1835 (2005).

[41] A. Boudjemâa and K. Abbas, Phys. Rev. A, **102**, 003300 (2020).

[42] K. Abbas and A. Boudjemâa, J. Phys.: Condens. Matter, **34**, 125102 (2022).

[43] A. Boudjemâa, Phys. Lett. A **424**, 127867 (2022).

[44] D. S. Petrov, Phys. Rev. Lett. **115**, 155302 (2015).

[45] T. D. Lee, K. Huang and C. N. Yang, Phys. Rev **106**, 1135 (1957).

[46] H. Kadau, M. Schmitt, M. Wenzel, C. Wink, T. Maier, I. Ferrier-Barbut and T. Pfau, Nature **530** ,194 (2016).

[47] M.Schmitt, M. Wenzel, F.Böttcher, I. Ferrier-Barbut and T. Pfau, Nature **539**, 259 (2016).

[48] L. Chomaz, S. Baier, D. Petter, M. J. Mark, F. Wächtler, L. Santos and F. Ferlaino, Phys. Rev. X **6**, 041039 (2016).

[49] A. Boudjemâa, Phys. Rev. A **98**, 033612 (2018).

[50] A. Boudjemâa, and N. Guebli, Phys. Rev. A **102**, 023302 (2020).

[51] R.N. Bisset, L.A. Pea Ardila, and L. Santos, Phys. Rev. Lett. **126**, 025301 (2021).

[52] G. E. Volovik, The Universe in a Helium Droplet, page 27-29 (Oxford University Press, Cambridge, 2009).

[53] F. Wachtler and L. Santos, Phys. Rev. A **93**, 061603(R) (2016).

[54] D. Baillie, R. M. Wilson, R. N. Bisset, and P. B. Blakie, Phys. Rev. A **94**, 021602(R) (2016).

[55] H. Buljan, M. Segev, and A. Vardi, Phys. Rev. Lett. **95**, 180401 (2005).

[56] C. R. Cabrera, L. Tanzi, J. Sanz, B. Naylor, P. Thomas, P. Cheiney, L. Tarruell, Science **359**, 301 (2018).

[57] P. Cheiney, C. R. Cabrera, J. Sanz, B. Naylor, L. Tanzi, and L. Tarruell, Phys. Rev. Lett. **120**, 135301 (2018).

[58] G. Semeghini, G. Ferioli, L. Masi, C. Mazzinghi, L. Wolswijk, F.Minardi, M. Modugno, G. Modugno, M. Inguscio, and M. Fattori, Phys. Rev. Lett. **120**, 235301 (2018).

[59] C. D'Errico, A. Burchianti, M. Prevedelli, L. Salasnich, F. Ancilotto, M. Modugno, F. Minardi, and C. Fort, Phys. Rev. Research **1**, 033155 (2019).

[60] Z. Guo, F. Jia, L. Li, Y. Ma, J. Hutson, X. Cui, and D. Wang, Phys. Rev. Research **3**, 033247 (2021).

[61] G. Natale, R. van Bijnen, A. Patscheider, D. Petter, M. Mark, L. Chomaz, and F. Ferlaino, Phys. Rev. Lett. **123**, 050402 (2019).

[62] L. Tanzi, S. Roccuzzo, E. Lucioni, F. Fama, A. Fioretti, C. Gabbanini, G. Modugno, A. Recati, and S. Stringari, Nature **574**, 382 (2019).

[63] A.Cidrim, F. E. A. dos Santos, E. A. L. Henn, and T. Macr, Phys. Rev. A **98**, 023618 (2018).

[64] M. Caldara, F. Ancilotto, arXiv:2202.02230 (2022).

[65] G. Ferioli, G. Semeghini, L. Masi, G. Giusti, G. Modugno, M. Inguscio, A. Gallem, A. Recati and M. Fattori, Phys. Rev. Lett. **122**, 090401 (2019),

[66] F. Böttcher, J.-N. Schmidt, M. Wenzel, J. Hertkorn,M. Guo, T. Langen, and T. Pfau, Phys. Rev. X **9**, 011051 (2019),

[67] L. Tanzi, E. Lucioni, F. Fama, J. Catani, A. Fioretti, C. Gabbanini, R. N. Bisset, L. Santos, and G. Modugno, Phys. Rev. Lett. **122**, 130405 (2019),

[68] L. Chomaz, D. Petter, P. Ilzhofer, G. Natale, A. Trautmann, C. Politi, G. Durastante, R. M. W. V. Bijnen, A. Patscheider, M. Sohmen, et al., Phys. Rev. X **9**, 021012 (2019).

[69] R. Sachdeva, M. N. Tengstrand, S. M. Reimann, Phys. Rev. A **102**, 043304 (2020).

[70] D. S. Petrov and G. E. Astrakharchik, Phys. Rev. Lett. **117**, 100401 (2016).

[71] D. Edler, C. Mishra, F. Wächtler, R. Nath, S. Sinha, and L. Santos, Phys. Rev. Lett. **119**, 050403 (2017).

[72] A. Boudjemâa, New. J. Phys. **21**, 093027 (2019).

[73] A. Boudjemâa, Sci. Rep. **11**, 21765 (2021).

[74] A. Boudjemâa, Annals of Physics. **381**, 68 (2017).

[75] E. Aybar and M. Ö. Oktel, Phys. Rev. A **99**, 013620 (2019).

[76] M. Ota, and G. E. Astrakharchik, SciPost Phys. **9**, 020 (2020).

[77] H. Hu and X-J. Liu, Phys. Rev. Lett. **125**, 195302 (2020).

[78] N. Guebli and A. Boudjemâa, Phys. Rev. A **104**, 023310 (2021).

[79] A. Boudjemâa, K. Abbas, and N. Guebli, Atoms, **10**, 64 (2022).

[80] Z.-H. Luo, W. Pang, B. Liu, Y.-Y. Li, and B. A. Malomed, A new form of liquid matter: quantum droplets, Frontiers of Physics **16**, 32201 (2021).

[81] M. Guo and T. Pfau, A new state of matter of quantum droplets, Frontiers of Physics **16**, 32202 (2021).

[82] H. Saito, J. Phys. Soc. Jpn. **85**, 053001 (2016).

[83] A. Macia, J. Sánchez-Baena, J. Boronat, and F. Mazzanti, Phys. Rev. Lett. **117**, 205301 (2016).

[84] C. Staudinger, F. Mazzanti, and R. E. Zillich, Phys. Rev. A **98**, 023633 (2018).

[85] V. Cikojevic, L. V. Markic, G. E. Astrakharchik and J. Boronat, Phys. Rev. A **99**, 023618 (2019).

[86] L. Parisi, G. E. Astrakharchik and S. Giorgini, Phys. Rev. Lett. **122**, 105302 (2019).

[87] F. Böttcher, M. Wenzel, J-N. Schmidt, M. Guo, T. Langen, I. Ferrier-Barbut, T. Pfau, R. Bombn, J. Sánchez-Baena, J. Boronat, F. Mazzanti, Phys. Rev. Research **1**, 033088 (2019).

[88] V. Cikojevic, L. V. Markic and J. Boronat, New. J. Phy **22**, 053045 (2020).

[89] V. Cikojevi, E. Poli, F. Ancilotto, L. Vranje-Marki, and J. Boronat, Phys. Rev. A **104**, 033319 (2021).

[90] M. Trippenbach, K. Goŕal, K. Rzaewski, B. Malomed, Y. B. Band, J. Phys. B **33**, 4017 (2000).

[91] E. Timmermans, Phys. Rev. Lett. **81**, 5718 (1998).

[92] B. D. Esry and C. H. Greene, Phys. Rev. A **59**, 1457 (1997).

[93] F. Riboli and M. Modugno, Phys. Rev. A **65**, 063614 (2002).

[94] D. M. Jezek and P. Capuzzi, Phys. Rev. A **66**, 015602 (2002).

[95] A. A. Svidzinsky and S. T. Chui, Phys. Rev. A **67**, 053608 (2003).

[96] A. Sinatra, P. O. Fedichev, Y. Castin, J. Dalibard, and G. V. Shlyapnikov, Phys. Rev. Lett. **82**, 251 (1999).

[97] K. Kasamatsu, M. Tsubota, and M. Ueda, Phys. Rev. A **69**, 043621 (2004).

[98] D. M. Larsen, Ann. Phys. (N.Y.) **24**, 89 (1963).

[99] W. H. Bassichis, Phys. Rev **134**, A 543 (1964).

[100] Y. A. Nepomnyashchii, Y. A. Nepomnnyashchii, Zh. Eksp. Teor. Fiz. **70**, 1070 (1976) [Sov. Phys. - JETP **43**, 559 (1976)]; Teor. Mat. Fiz. **20**, 399 (1974).

[101] A. S. Sorensen, Phys. Rev. A **65**, 043610 (2002).

[102] P.Tommasini, E. J. V. de Passos, A. F. R. de T. Piza, and M. S. Hussein, Phys. Rev. A **67**, 023619 (2003).

[103] W. B. Colson and A. L. Fetter, J. Low. Temp. Phys. **33**, 231 (1978).

[104] B. V. Schaeybroeck, Physica A **392**, 3806 (2013).

[105] C.-C. Chien, F. Cooper, and E. Timmermans, Phys. Rev. A **86**, 023634 (2012).

[106] H. Shi, W.-M. Zheng, and S.-T. Chui, Phys. Rev. A **61**, 063613 (2000).

[107] Arko Roy and D. Angom, Phys. Rev. A **92**, 011601(R) (2015).

[108] Xiao-Long Chen, Xia-Ji Liu, and Hui Hu, Phys. Rev. A **96**, 013625 (2017).

[109] M. J. Edmonds, K. L. Lee, and N. P. Proukakis, Phys. Rev. A **91**, 011602 (2015); **92**, 063607 (2015).

[110] K-L. Lee and N. P. Proukakis J. Phys. B: At. Mol. Opt. Phys. **49**, 214003 (2016).

[111] J. Wehr, A. Niederberger, L. Sanchez-Palencia, and M. Lewenstein, Phys. Rev. B **74**, 224448 (2006).

[112] A. Niederberger, T. Schulte, J. Wehr, M. Lewenstein, L. Sanchez-Palencia, and K. Sacha, Phys. Rev. Lett. **100**, 030403 (2008).

[113] K-T. Xi, J. Li and D-N. Shi, Physica B: Condensed Matter, **459**, 6 (2015).

[114] Sh. Mardonov, M. Modugno, and E. Ya. Sherman, Phys. Rev. Lett. **115**, 180402 (2015).

[115] A. Boudjemâa and M. Benarous, Eur. Phys. J. D **59**, 427 (2010) .

[116] A. Boudjemâa and M. Benarous, Phys. Rev. A **84**, 043633 (2011).

[117] A. Boudjemâa, Phys. Rev. A **86**, 043608 (2012).

[118] A. Boudjemâa, Phys. Rev. A **88**, 023619 (2013).

[119] A. Boudjemâa, Phys. Rev. A **90**, 013628 (2014).

[120] A. Boudjemâa, J. Phys. A: Math. Theor. **48** 045002 (2015).

[121] A. Boudjemâa, Phys. Rev. A **91**, 063633 (2015).

[122] A. Boudjemâa, Commun. Nonlinear Sci. Numer. Simul. **33**, 85 (2016).

[123] A. Boudjemâa, Commun. Nonlinear Sci. Numer. Simul. **48**, 376 (2017).

[124] A. Boudjemâa, Phys. Rev. A **94**, 053629 (2016).

[125] A. Boudjemâa, and Nadia Guebli, J. Phys. A: Math. Theor. **50**, 425004 (2017).

[126] N. M. Hugenholtz and D. Pines, Phys. Rev. **116**, 489 (1959).

[127] R.A. Duine and H.T.C. Stoof, J. Opt. B: Quantum Semiclass. Opt. **5**, S212 (2003).

[128] D. A. W. Hutchinson, R. J. Dodd, K. Burnett, S. A. Morgan, M. Rush, E. Zaremba, N. P. Proukakis, M. Edwards, and C. W. Clark, J. Phys. B **33**, 3825 (2000).

[129] S. Tojo, Y. Taguchi, Y. Masuyama, T. Hayashi, H. Saito, and T. Hirano, Phys. Rev. A **82**, 033609 (2010).

[130] E. Nicklas, H. Strobel, T. Zibold, C. Gross, B. A. Mal- omed, P. G. Kevrekidis, and M. K. Oberthaler, Phys. Rev. Lett. **107**, 193001 (2011).

[131] S. Ospelkaus, C. Ospelkaus, L. Humbert, K. Sengstock, and K. Bongs, Phys. Rev. Lett. **97**, 120403 (2006).

[132] M. Zaccanti, C. DErrico, F. Ferlaino, G. Roati, M. Inguscio, and G. Modugno, Phys. Rev. A **74**, 041605 (2006).

[133] S. Giorgini, Phys. Rev. A **57**, 2949 (1998); Phys. Rev. A **61**, 063615 (2000).

[134] Xia-Ji Liu, Hui Hu, A. Minguzzi, and M. P. Tosi, Phys. Rev. A **69**, 043605 (2004).

[135] de Gennes. P G Superconductivity of Metals and Alloys (Perseus Books Advanced Book Classics, 1999).

[136] S. T. Beliaev, Sov. Phys. JETP **7**, 289 (1958).

[137] P. O. Fedichev and G. V. Shlyapnikov, Phys. Rev. A **58**, 3146 (1998).

[138] J. Zinn-Justin, Quantum field Theory and Critical Phenomena (Oxford University Press, New York, 2002)

[139] Kleinert H, Path Integrals, World Scientific, Singapore, (2004)

[140] J. O. Andersen, Rev. Mod. Phys **76**, 599 (2004).

[141] V. I. Yukalov, Ann. Phys. **323**, 461 (2008); Phys. Part. Nucl. **42**, 460 (2011).

[142] A. N. Bohr and B. R. Mottelson. Nuclear Structure (Vol. 1). (World Scientific Publishing Company, 1998).

[143] G. E. Volovik, The Universe in a Helium Droplet, (Oxford University Press, Cambridge, 2009).

[144] H. Michinel, J. Campo-Táboas, R. Garcia-Fernández, J. R. Salgueiro, and M. L. Quiroga-Teixeiro, Phys. Rev. E **65**, 066604 (2002).

[145] A. Gammal, T. Frederico, L. Tomio and L. P. Chomaz, J. Phys. B: At. Mol. Opt. Phys. **33**, 4053 (2000).

[146] H. Saito, R. G. Hulet and M. Ueda Phys. Rev. A **76**, 053619 (2007).

[147] S. Gautam and S. K. Adhikari, Ann. Phys. **409**, 167917 (2019).

[148] A. Burchianti, C. D'Errico, M. Prevedelli, L. Salasnich, F. Ancilotto, M. Modugno, F. Minardi and C. Fort, Condensed Matter **5**, 1 (2020).

[149] F. Minardi, F. Ancilotto, A. Burchianti, C. D'Errico, C. Fort, and M. Modugno, Phys. Rev. A **100**, 063636 (2019).

[150] F. Ancilotto, M. Barranco, M. Guilleumas, and M. Pi, Phys. Rev. A **98**, 053623 (2018).

[151] C. D'Errico, M. Zaccanti, M. Fattori, G. Roati, M. Inguscio, G. Modugno, and A. Simoni, New.J. Phys **9**, 223 (2007).

[152] A. Marte, T. Volz, J. Schuster, S. Dürr, G. Rempe, E. G. M. van Kempen, and B. J. Verhaar, Phys. Rev. Lett. **89**, 283202 (2002).

[153] S. Stringari and J. Treiner, Phys. Rev. B **36**, 8369 (1987).

[154] J. Wang, X-J Liu and H. Hu, Chin. Phys. **30**, 010306 (2021).

[155] M. Barranco, R. Guardiola, S. Hernández, R. Mayol, J. Navarro, and M. Pi, J. Low Temp. Phys. **142**, 1 (2006).

[156] A. Boudjemâa, J. Phys. B: At. Mol. Opt. Phys. **48**, 035302 (2015).

[157] O. Penrose and L. Onsager, Phys. Rev. **104**, 576 (1956).

[158] A. F. Andreev and I. M. Lifshitz, Sov. Phys. JETP **29**, 2 (1969).

[159] D. J. Thouless, The Flow of a Dense Superfluid, Ann. Phys. (N.Y.) **52**, 403 (1969).

[160] A. J. Leggett, Phys. Rev.Lett. **25**, 1543 (1970).

[161] G. V. Chester, Phys. Rev. A **2**, 256 (1970).

[162] M. Boninsegni andN. V. Prokof'ev, Rev. Mod. Phys. **84**, 759 (2012).